Turun yliopisto
University of Turku

EVALUATION OF MACROPHAGE-TARGETING PET TRACERS FOR IMAGING INFLAMMATION IN ATHEROSCLEROSIS

Sanna Hellberg

TURUN YLIOPISTON JULKAISUJA – ANNALES UNIVERSITATIS TURKUENSIS
Sarja - ser. D osa - tom. 1268 | Medica - Odontologica | Turku 2017

University of Turku

Faculty of Medicine
Department of Clinical Physiology and Nuclear Medicine
Drug Research Doctoral Programme
Turku PET Centre

Supervised by

Professor Anne Roivainen, PhD
Turku PET Centre and Turku Center for Disease Modelling
University of Turku
Turku, Finland

Associate Professor Antti Saraste, MD, PhD
Turku PET Centre and Heart Center
University of Turku and Turku University Hospital
Turku, Finland

Reviewed by

Adjunct Professor Katariina Öörni, PhD
Wihuri Research Institute
Helsinki, Finland

Doctor Fabien Hyafil, MD, PhD
Hôpital Bichat-Claude Bernard
Paris, France

Opponent

Professor Katriina Aalto-Setälä, MD, PhD
School of Medicine and Institute for Biomedical Technology
BioMediTech
University of Tampere
Tampere, Finland

ISBN 978-951-29-6700-1 (PRINT)
ISBN 978-951-29-6701-8 (PDF)
ISSN 0355-9483 (Print)
ISSN 2343-3213 (Online)
Painosalama Oy - Turku, Finland 2017

To my family

ABSTRACT

Sanna Hellberg

EVALUATION OF MACROPHAGE-TARGETING PET TRACERS FOR IMAGING INFLAMMATION IN ATHEROSCLEROSIS

University of Turku, Faculty of Medicine, Department of Clinical Physiology and Nuclear Medicine, Drug Research Doctoral Programme, Turku PET Centre, Turku, Finland

Atherosclerosis is an inflammatory disease which is characterized by accumulation of lipids in the vascular wall. The rupture of atherosclerotic plaque is often behind the leading causes of death in the Western world: myocardial infarction and stroke. Plaques prone to rupture are often inflamed and contain large numbers of immune cells, especially macrophages. The detection of inflammation has been studied by new imaging techniques, such as positron emission tomography (PET).

The aim of this thesis was to evaluate macrophage-targeting PET tracers for the imaging of inflammation in atherosclerosis and to evaluate responses to interventions using an established PET tracer. The studies were conducted in two mouse models. *In vivo* imaging, *ex vivo* biodistribution and aortic autoradiography were utilized to assess the tracer uptake in atherosclerotic arteries. Plasma biomarker measurements and histological stainings were conducted to assess the inflammation and the presence of tracer targets. The effects of dietary and atorvastatin interventions on aortic inflammation and uptake of an established tracer, ^{18}F-FDG, were studied.

Of the studied tracers, ^{18}F-FMCH showed the highest potential. ^{18}F-FEMPA, ^{68}Ga-DOTANOC, and ^{68}Ga-DOTATATE also showed suitable characteristics for *in vivo* imaging with certain limitations, whereas ^{18}F-FDR-NOC was not suitable. Compared to mice on high-fat food, dietary intervention led to attenuated aortic inflammation and lower ^{18}F-FDG uptake, whereas atorvastatin alone had no effect.

In conclusion, the macrophage-targeting tracers showed potential for the imaging of inflammation in atherosclerosis, especially ^{18}F-FMCH, which will be further studied in a clinical setting. The therapy responses could be assessed in a mouse model with ^{18}F-FDG.

Keywords: Atherosclerosis, inflammation, macrophage, positron emission tomography (PET) imaging

TIIVISTELMÄ

Sanna Hellberg

MAKROFAGISOLUIHIN KOHDENTUVAT PET-MERKKIAINEET ATEROSKLEROOSIN TULEHDUKSEN KUVANTAMISESSA

Turun yliopisto, Lääketieteellinen tiedekunta, Kliininen fysiologia ja isotooppilääketiede, Lääketutkimuksen tohtoriohjelma, Valtakunnallinen PET-keskus, Turku, Suomi

Ateroskleroosi on tulehduksellinen sairaus, jossa rasvaa kertyy verisuonten seinämiin. Ateroskleroottisen plakin repeäminen voi johtaa sydäninfarktiin ja aivohalvaukseen, jotka ovat yleisimpiä kuolinsyitä länsimaissa. Ateroskleroottisisen plakin repeämisriskiä lisää tulehdusreaktio. Plakeissa esiintyy runsaasti tulehdussoluja, erityisesti syöjäsoluja eli makrofageja. Tulehduksen havaitsemista on tutkittu uusilla kuvantamismenetelmillä, kuten positroniemissiotomografialla (PET).

Tämän väitöskirjatyön tarkoituksena oli tutkia makrofagisoluihin kohdentuvien PET-merkkiaineiden soveltuvuutta ateroskleroottisen plakin tulehduksen kuvantamiseen. Tutkimukset toteutettiin kahdella ateroskleroosin hiirimallilla. Merkkiaineiden kertymistä tutkittiin *In vivo* -kuvantamisella, *ex vivo* kudosjakaantumisen määrittämisellä ja aortan autoradiografialla. Plasmasta tehtyjen biomarkkerimääritysten ja kudosvärjäysten avulla tutkittiin tulehdusta ja merkkiaineiden kohteita plakeissa. Lisäksi tutkittiin vähärasvaisen ruokavalion ja atorvastatiinin vaikutusta aortan tulehdukseen ja yleisesti käytössä olevan merkkiaineen, ^{18}F-FDG:n, kertymään aortassa.

Tutkituista merkkiaineista ^{18}F-FMCH oli lupaavin ateroskleroottisen plakin tulehduksen kuvantamiseen. ^{18}F-FEMPA, ^{68}Ga-DOTANOC ja ^{68}Ga-DOTATATE olivat myös soveltuvia *in vivo* -kuvantamiseen tietyin rajoituksin. ^{18}F-FDR-NOC sen sijaan ei soveltunut kuvantamistarkoituksiin. Verrattuna rasvaista ruokaa syöneisiin hiiriin, vähärasvainen ruokavalio hiirillä vähensi aortan tulehdusta ja ^{18}F-FDG-kertymää, kun taas pelkällä atorvastatiinihoidolla ei ollut vaikutusta.

Yhteenvetona voidaan todeta, että makrofagisoluihin kohdentuvat merkkiaineet ovat soveltuvia ateroskleroottisen plakin tulehduksen kuvantamiseen. Erityisesti ^{18}F-FMCH oli lupaava ja sitä aiotaan tutkia jatkossa potilailla. Hoidon vaikutuksia pystyttiin arvioimaan ^{18}F-FDG:n avulla hiirimallissa.

Avainsanat: Ateroskleroosi, makrofagi, positroniemissiotomografia (PET)-kuvantaminen, tulehdus

TABLE OF CONTENTS

ABSTRACT 4
TIIVISTELMÄ 5
ABBREVIATIONS 9
LIST OF ORIGINAL PUBLICATIONS 12
1 INTRODUCTION 13
2 REVIEW OF LITERATURE 14
2.1 Atherosclerosis 14
2.1.1 Blood lipids and vascular structure in healthy state 14
2.1.2 Pathogenesis of atherosclerosis 14
2.1.3 Risk factors associated with atherosclerosis 16
2.1.4 Mouse models of atherosclerosis 16
2.2 Inflammation in atherosclerosis 18
2.2.1 Factors affecting the inflammatory process 19
2.2.2 Macrophages in atherosclerosis 21
2.2.3 Other inflammatory cells in atherosclerotic plaques 25
2.2.4 Pharmacological treatment of inflammation in atherosclerosis 26
2.3 Imaging of atherosclerosis 27
2.3.1 Anatomical imaging 28
2.3.2 Targeted molecular imaging 29
2.4 PET imaging of inflammation in atherosclerosis 31
2.4.1 Technical challenges and quantitation in vascular PET imaging 31
2.4.2 ^{18}F-FDG PET imaging 32
2.4.3 PET imaging with other tracers 35
3 AIMS OF THE STUDY 39
4 MATERIALS AND METHODS 40
4.1 Experimental animals 40
4.2 General study design 40
4.2.1 Interventional protocol (IV) 40
4.3 Tracer radiosyntheses 41
4.4 In vivo tracer stability measurements 42
4.5 PET/CT imaging 43
4.6 Ex vivo biodistribution 44
4.7 Autoradiography studies 45

4.8 Histology and immunohistochemistry 47
4.9 Measurement of plasma biomarkers (I, II, IV) 49
4.10 Statistical analyses 50

5 RESULTS 51

5.1 Characterization of mouse models 51
5.1.1 Histology and immunohistochemistry 51
5.1.2 Plasma biomarkers 52
5.2 In vivo stability of the tracers (I-III) 52
5.3 PET/CT imaging 53
5.4 Ex vivo biodistribution 56
5.5 Autoradiography studies 57
5.6 Correlation of plasma biomarkers and tracer uptake (I, II, IV) 58

6 DISCUSSION 60

6.1 Animal models 60
6.2 Experimental methods 61
6.2.1 In vivo imaging 61
6.2.2 Autoradiography 61
6.2.3 Detection of macrophages and assessing plaque burden 62
6.2.4 Plasma biomarker measurements 63
6.3 Evaluation of the tracers for imaging atherosclerotic plaque inflammation 63
6.3.1 SSTR-2-targeting tracers 63
6.3.2 ^{18}F-FMCH 65
6.3.3 ^{18}F-FEMPA 66
6.3.4 Diet and atorvastatin interventions and ^{18}F-FDG 67
6.4 Future aspects 69

7 SUMMARY AND CONCLUSIONS 71

8 ACKNOWLEDGEMENTS 72

9 REFERENCES 75

ORIGINAL PUBLICATIONS 87

ABBREVIATIONS

^{18}F-FDG	2-deoxy-2-[^{18}F]-fluoro-D-glucose
^{18}F-FDR-NOC	5-deoxy-5-[^{18}F]fluororibose- NaI^{3}-octreotide
^{18}F-FEMPA	N-{2-[2-^{18}F-fluoroethoxy]-5-methoxybenzyl}-N-[2-(4methoxyphenoxy)pyridin-3-yl]acetamide
^{18}F-FMCH	^{18}F-fluoromethylcholine
^{68}Ga-DOTANOC	^{68}Ga-DOTA-NaI^{3}-octreotide
^{68}Ga-DOTATATE	^{68}Ga-DOTA-d-Phe^{1}-Tyr^{3}-octreotate
α-SMA	Alpha-smooth muscle actin
ABCA1	ATP-binding cassette subfamily A 1 protein
ABCG1	ATP-binding cassette subfamily G 1 protein
ACS	Acute coronary syndrome
AGE	Advanced glycation end-product
ApoB48	Apolipoprotein B48
ApoB100	Apolipoprotein B100
ApoE	Apolipoprotein E
ApoE$^{-/-}$	Mouse model deficient in ApoE
ARG	Autoradiography
C57BL/6N	C57-Black-6N mouse strain
CD	Cluster of differentiation (e.g. CD14, CD68)
CETP	Cholesteryl ester transfer protein
CT	Computed tomography
CXCL4	Chemokine (C-X-C motif) ligand 4
DAB	3,3' diaminobenzidine tetrahydrochloride hydrate
DC	Dendritic cell
DOTA	1,4,7,10-tetraazacyclododecane-N,N',N'',N'''-tetraacetic acid
ECM	Extracellular matrix
FH	Familial hypercholesterolemia
H&E	Hematoxylin and eosin
HDL	High-density lipoprotein
HFD	High-fat diet (in study IV)
HFD+A	High-fat diet plus added atorvastatin (in study IV)
HIV	Human immunodeficiency virus
HMG-CoA	3-hydroxy-3-methyl-glutaryl-coenzyme A
HMOX1	Heme oxygenase 1
HPLC	High-performance liquid chromatography
HRP	Horseradish peroxidase
hs-CRP	High-sensitivity c-reactive protein
ICAM-1	Intercellular adhesion molecule 1
IFN-γ	Interferon gamma
IGF-II/LDLR$^{-/-}$ApoB$^{100/100}$	LDLR$^{-/-}$ApoB$^{100/100}$ mouse with IGF-II overexpression in pancreatic beta cells
IL	Interleukin
IMR	Intima-to-media ratio
IMT	Intima-media thickness

iNOS	Inducible nitric oxide synthase
i.v.	Intravenous
IVUS	Intravascular ultrasound
LDL	Low-density lipoprotein
LDLR	LDL receptor
$LDLR^{-/-}$	Mouse model deficient in LDL receptor
$LDLR^{-/-}ApoB^{100/100}$	Mouse model deficient in LDL receptor expressing only apolipoprotein B100
LOX-1	Lectin-like oxidized LDL receptor
LPS	Lipopolysaccharide
LRP	LDLR related protein
Ly6C	Lymphocyte antigen 6 complex
M1	Pro-inflammatory macrophage
M2	Anti-inflammatory macrophage
M4	Platelet chemokine-induced macrophage
Mac-3	Mouse CD107b antigen
MCP-1	Monocyte chemoattractant protein-1 (also known as CCL2)
M-CSF	Macrophage colony-stimulating factor
Mφ	Macrophage
M(Hb)	Hemoglobin-stimulated macrophage
MHC	Major histocompatibility complex
Mhem	Heme-induced macrophage
MMP	Matrix metalloproteinase
Mox	Oxidized phospholipid induced macrophage
MR	Mannose receptor
MRC-1	Mannose receptor, C type 1
MRI	Magnetic resonance imaging
NLRP3	NLR family, pyrin domain containing 3
NO	Nitric oxide
NZW	New Zealand White rabbit
OCT	Optical coherence tomography
PAD	Peripheral artery disease
PCSK9	Proprotein convertase subtilisin/kexin type-9
PET	Positron emission tomography
PK11195	1-(2-chlorophenyl)-N-methyl-N-(1-methylpropyl)-3-isoquinoline caboxamide
PLTP	Phospholipid transfer protein
PON-1	Paraoxonase-1
PSL/mm^2	Photo-stimulated luminescence per square millimeter
RANTES	Chemokine regulated on activation, normal T cell expressed and secreted (Also known as CCL5)
RGD	Arginine-glycine-aspartate motif
ROI	Region of interest
SMC	Smooth muscle cell
SPECT	Single-photon emission computed tomography
SPIO	Small paramagnetic particles of iron oxide

SSTR	Somatostatin receptor
SUV	Standardized uptake value
T_H	Helper T cell
T_{reg}	Regulatory T cell
TBR	Target-to-background ratio
TF	Tissue factor
TGFβ	Transforming growth factor beta
TLR	Toll-like receptor
TNF-α	Tumor necrosis factor alpha
TSPO	18 kDa translocator protein
USPIO	Ultra-small paramagnetic particles of iron oxide
VCAM-1	Vascular cell adhesion molecule 1
VLDL	Very low density lipoprotein
VSMC	Vascular smooth muscle cell
WHHL	Watanabe heritable hyperlipidemic rabbit

LIST OF ORIGINAL PUBLICATIONS

This thesis is based on the following original publications.

I. Rinne P*, Hellberg S*, Kiugel M, Virta J, Li XG, Käkelä M, Helariutta K, Luoto P, Liljenbäck H, Hakovirta H, Gardberg M, Airaksinen AJ, Knuuti J, Saraste A, Roivainen A. Comparison of Somatostatin Receptor 2-Targeting PET Tracers in the Detection of Mouse Atherosclerotic Plaques. Mol Imaging Biol. 2016;18(1):99-108.

II. Hellberg S, Silvola JM, Kiugel M, Liljenbäck H, Metsälä O, Viljanen T, Metso J, Jauhiainen M, Saukko P, Nuutila P, Ylä-Herttuala S, Knuuti J, Roivainen A, Saraste A. Type 2 diabetes enhances arterial uptake of choline in atherosclerotic mice: an imaging study with positron emission tomography tracer ^{18}F-fluoromethylcholine. Cardiovasc Diabetol. 2016;15(1):26.

III. Hellberg S, Silvola JMU, Kiugel M, Liljenbäck H, Savisto N, Li XG, Thiele A, Lehmann L, Heinrich T, Vollmer S, Hakovirta H, Laine VJO, Ylä-Herttuala S, Knuuti J, Roivainen A, Saraste A. 18-kDa Translocator Protein Ligand ^{18}F-FEMPA: Biodistribution and Uptake into Atherosclerotic Plaques in Mice. J Nucl Cardiol. Published online May 25, 2016.

IV. Hellberg S, Sippola S, Liljenbäck H, Virta J, Silvola JMU, Ståhle M, Savisto N, Metso J, Jauhiainen M, Saukko P, Ylä-Herttuala S, Nuutila P, Knuuti J, Roivainen A, Saraste A. Effects of atorvastatin and diet interventions on atherosclerotic plaque inflammation and [^{18}F]FDG uptake in *Ldlr$^{-/-}$Apob$^{100/100}$* mice. Manuscript submitted for publication.

* Equal contribution

The original publications have been reprinted with the permission of copyright holders.

The publications are referred to in the text by their corresponding Roman numerals, I-IV. In addition, some unpublished data are presented in this thesis.

1 INTRODUCTION

Atherosclerosis is characterized by accumulation of lipids in the arterial walls, which can eventually lead to severe complications. It is a major cause of morbidity and mortality especially in developed countries. The clinical manifestations of atherosclerosis include ischemic heart disease and stroke, which still remain the largest mortality-causing diseases worldwide, although the prevalence has diminished during the recent decades (GBD 2013 Mortality and Causes of Death Collaborators 2015; Herrington et al. 2016).

Atherosclerosis is initiated when lipoproteins accumulate in the vessel wall. Modification of the lipoproteins evokes an inflammatory response including recruitment of monocytes from bloodstream to the lesion area. Monocytes differentiate into macrophages in the vessel intima and phagocytose the lipids. Macrophages can further promote disease progression by secreting pro-inflammatory cytokines, and at later stages of the disease, also take part in plaque erosion or rupture by secreting proteolytic enzymes. Therefore, inflammation is a key feature of plaques at high risk of rupture. (Rudd et al. 2010, Moore and Tabas 2011)

Positron emission tomography (PET) imaging is a possible method to non-invasively assess inflammation in atherosclerosis. Glucose analogue 2-deoxy-2-[^{18}F]-fluoro-*D*-glucose (^{18}F-FDG) is the most studied tracer, which shows increased uptake in activated and pro-inflammatory macrophages (Rudd et al. 2002; Davies et al. 2010; Tavakoli et al. 2013). In addition to detecting inflammation in atherosclerosis, ^{18}F-FDG imaging has been utilized in the assessment of therapy responses (Tahara et al. 2006; Tawakol et al. 2013).

^{18}F-FDG imaging, however, has some limitations, and therefore other tracers might be more suitable for detecting inflammation in atherosclerosis. In this thesis, new PET tracers targeting macrophages in atherosclerotic lesions are studied in mouse models of atherosclerosis. In addition, ^{18}F-FDG is evaluated in the *in vivo* imaging of therapy responses in a hypercholesterolemic mouse model.

2 REVIEW OF LITERATURE

2.1 Atherosclerosis

2.1.1 Blood lipids and vascular structure in healthy state

Lipids in the bloodstream are derived from dietary intake and endogenous biosynthesis. As insoluble molecules, they are always carried in association with proteins called apoproteins. The combination of lipid and apoprotein is referred to as lipoprotein, and one lipoprotein often has several apoproteins on the surface. The lipoproteins are classified, based on their size and density, as chylomicrons, very low-, low- or high density lipoproteins (VLDL, LDL and HDL, respectively). Chylomicrons are produced in the intestine and they are involved in transportation of dietary lipids. VLDL particles are mainly produced in the liver, and LDL particles are derived from VLDL in the bloodstream. Both are considered pro-atherogenic. LDL is the most important carrier of cholesterol, whereas VLDL carries mainly triglycerides. The major structural apoprotein of VLDL and LDL is apolipoprotein B100 (ApoB100). The intake of LDL to hepatic cells and cells in peripheral tissues is mediated by LDL receptor (LDLR). HDL particles contain apolipoprotein A1 as the major structural apoprotein, and they transport cholesterol and phospholipids from peripheral tissues to the liver. HDL is therefore considered anti-atherogenic. (Tall and Yvan-Charvet 2015)

Normal arteries have dedicated structure consisting of separate layers: intima, media and adventitia. Intima consists of endothelial cells and sub-endothelial connective tissue and smooth muscle cells (SMCs). The endothelial cells cover the inner surface of blood vessels and control contractility as well as regulate permeability and inhibit leukocyte adhesion (Cines et al. 1998). Media consists of several layers of SMCs, and is responsible for the elasticity of the vessel. Adventitia is adipose and connective tissue with small blood and lymphatic vessels, and nerves.

2.1.2 Pathogenesis of atherosclerosis

The initiation of atherosclerosis involves accumulation of lipids from the bloodstream into the vessel intima. This process is associated with endothelial dysfunction, a process where the endothelial cells lose their ability to maintain the homeostasis of vascular tone. The production of vascular relaxation mediators, such as nitric oxide (NO), is impaired leading to increased vasoconstriction and permeability. Lipids from the bloodstream, as well as immune cells, can adhere to the vessel wall and penetrate to the intima. This leads to mild inflammation and the formation of the initial lesions, referred as fatty streaks or intimal xanthomata. These lesions are characterized by the presence of foam cells, which are macrophages that have ingested lipids.

Macrophages are monocyte-derived phagocytic cells, which are a part of innate immune system, and they have a critical role in atherosclerosis, discussed further in Chapter 2.2. (Stary et al. 1994; Cines et al. 1998; Virmani et al. 2000)

The initial lesions may increase in size and have increased fibrosis, leading to pathological intimal thickening characterized by collagen, foam cells and small extracellular lipid pools. Macrophages normally phagocytose the material from cells undergoing programmed cell death, apoptosis. When this progress becomes defective, the cell debris forms the necrotic core of the plaque. The pro-inflammatory milieu in plaques also leads to SMC proliferation and increased deposition of extracellular matrix (ECM), leading to formation of a covering layer of connective tissue, which is termed fibrous cap. The size of the lesions is very variable, and does not indicate the severity. The lesions may also undergo positive remodeling, which means enlargement without luminal narrowing. At this stage, the classical plaque structure with lipid core and fibrous cap is present, and the lesions are classified as fibroatheromas. (Virmani et al. 2000)

Some of the plaques may develop further to become thin cap fibroatheromas. The thinning of the fibrous cap is caused by matrix-degrading proteases produced by inflammatory cells. Thin cap fibroatheromas are defined as having less than 65 µm-thick fibrous cap, and they may contain crystallized cholesterol and intraplaque hemorrhages. They are more disorganized by structure than less-advanced lesion types. Deposits of calcium may also emerge. The calcification process is highly regulated, and the sizes of calcifications vary from few-micrometer microcalcifications to calcified nodules and large whole-plaque calcifications. The inflammatory process in plaques is also prominent. As the lesion becomes larger, some of the plaque areas may be poorly oxygenated (hypoxic). This leads to formation of new blood vessels (neovascularization) in order to oxygenate the arterial wall. Lesions with these features are at high risk of rupture or erosion. Rupture of the plaque can be caused by active degradation process and physical factors, such as blood flow pressure or calcifications, and it occurs commonly in the areas at the junction of plaque and lesion-free vascular wall (shoulder regions). In erosion, the endothelium of vascular wall is often absent, which predisposes the underlying material to blood, causing thrombosis. Thrombosis does not always lead to coronary or cerebral events, but may heal and increase the lesion size. (Virmani et al. 2000; Libby and Theroux 2005; Sage et al. 2010)

The main complications of atherosclerosis include ischemic heart disease, stroke and peripheral artery disease (PAD). Ischemic heart disease is the complication when a coronary vessel is blocked by either an obstructive lesion, leading to diminished perfusion of the myocardial tissue, or when a thrombus blocks the blood flow to the myocardial tissue. Thrombosis following rupture or erosion of plaque is the most common cause of myocardial infarction (MI) leading to sudden death (Virmani et al. 2000). In MI, the blood flow in the coronary artery is blocked leading to uncontrolled cell death, necrosis, in the myocardium. In

stroke, the blood flow to brain tissue is blocked by a thrombus leading to tissue damage. PAD affects the peripheral blood vessels, usually in limbs or kidneys. PAD is not a major cause of mortality, but instead, causes morbidity by critically lowering the patient's mobility (Herrington et al. 2016).

2.1.3 Risk factors associated with atherosclerosis

The risk of developing atherosclerosis during one's lifetime is dependent on numerous genetic and environmental factors. Age, male gender, genetic susceptibility, increased cholesterol levels, diabetes, elevated blood pressure (hypertension) and smoking have been recognized as the most important risk factors for atherosclerosis (Herrington et al. 2016). Additionally, some systemic inflammatory diseases, such as rheumatoid arthritis or human immunodeficiency virus (HIV) infection, can increase risk. The risk of individual subjects developing cardiovascular disease can be estimated by calculated risk scores, such as the Framingham risk score.

Familial hypercholesterolemia (FH) is a monogenetic disease which is characterized by highly elevated LDL cholesterol levels and high risk of cardiovascular diseases. FH patients have a mutation in the LDL receptor or the ApoB gene, leading to elevated cholesterol. Other genetic variants affect the risk of atherosclerosis, but not as severely as in FH. (Rader et al. 2003)

High cholesterol levels are an important risk factor for cardiovascular mortality, which has been proven in numerous large studies. The risk of cardiovascular mortality is positively correlated with non-HDL cholesterol in a log-linear manner, whereas HDL cholesterol has a negative correlation. Although high cholesterol levels increase the risk of ischemic heart disease, the association of cholesterol to risk of stroke is less clear. (Di Angelantonio et al. 2009; Herrington et al. 2016)

Diabetic patients are at higher risk of atherosclerosis and its complications. Their risk for PAD, MI or stroke is two to four times higher than for people without diabetes. Diabetes is often combined with obesity, which further raises the risk. The mechanisms of diabetes increasing the risk of complications also include increased coagulation, proteolysis and thrombotic activity. Advanced glycation end-products (AGEs) may also increase vascular inflammatory responses. (Pasterkamp 2013; Herrington et al. 2016)

2.1.4 Mouse models of atherosclerosis

Animal models are an important tool in gaining understanding of the pathogenesis of atherosclerosis as well as in the search of new treatments. The most commonly-utilized species for atherosclerosis research is mouse, mainly because of convenience. They are inexpensive, have a relatively short lifespan and are easy to breed and maintain. Larger animal models such as rabbits, swine and non-human primates, are better for *in vivo* imaging purposes, but the

development of disease is slower and the models are more costly and laborious to handle. Most of the disease models are based on genetic modifications. In addition, models with physical damage to the vessel, for example balloon injury, denudation or cuffing, combined with high-fat diet, are utilized. Commonly utilized rabbit models include Watanabe heritable hyperlipidemic rabbit (WHHL), which is genetically susceptible to atherosclerosis, and balloon injury model on New Zealand White (NZW) rabbit. Ideally, the animal model would have a human-like lipid profile and rapidly developing atherosclerosis with all the features of the disease. The model should also be responsive to similar treatments, such as statins, as humans. The ideal model would also represent the complicated lesions, plaque rupture and thrombosis.

Mice are generally resistant to atherosclerosis. This is mainly caused by the differences in lipoprotein profile compared to humans. Mice have a vast majority of HDL in the plasma, and LDL and VLDL are only a very small proportion. Mice also lack cholesteryl ester transfer protein (CETP). Most of the atherosclerotic mouse models are developed on C57BL/6 background, since these mice are prone to gain weight and have increased pro-inflammatory immunological responses (Paigen et al. 1985; Huber et al. 2001). ApoE knockout ($ApoE^{-/-}$) mouse, which was developed in the early 1990s, is the most-utilized model of atherosclerosis (Piedrahita et al. 1992; Plump et al. 1992). ApoE is present in lipoprotein particles, especially in chylomicrons, and it takes part in lipoprotein clearance. The lipoprotein profile of $ApoE^{-/-}$ mice is distinct from healthy mice, but on the other hand, also very different from humans. $ApoE^{-/-}$ mice develop atherosclerosis even on low-fat chow diet, but feeding with high-fat diet is often utilized to accelerate the disease. Atherosclerosis in these mice is present in the aorta and carotid arteries (Zhang et al. 1992). The ApoE*3-Leiden mouse model has a mutant form of ApoE, and it resembles human dysbetalipoproteinemia. These mice have spontaneously increased plasma cholesterol levels, but the development of prominent atherosclerosis requires feeding with high-fat diet (van den Maagdenberg et al. 1993; Van Vlijmen et al. 1994). LDL receptor knockout ($LDLR^{-/-}$) mouse is another widely-utilized model of atherosclerosis. It resembles human FH by lipid profile and lesion formation. The lipid profile of these mice is only modestly modified when fed with chow diet compared to healthy mice, but high-fat diet feeding causes highly elevated VLDL and LDL cholesterol as well as large atherosclerotic lesions throughout the arterial tree (Ishibashi et al. 1993).

The above-mentioned mouse models have also been combined with other genetic modifications in order to develop models that better mimic human atherosclerosis. In mice, but not in humans, a large portion of ApoB100 is edited to ApoB48 in the liver via APOBEC-1 enzyme complex. Targeted mutation in the ApoB gene (Farese et al. 1996; Powell-Braxton et al. 1998) or lack of APOBEC-1 enzyme (Hirano et al. 1996) leads to expression of only ApoB100 ($ApoB^{100/100}$). Lack of ApoB48 combined with LDLR deficiency ($LDLR^{-/-}ApoB^{100/100}$) further impairs the lipoprotein clearance, since ApoB100-containing lipoproteins cannot be taken up in cells via LDLR related protein

(LRP), which would facilitate the clearance in the absence of LDLR (Véniant et al. 1998). This further raises LDL cholesterol and makes the lipoprotein profile closer to that of humans (Véniant et al. 1998; Powell-Braxton et al. 1998). Another approach to making more human-like disease is to add expression of human CETP. CETP mediates exchange of cholesterol and triglycerides (TG) between ApoB-containing lipoproteins and HDL, and therefore affects the VLDL/LDL–HDL ratio. Addition of human CETP expression in $LDLR^{-/-}$, $ApoE^{-/-}$ or ApoE*3-Leiden mice decreases HDL, increases VLDL and LDL and accelerates the disease development (Plump et al. 1999; Westerterp et al. 2006). Several models have also been created to mimic the combination of diabetes and atherosclerosis (Heinonen et al. 2015). Since plaque ruptures are extremely rare in mice, models have been developed to increase the rate of spontaneous plaque rupture. For example, $ApoE^{-/-}$ mice with mutant fibrillin-1 gene represent increased presence of rupture-prone plaques (Van Herck et al. 2009).

2.2 Inflammation in atherosclerosis

The involvement of immune cells in atheromas was observed already in the mid-19th century by pathologists von Rokitansky and Virchow. The widely-known view of atherosclerosis has, however, been a disease of arteries hardening by accumulation of cholesterol. Smooth muscle cell proliferation as a response to injury was added to the concept in the 1970s (Ross and Glomset 1976a; Ross and Glomset 1976b). In the 1990s, two hypotheses of atherogenesis were presented: The response to retention -hypothesis, where the lipoprotein retention in the arterial wall is considered as the key factor in atherogenesis (Williams and Tabas 1995; Tabas et al. 2007), and the concept of inflammation being the driving force (Libby 2002). In today's view, inflammation in atherosclerosis is a complex process involving numerous components of innate and adaptive immunity, including different types of cells and various physical and chemical factors, and involving both a systemic component as well as local reactions in individual plaques. Systemic inflammatory process, measured as blood levels of C-reactive protein by high-sensitivity assays (hs-CRP), is linked to increased risk of cardiovascular disease (Ridker et al. 2009). On the other hand, inflammation in individual atherosclerotic plaques has been linked to higher risk of rupture (Narula et al. 2008). A schematic view of atherosclerotic plaque components and the inflammatory process is shown in Figure 1.

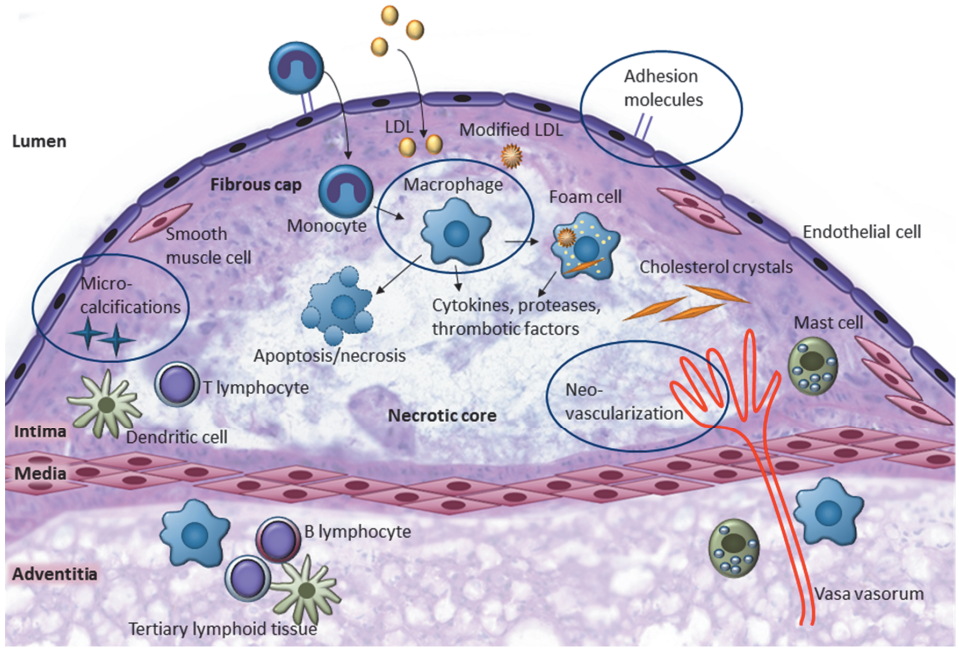

Figure 1. Features and molecular imaging targets of atherosclerotic plaques. Inflammatory cells are recruited to plaques by cytokines and expression of adhesion molecules in the vascular endothelium. Monocytes differentiate to macrophages, ingest modified LDL and become foam cells. Also other types of inflammatory cells, such as mast cells, dendritic cells and B and T lymphocytes are present in the plaque intima and in adventitia. The most-studied targets for molecular imaging of atherosclerosis include adhesion molecules, macrophages, microcalcifications and neovascularization.

2.2.1 Factors affecting the inflammatory process

Atherosclerotic lesions tend to form in areas where the blood flow is turbulent. The term "shear stress" refers to the pressure effect of blood flow on the arterial walls. Shear stress is needed for normal endothelial function, but where there is less flow, especially in the inner curvatures and bifurcations, those areas are more prone to develop lesions. Low shear stress can lead to endothelial dysfunction, which predisposes the area to plaque progression (Chiu and Chien 2011; Hsieh et al. 2014). Adhesion molecules are also expressed in the sites of low shear stress (Nakashima et al. 1998).

The immune system reacts to molecular structures which are altered or exist in places where they should not exist. These are recognized by immune cells, such as macrophages, via toll-like receptors (TLRs). In atherosclerosis, these altered structures include, for example, oxidatively modified or aggregated lipoproteins, crystallized cholesterol and AGEs. Material from ECM degradation and debris from necrotic cells are also triggers to the immune system. (Zimmer et al. 2015)

The accumulation of free, non-esterified cholesterol in plaques can lead to the formation of cholesterol crystals. Free cholesterol is derived from cholesterol de-

esterification as well as from dying foam cells and red blood cells. Cholesterol crystals can be present already in early stages of the disease. They are very pro-inflammatory in nature: they can promote the activation of NLRP3 inflammasome and thus lead to secretion of pro-inflammatory cytokines, such as interleukins IL-1β and IL-6 (Duewell et al. 2010; Rajamäki et al. 2010; Janoudi et al. 2016). In addition to causing inflammatory response, the cholesterol crystals may also physically perforate the plaque intima and trigger plaque rupture (Abela and Aziz 2006). In addition to cholesterol crystals, small, spotty calcifications in plaques may also be related to the pathogenesis and complications of atherosclerosis (Ehara et al. 2004).

Intraplaque hemorrhage leads to leakage of blood cells and hemoglobin into the plaque. The red blood cell membranes are rich with cholesterol, which increases the plaque size, and hemoglobin deposition leads to increased iron concentration in plaques. Iron is thought to have a pro-inflammatory effect and a role in catalyzing lipoprotein oxidation, but consensus is still lacking in the field. Red blood cells are also a source of cholesterol, and platelets can lead to the deposition of beta-amyloid in the plaques, which further promotes plaque development. (De Meyer et al. 2002; Sullivan 2009; Habib and Finn 2014)

Systemic inflammatory diseases, such as rheumatoid arthritis and HIV infection increase the risk of atherosclerosis. The risk of myocardial infarction and stroke is also increased during certain infections. Interestingly, DNA from multiple pathogens have been detected inside atherosclerotic lesions, and therefore, the inflammation in atherosclerotic plaques is not necessarily sterile. For example *Chlamydia pneumoniae* and *Helicobacter pylori* can be found in lesions. Viable *C. pneumoniae* bacteria have been detected in addition to only the DNA, and this is the bacterium that has the most evidence of having a role in atherogenesis. The role of pathogens in atherosclerosis is not well-understood, and it must be borne in mind, that bacteria can also be innocent bystanders in the plaque. (Zimmer et al. 2015)

Factors affecting the trafficking of cells

Cytokines have a major role in the development of atherosclerosis, but on the other hand, also in the regression of the disease. Cytokines are cell-produced signaling molecules. These soluble factors affect the immune cells by controlling their extravasation to the plaques as well as their differentiation and polarization. Cells recognize cytokines via specific receptors. Chemokines are a sub-class of cytokines, which are involved in attracting cells to enter tissues (chemotaxis). Cytokines effecting atherosclerotic plaque progression are, for example, interferon gamma (IFN-γ), tumor necrosis factor alpha (TNF-α), IL-1β, IL-6, IL-12, IL-15 and IL-18. Atheroprotective cytokines include IL-4, IL-10 and transforming growth factor beta (TGFβ). Key chemokines in atherogenesis are monocyte chemoattractant protein-1 (MCP-1/ CCL2), which attracts monocytes to penetrate the intima, and chemokine regulated on activation, normal T cell expressed and secreted (RANTES/ CCL5), which attracts T cells to plaques.

Adhesion molecules are up-regulated in the induction of inflammation and they have a key role in the recruitment of immune cells to atherosclerotic plaques. Immune cells recognize the adhesion molecules via their surface antigens, attach to the molecules, and finally transmigrate to the intima. The most important adhesion molecules in atherosclerosis are vascular cell adhesion molecule 1 (VCAM-1), intercellular adhesion molecule 1 (ICAM-1) and P-selectin. The expression of adhesion molecules is regulated by the inflammatory process, and their meaning in the pathogenesis of atherosclerosis has been widely studied. Lack of adhesion molecules generally leads to attenuated atherosclerosis. (Johnson et al. 1997; Nakashima et al. 1998; Patel et al. 1998; Cybulsky et al. 2001; Hansson and Libby 2006)

2.2.2 Macrophages in atherosclerosis

Macrophages are the most numerous cells in atherosclerotic lesions. They are mononuclear phagocytes, which were discovered in 1884 by Ilya Metchnikoff. Macrophages arise from blood monocytes, which penetrate through the vascular wall into the intima and differentiate into macrophages. Monocytes in the bloodstream are a heterogeneous population; in mice they are most often divided into pro-inflammatory $Ly6C^{hi}$ and anti-inflammatory $Ly6C^{low}$ monocytes. The corresponding subsets in humans are $CD14^{high}CD16^{-}$ and $CD14^{low}CD16^{+}$, respectively. The proportions of these subsets are affected by hyperlipidemia and inflammation. In the intima, the macrophages are affected by many factors, which lead to different activation and polarization states. Macrophages sustain the pro-inflammatory environment in atherosclerotic plaques and also contribute to fibrous cap thinning and thrombosis. (Woollard and Geissmann 2010; Moore and Tabas 2011)

Origins of macrophages

Most of the macrophages in atherosclerotic plaques arise from bone marrow derived blood monocytes. These myeloid progenitor cells can differentiate to monocytes, but also to neutrophils, mast cells or dendritic cells. In recent years, judging the bone marrow as the only source of plaque macrophages has been questioned. The contemporary view of the monocyte-macrophage system is that part of the tissue-resident macrophages originates from embryonic time and proliferate in the tissues (Ginhoux and Jung 2014). The spleen has also been identified as an important source of inflammatory monocytes (Cochain and Zernecke 2015). One newly recognized source of macrophages in atherosclerosis is the transdifferentiation of VSMCs. This has been recognized *in vitro* and in animal model, but evidence from clinical samples is still lacking (Rong et al. 2003; Feil et al. 2014).

Macrophages in the pathogenesis of atherosclerosis

Macrophages have a central role in the initiation, development and complications of atherosclerosis. Inhibiting macrophage differentiation diminishes atherosclerosis

(Smith et al. 1995). In the early atherogenesis, endothelial dysfunction leads to accumulation of lipoproteins to the intima, secretion of chemokines and expression of adhesion molecules in the endothelial cells. The details of this process still remain poorly understood. The monocytes from the bloodstream enter the intima and differentiate to macrophages. The differentiation process is mediated by cytokines, such as macrophage colony-stimulating factor (M-CSF). Macrophages ingest the lipoproteins via scavenger receptors, such as CD36, type A scavenger receptor, lectin-like oxidized LDL receptor (LOX-1) and TLRs. The macrophages with ingested lipids are referred to as "foam cells". In normally functioning macrophages, cholesteryl esters are digested in lysosomes and effluxed to HDL particles via ATP-binding cassette subfamily A and G 1 proteins (ABCA1 and ABCG1). The free cholesterol may also be re-esterified if it is not effluxed and this cycle may be repeated. At this point, the role of macrophages can be seen as positive and disease-controlling, since they participate in the removal of the lipids from the arterial wall. However, if the process becomes defective, for example due to excess amount of lipids, macrophages may start to promote the disease development. Overload with free cholesterol may lead to endoplasmic reticulum stress in macrophages, which can lead to pro-inflammatory signaling and eventually to apoptosis. The apoptotic cell debris is also cleared by macrophages. If the clearance mechanisms become defective, it can cause secondary necrosis. This leads to the formation of lipid-rich necrotic core areas of the plaques. Macrophages in the plaques keep up the pro-inflammatory state in the plaques by secreting cytokines and chemokines, which can lead to increased recruitment of leukocytes, decreased collagen production in SMCs and also cell death. This in addition to secreted matrix metalloproteinases (MMPs) and other proteases lead to weakening of the fibrous cap. Macrophages also have a role in the complications of atherosclerosis by secreting pro-thrombotic tissue factor (TF), which promotes the thrombus formation. (Moore and Tabas 2011)

Macrophage polarization

Macrophages can switch their phenotype profile based on environmental signals. The phenotype switch changes the gene transcription and leads to expression of different surface molecules and secretion of soluble mediators (Table 1). The different polarization states of macrophages are mainly reversible, with the exception of M4 polarization (Gleissner et al. 2010). The polarization can be seen more as a continuum, not as a clear separation of segregated cell types which have distinct functions.

Generally, macrophages are divided into two major groups based on their polarization: pro-inflammatory M1 and anti-inflammatory M2 macrophages. These correspond to Th1 and Th2 responses in T cells, respectively. Both M1 and M2 macrophages have been detected in the fibrous cap of atherosclerotic plaques, but M1 macrophages dominate the shoulder areas (Stöger et al. 2012). M1 macrophages are also referred to as classically activated and M2 as alternatively activated. M1 polarization is driven by pro-inflammatory cytokines,

such as IFN-γ and TNF-α, as well as bacterial lipopolysaccharide (LPS). In atherosclerosis, oxidized LDL (ox-LDL) and cholesterol crystals may also trigger M1 polarization. Characteristic surface markers for M1-polarized macrophages are, for example, CD86 and TLR4. M1 polarization leads to the secretion of pro-inflammatory mediators, such as IL-1β, IL-6, IL-12, TNF-α, chemokine receptor ligands, and activation of inducible nitric oxide synthase (iNOS), which further promote the recruitment of new inflammatory cells from the bloodstream. They also produce reactive oxygen species which further take part in lipid oxidation. This response is relevant in acute infections, but can lead to tissue damage when the response is chronic. (Mosser and Edwards 2008; Mantovani et al. 2009; Colin et al. 2014)

M2 polarization has opposite effects from M1 polarization. M2-polarized macrophages are generally seen as atheroprotective, although they are also present in plaques with high-risk features (Tahara et al. 2014). M2-polarized macrophages can be further divided to M2a, M2b and M2c. M2a macrophages are induced by cytokines IL-4 and IL-13, and show a high expression of mannose receptor (MR). These cells secrete, for example, fibronectin and TGFβ and therefore have a role in wound healing. M2b macrophages are induced by immune complexes and IL-1β and M2c macrophages by glucocorticoids and IL-10. M2b and M2c macrophages are suggested to take part in the cleaning of apoptotic cells and to have an immunoregulatory role. (Colin et al. 2014)

Division into M1 and M2 macrophages does not cover the full spectrum of macrophage polarization; other kinds of polarization states have also been recognized. Oxidation of phospholipids leads to formation of new epitopes, which are recognized by immune cells. Macrophages recognize these epitopes via scavenger- and toll-like receptors, which may lead to a polarization state referred to as Mox. Mox macrophages express antioxidant genes, such as heme oxygenase 1 (HMOX1) and have reduced phagocytic capacity. They can build up to 30 % of lesion macrophages in mice, but have not been recognized in humans (Kadl et al. 2010). The role of these macrophages is still controversial, since there are studies showing atheroprotective effects, but also activation of pro-inflammatory pathways (Colin et al. 2014). Macrophage polarization induced by intraplaque hemorrhage has also been recognized. Hemoglobin-stimulated macrophages (M(Hb)) express MR and CD163, a scavenger receptor recognizing hemoglobin/haptoglobin complexes. Mhem macrophages express HMOX1 and CD163, and the polarization is induced by ingestion of heme. M(Hb) and Mhem macrophages have partially similar functions and properties, since they both have a role in iron handling and are therefore seen as atheroprotective (Colin et al. 2014; Chistiakov et al. 2015). M4 macrophages are induced by platelet chemokine CXCL4. They are regarded as pro-inflammatory and pro-atherogenic, since they are prone to foam cell formation, have a low phagocytic capacity due to CD163 down-regulation and they secrete pro-inflammatory IL-6 and TNF-α (Gleissner et al. 2010).

Table 1. Inflammatory cells in atherosclerotic plaques

Immune cell	Induced by	Functions and properties	Phenotypic markers, surface molecules	Cytokines and other secreted factors	Identified in
Monocytes					
$Ly6C^{hi}$	Hyperlipidemia	Pro-inflammatory, differentiates to M1 macrophage	CCR2, CD62L	IL-1β, proteases, ROS	Mouse
$Ly6C^{low}$	N/A (resident/ patrolling)	Anti-inflammatory, differentiates to M2 macrophage	CX_3CR1, CD11a	N/A	Mouse
$CD14^{high}CD16^{-}$	N/A (resident/ patrolling)	Classical monocytes, 85-95% of blood monocytes in healthy state	CCR2, CD62L, CD64	CCL2 (MCP-1), IL-6, IL-8, IL-10, ROS, myeloperoxidase	Human
$CD14^{low}CD16^{+}$	Inflammation	Pro-inflammatory	CX_3CR1, CD32, MHC-II	TNF-α	Human
Macrophages					
M1	LPS, IFN-γ, TNF-α, ox-LDL, cholesterol crystals	Pro-inflammatory, Th1 response	CD86, iNOS Mouse: Arg-2	IL-1β, IL-6, IL12, TNF-α, CCL5 (RANTES), NO, ROS	Human, mouse
M2a	IL-4, IL-13	Anti-inflammatory, tissue remodeling, plaque regression	Human: MR, IL1RN Mouse: Arg-1, FIZZ-1	IL-10, TGF-β, CCL17, CCL22, collagen, fibronectin	Human, mouse
M2b	IL-1β, LPS, immune complexes	Immunoregulation	$IL\text{-}10^{high}$, $IL\text{-}12^{low}$	IL-6, IL-10, TNF-α	Human, mouse
M2c	IL-1β, TGF-β, glucocorticoids	Phagocytosis of apoptotic cells	Human: MR Mouse: Arg-1	IL-10, TGF-β	Human, mouse
Mox	ox-LDL	Weak phagocytosis, pro-atherogenic	HMOX1	IL-1β, IL-10, ROS	Mouse
Mhem	Heme	Phagocytosis of erythrocytes, atheroprotective	CD163, HMOX1	IL-10, ApoE	Human, mouse
M(hb)	Hemoglobin/ haptoglobin	Hemoglobin clearance, atheroprotective	CD163, MR, ABCG1, ABCA1	IL-10	Human
M4	CXCL4	Weak phagocytosis, pro-atherogenic	MR, S100A8	IL-6, TNF-α, MMP-7, MMP-12	Human
Lymphocytes					
T_H1 T cells	IL-12, IL-18 (Th1 response)	Pro-inflammatory, antigen-mediated immunity	CD4, CD40L, CD154	IFN-γ, TNF-α	Human, mouse
Cytotoxic T cells	N/A	Cytotoxic, proatherogenic	CD8	TNF-α	Human, mouse
T_{reg} cells	N/A	Anti-inflammatory, suppression of immune responses	CTLA-4	IL-10, TGF-β	Human, mouse
B cells	N/A	Production of protective antibodies/ enhancing pro-atherogenic T cell responses	CD19	IgM, IgA, IgG, IgE	Human, mouse
Other cell types					
Dendritic cells	N/A	Antigen presenting, Th1 response, link between innate and adaptive immunity / T_{reg} expansion, atheroprotection	CD11c	IFN-α, IFN-β / CCL17, IL-12	Human, mouse
Mast cells	N/A	Matrix degradation, recruitment of inflammatory cells, weakening of neovessels	Granule neutral proteases, CCR3	Chymase, tryptase, histamin, heparin, IL-6, IFN-γ	Human, mouse
Neutrophils	Hyperlipidemia	Recruitment of inflammatory cells, pro-atherogenic, pro-thrombotic	CCR1, CCR5, CD11b	Azurocidin, cathepsin G, elastase	Human, mouse

Table data from references: (Hansson and Libby 2006; Drechsler et al. 2010; Weber and Noels 2011; Hilgendorf and Swirski 2012; Colin et al. 2014; Tsiantoulas et al. 2014; Witztum and Lichtman 2014; Chistiakov et al. 2015; Cochain and Zernecke 2015; Zernecke 2015; Bot et al. 2015)

2.2.3 Other inflammatory cells in atherosclerotic plaques

Lymphocytes

Lymphocytes are an essential part of adaptive immunity. They include T and B cells, which have distinct origins and functions. Mice without lymphocytes have significantly less atherosclerosis (Reardon et al. 2001). T cells in atherosclerotic plaques have a central role in the atherogenesis. Naïve T cells enter the bloodstream from thymus, and are recruited to plaques. They undergo activation, when antigens are presented to them by antigen-presenting cells, usually dendritic cells or macrophages. T cells in plaques, especially plaques of vulnerable phenotype, undergo clonal expansion, which suggests antigen-specific reactions in the lesion (Liuzzo et al. 2000). The putative antigens in atherosclerosis include ox-LDL, heat shock protein 60 and, as well as bacterial antigens from foreign microorganisms, such as *C. pneumoniae*. Most of the T cells in the lesions are $CD4^+$ T cells (regulatory or helper T cells, T_{reg} and T_H), but also $CD8^+$ T cells (cytotoxic T cells) are present. The T cell response is mainly pro-inflammatory T_H1-type. The T_H1 cells have a major role in the development of atherosclerotic lesions: they produce pro-inflammatory IFN-γ and activate macrophages. The depletion of T_H1 differentiation leads to reduced atherosclerosis in mice (Buono et al. 2005).

T cells are abundantly present in the intima of inflamed atherosclerotic lesions, whereas bone-marrow derived B cells are mainly localized in the adventitia below the atherosclerotic lesion. B cells are generally considered to be atheroprotective, but also contradictory findings have been obtained for some B cell subtypes. IgM antibodies produced by B-cell derived plasma cells can be particularly atheroprotective, such as anti-ox-LDL antibodies and anti-phosphorylcholine antibodies. (Hansson and Hermansson 2011)

Dendritic cells

Dendritic cells (DCs) are derived from blood monocytes (classical DCs) or lymphoid precursors (plasmacytoid DCs) and are present in atherosclerotic plaques, plaque-neighbouring lymph nodes and tertiary lymphoid tissues in the adventitia. In normal conditions, DCs participate in keeping up the immunological tolerance by suppressing T cells. In atherosclerosis they act as a mediator between innate and adaptive immunity. DCs are antigen-presenting cells, which internalize particles, such as ox-LDL, and present the fragments to lymphocytes in class II major histocompatibility complex (MHC) molecule resulting in immune response. (Zernecke 2015)

Mast cells

Mast cells are derived from myeloid precursor cells. In mice, they are present in plaques in relatively low numbers, but are abundant in the plaque-surrounding

adventitial tissue. In humans, however, mast cells are also abundant in the plaque intima. Mast cells are localized near plaque neovessels and might have a role in promoting the neovascularization and intraplaque hemorrhage by increasing the leakiness of neovessels. They contain neutral proteases, such as chymase and tryptase, in granules, and therefore might also contribute to plaque rupture by releasing the granule contents. Mast cells also produce pro-inflammatory cytokines, such as IFN-γ and IL-6, which further promotes their pro-inflammatory function. (Bot et al. 2015)

Neutrophils

In the acute inflammatory response, neutrophils are the first inflammatory cells to enter the tissue. Hyperlipidemia leads to increased numbers of neutrophils in blood and recruitment of neutrophils to lesions. They are mainly involved in the early phases of atherosclerosis. The neutrophil numbers in blood are correlated with plaque size, and early depletion of these cells reduces the plaque burden. (Drechsler et al. 2010; Weber and Noels 2011)

2.2.4 Pharmacological treatment of inflammation in atherosclerosis

The prevention and treatment of atherosclerosis has concentrated on lifestyle interventions affecting risk factors of atherosclerosis, as well as on lipid lowering and anti-thrombotic medication. Numerous lipid-lowering trials have established that reduction of cholesterol inhibits progression of atherosclerotic plaques and vascular events. Statins are proven to be efficient in lowering LDL cholesterol in a dose-dependent manner (Collins et al. 2004; Baigent et al. 2005; Nissen et al. 2005). Statins inhibit the enzyme 3-hydroxy-3-methyl-glutaryl-coenzyme A (HMG-CoA) reductase, which is involved in the cholesterol biosynthesis in hepatocytes. The HMG-CoA inhibition leads to increased expression of LDLR in hepatocytes, and therefore increased cellular LDL intake. Statins also have anti-inflammatory actions in addition to cholesterol lowering (Scalia et al. 2001; Schwartz et al. 2001). In addition to statins, other types of lipid-lowering drugs have also been utilized. Ezetimibe inhibits cholesterol absorption from the small intestine and lowers LDL in combination with statins (Shapiro and Fazio 2016). Fibrates or resins can also be utilized in statin-intolerant patients or in combination with statin. New biological drugs inhibiting the proprotein convertase subtilisin/kexin type-9 (PCSK9), evalocumab and alirocumab, have now emerged in the market. PCSK9 is involved in LDLR destruction in lysosomes, and inhibiting it leads to increased numbers of LDLRs on the cellular surface. This augments the cellular intake of LDL and thus lowers cholesterol levels. CETP inhibition with dalcetrapib or torcetrapib has been one approach to altering lipid profiles from LDL towards HDL, but large studies have recently failed to show reduction of cardiovascular events using these therapies (Barter et al. 2007; Schwartz et al. 2012). However, new CETP inhibitors are in clinical trials.

Despite efficient lipid-lowering therapies, atherosclerosis-related mortality remains high. Since inflammation is a key player in atherogenesis and increases the risk of plaque rupture, suppression of it could have plaque-stabilizing effects. This has been observed in clinical studies, where anti-inflammatory therapies for non-cardiac diseases have been beneficial also for the reduction of cardiovascular events. In recent years, the research in anti-atherosclerotic therapies has expanded from lipid lowering to anti-inflammatory treatments. Preclinical studies have shown beneficial effects of multiple anti-inflammatory therapies and clinical trials are ongoing based on the results. (Bäck and Hansson 2015)

Blocking of IL-1β by IL-1 receptor antagonist reduces lesion formation in $ApoE^{-/-}$ mice (Elhage et al. 1998) and modulation of IL-1β signaling diminishes neointimal formation in rat carotid denudation model (Roubille et al. 2014). A large clinical trial studying the effects of anti-IL-1β monoclonal antibody canakinumab on reducing recurrent cardiovascular events is ongoing (Canakinumab Anti-inflammatory Thrombosis Outcomes Study, CANTOS) (Ridker et al. 2011).

Treatment of atherosclerosis has also been experimented on with small-dose methotrexate. Methotrexate is a folic acid antagonist, which is utilized in cancer treatment and in smaller doses in treating systemic inflammatory diseases, such as rheumatoid arthritis. Several studies of rheumatoid arthritis patients have shown reduced risk of cardiovascular events in patients with methotrexate treatment (Westlake et al. 2010). Methotrexate treatment has atheroprotective effects, such as promotion of reverse cholesterol transport (Reiss et al. 2008) and reduction of lesion formation and macrophage content in rabbits (Bulgarelli et al. 2012; Bulgarelli et al. 2013). Methotrexate treatment in atherosclerotic patients without rheumatoid diseases is currently ongoing (Cardiovascular Inflammation Reduction Trial, CIRT). (Everett et al. 2013)

Reducing the lipid mediators of inflammation has also been studied for the treatment of atherosclerosis. 5-lipoxygenase inhibition with atreleuton and phospholipase A_2 inhibition with varespladib and darapladib have shown some positive effects in animal models, but in clinical studies these approaches have shown not to be effective (Vidal et al. 2007; Nicholls et al. 2014; White et al. 2014; Gaztanaga et al. 2015). Other approaches for reducing risk of acute coronary syndromes (ACS) via reducing inflammation include, for example, low-dose colchisine (Nidorf et al. 2013) and TNF-α blockade with etanercept or infliximab (Jacobsson et al. 2005), but these lack large-scale clinical studies as evidence. One potential future approach for attacking inflammation in atherosclerosis is vaccination against native or modified LDL, which is expected to be tested in clinical trials in the future (Shah et al. 2014).

2.3 Imaging of atherosclerosis

The *in vivo* imaging of blood vessels was studied already in the 1920s, and the coronary angiography method was invented and developed in the 1950s and

1960s (Mueller and Sanborn 1995). Today, *in vivo* imaging of atherosclerosis is utilized in clinical practice and as a research tool. The *in vivo* imaging methods can be divided into two categories: anatomical and functional. Anatomical imaging methods aim to visualize the physical existence and structure of the lesions; these are useful in clinical diagnostics. Functional imaging methods aim to detect the biological processes, and they have applications as research tools. They help to increase knowledge about disease mechanisms and are valuable for example in assessing therapy responses. Functional imaging is often carried out by means of molecular imaging, which is defined as "visualization, characterization, and measurement of biological processes at the molecular and cellular levels in humans and other living systems" (Mankoff 2007). Functional imaging modalities are often accompanied with anatomical imaging to gain information on the localization of the visualized function. These combined imaging methods are referred to as multimodality imaging.

2.3.1 Anatomical imaging

Invasive angiography is based on the radio-opaque effect of intra-arterially injected iodinated contrast agent visualized by X-rays. This method has been traditionally considered as the "gold standard" of imaging of vascular disease. It provides a good spatial resolution and a very precise knowledge of the presence of stenosis, but on the other hand, is an invasive procedure with risks and does not give information about the vessel components beyond the luminal narrowing. Therefore, its use is generally limited to selected symptomatic high-risk patients and it is often accompanied by opening of the coronary vessel by percutaneous coronary intervention. (Aikawa 2015; Tarkin et al. 2016)

X-ray computed tomography (CT) angiography is a non-invasive method for visualizing the vessel lumen and atherosclerotic lesions. It is based on a rotating X-ray source and detector, and the data from several projections can be reconstructed to images of multiple planes. Vessels are visualized in CT with iodinated contrast agent. The spatial resolution of CT angiography is lower than that of invasive angiography, but it can differentiate soft and calcified lesions and therefore can also be utilized in assessing e.g. the amount of calcium burden in the vessels (calcium score). Measurement of calcium score is useful in negative predictive value, i.e. if the coronary arteries are free of calcium, the risk of cardiovascular events is low. However, it is not the optimal method for following disease progression, since the calcification process tends to continue despite efficient risk-lowering therapy, such as statins (McEvoy et al. 2010). CT angiography can also be combined with myocardial perfusion imaging to assess whether the lesions limit blood flow to myocardial tissue. (Aikawa 2015; Tarkin et al. 2016)

Magnetic resonance imaging (MRI) is based on the magnetic properties of hydrogen atoms. The magnetic field of the MRI aligns the magnetic dipoles (spins) of atoms and radiofrequency pulses are applied to change the polarization. After the pulse, the spins return back to the orientation of the

magnetic field, and this relaxation can be detected. Non-invasive angiography can be performed with MRI. It also enables the detection of plaque characteristics, such as differentiating lipid-rich, fibrotic and calcified lesions in larger vessels, such as aorta and carotid arteries, using gadolinium contrast agents. (Aikawa 2015; Tarkin et al. 2016)

Ultrasound is based on high frequency sound waves and their echoes and diffractions from the tissue. Conventional ultrasound can also be utilized in assessing atherosclerotic lesions. Mainly it is utilized in the assessment of intima-media thickness, most commonly in carotid arteries. Intima-media thickness measures the thickness of arterial wall, including the intimal and medial layers. This method is useful because of its availability and non-invasiveness, as well as the fact that it does not predispose the patient to ionizing radiation or contrast agents. The main limitation is the low tissue penetration, which limits its use to only superficial vessels. (Ehlgen et al. 2015)

More modernized versions of arterial imaging include intravascular ultrasound (IVUS) and optical coherence tomography (OCT). IVUS utilizes an intravascular ultrasound catheter. It can detect plaques and has high spatial resolution, and the detection of lesions is far more detailed than conventional ultrasound or angiography. IVUS can also be combined with virtual histology to enable differentiation of necrotic core, fibrous and fibrofatty plaques, as well as calcium. OCT utilizes near-infrared light and results in a detailed view of the vessel wall structure. The spatial resolution of this method is particularly good, but on the other hand, the tissue penetration is only up to 3 mm which often makes it impossible to image the whole plaque. The other disadvantage is the need for blood clearance during the acquisition, but this can be overcome by advanced imaging technologies. OCT is a good and precise method for detecting plaque characteristics, and has shown to have the capacity of visualizing immune cells. (Aikawa 2015; Tarkin et al. 2016)

2.3.2 Targeted molecular imaging

Targeted molecular imaging utilizes molecules as probes to detect biological functions. Both endogenous molecules and exogenous probes can be molecular imaging agents, and the imaging can be performed with multiple modalities. In general, the molecular imaging is based on target-specific ligands accompanied with a signal-forming element which can be detected by the respective imaging modality. The most commonly clinically-utilized molecular imaging modalities include MRI, CT, ultrasound, PET and single-photon emission computed tomography (SPECT). These methods would provide information beyond plaque structure, for example on the inflammation. In pre-clinical models, imaging with fluorescence and bioluminescence-based methods as well as photoacoustic imaging are emerging, but will not be discussed in this thesis.

Nanoparticle imaging with MRI, CT and ultrasound

MRI, CT and ultrasound can all be utilized in nanoparticle imaging. Nanoparticles are 10 to 100 nm diameter particles which can comprise very different molecules, such as liposomes, lipoproteins, dendrimers and metals. They can be designed so that they are useful in multiple imaging platforms, and they can also be utilized in drug delivery.

In molecular imaging of atherosclerosis with MRI, the most commonly-utilized imaging agents include small and ultra-small paramagnetic particles of iron oxide (SPIO and USPIO) as well as gadolinium-based liposomes, micelles and lipoproteins. USPIO signal is found in macrophage-rich areas of lesions, and the effect of treatment can be seen with this imaging method (Ruehm et al. 2001; Trivedi et al. 2006; Tang et al. 2009). However, the USPIO uptake is greater in M2 macrophages than in M1 macrophages, which might make it less attractive for imaging atherosclerotic plaque inflammation (Satomi et al. 2013). CT imaging with nanoparticles is a less-studied field, but has been shown to be feasible. In a couple of studies, HDL nanoparticles have been labelled with contrast agents, such as gold or iodine, to be visualized with CT (Hyafil et al. 2007; Skajaa et al. 2010; Cormode et al. 2010).

Ultrasound signal can be enhanced with targeted microbubbles or other nanoscale particles. Microbubbles are intravascular tracers, which are composed of inert gas in a shell. The shell can be composed of e.g. phospholipids, albumin or biodegradable polymers. Their diameter is 1-4 μm. Microbubbles are suitable for imaging of inflammation-associated targets in the vascular wall, such as integrins or adhesion molecules (Villanueva et al. 1998; Villanueva and Wagner 2008; Lindner 2009).

Nuclear imaging

SPECT is a non-invasive and sensitive imaging method which has multiple applications in medical imaging. SPECT is based on gamma-ray emitting radionuclides, such as ^{99m}Tc, ^{111}In or ^{123}I. The SPECT camera has a set of rotating detectors which obtain data of emitted gamma rays from several projections. The data can be reconstructed into three-dimensional images. SPECT tracers are generally relatively long-lived (physical half-life of several days), which means that production does not have to be on-site. Clinical SPECT scanners are widely available, which makes this modality attractive for use. However, the spatial resolution of this method in clinical scanners is limited (7-15 mm), which compromises imaging of the lesions of small size. SPECT is usually coupled with an anatomical imaging modality, most often CT, which is utilized as an anatomical reference as well as for attenuation correction, i.e. to take into account the soft tissues and bone attenuating the penetration of gamma rays to the detectors. (Aikawa 2015)

PET is a very sensitive molecular imaging method, which is based on positron-emitting radionuclides. When a positron is emitted, it goes forward through tissue

until it encounters an electron, which leads to annihilation and formation of two 511 kiloelectron volt gamma rays in opposite directions. The PET camera has ring-like detector systems, which detect the gamma rays on opposite sides. The data from detectors can be transferred to three-dimensional images via computational reconstruction algorithms. The most commonly utilized PET radionuclides include ^{18}F (physical half-life 110 min), ^{11}C (20 min) and ^{68}Ga (68 min). Like SPECT, PET is also usually combined with CT, and PET/MRI is also becoming more and more common. The availability of PET tracers is more limited because of their short physical half-life, and the PET cameras are not as widely available as SPECT devices. However, the spatial resolution of PET is higher than with SPECT, in clinical cameras around 3-5 mm, which makes it a more attractive method for imaging atherosclerotic plaques. The advantages of PET over other imaging modalities include also high sensitivity and possibility to quantitate the data. (Aikawa 2015)

2.4 PET imaging of inflammation in atherosclerosis

The field of PET imaging in atherosclerosis has been very active in the last decade. The investigations vary from testing new potential PET tracers in cell and animal models to large-scale clinical studies, and from simple proof-of-concept studies to thorough evaluations. Recently, the focus has moved from testing new radiopharmaceuticals to the direction of association with drug development and gaining more understanding of the disease pathology. There are many potential targets for imaging atherosclerotic plaques. For example, the imaging of hypoxia (Silvola et al. 2011a; Mateo et al. 2014) and thrombosis (Elmaleh et al. 2006) have been studied and have shown promise for the imaging of high-risk plaques. Imaging of plaque microcalcifications with sodium fluoride (^{18}F-NaF) has also gained a lot of attention in the last five years (Joshi et al. 2014; Irkle et al. 2015). However, the most studied imaging target in atherosclerosis PET imaging is the inflammatory process in the plaques. Inflammation is crucial in the development of atherosclerosis and is related to higher risk of plaque rupture, which makes it an attractive target.

2.4.1 Technical challenges and quantitation in vascular PET imaging

When imaging small targets, CT or MRI as an anatomical reference and for attenuation correction is essential. The development of multimodality devices, such as PET/CT and PET/MRI, has increased the use of PET in vascular imaging. Despite these advances, spatial resolution remains a major limitation of PET. This is a major issue especially in the imaging of small targets, even when using the ^{18}F isotope with favorable physical properties for imaging (low positron energy and positron range, resulting in better resolution). When the targets are smaller than the voxel (three-dimensional pixel) size, they are subject to partial volume effects, resulting in underestimation in measured radioactivity. Surrounding radioactivity – in the case of vascular imaging, from the blood – also affects the imaging. Therefore, the aim in vascular imaging is to yield high

uptake in the lesions and low remaining radioactivity in the blood pool. The constant motion of the heart from breathing and the cardiac cycle affects the imaging of coronary vessels and needs specific motion correction methods. Also, the radioactivity in surrounding tissues such as myocardium, lungs and liver, must be taken into account when analyzing the vascular uptake. (Bucerius et al. 2016)

There are multiple methods for the quantitation of PET tracer uptake in vascular wall. Standardized uptake value (SUV) is the most commonly utilized measure in PET imaging. Both mean and maximum SUV values can be evaluated. SUV is calculated by formula: (radioactivity in tissue / tissue volume) / (injected radioactivity / patient weight). However, particularly in vascular imaging, target-to-background ratio (TBR) is also used. It can be calculated as the ratio of SUV in target tissue (lesion) and SUV in background (blood). TBR_{mean} refers to the use of mean SUVs in both of the measurements, whereas in TBR_{max} the maximum SUV in lesion and mean SUV in blood are utilized. In addition to differences in quantitation methods, variability in measurements comes also from the choice of areas to analyze: whether to measure the whole vessel or only the most diseased segment. The timing of imaging and the pre-study conditions, such as fasting or high-fat meal, may also affect the tracer uptake.

In preclinical studies, radiation safety applies primary to the researchers, whereas when the imaging procedures are applied to man, the radiation dose for the imaging subject must be taken into account. Therefore, the numbers of imaging sessions and tracer doses have limitations, especially in studies with repeated imaging.

2.4.2 ^{18}F-FDG PET imaging

^{18}F-FDG is a glucose analogue and the most commonly-utilized PET tracer. ^{18}F-FDG is taken up in cells via glucose transporters and phosphorylated by hexokinase to ^{18}F-FDG-6-phosphate. Unlike glucose-6-phosphate, ^{18}F-FDG-6-phosphate cannot be further metabolized, and it is trapped in cells. The cellular uptake of ^{18}F-FDG is directly associated with the glucose utilization and glycolytic energy metabolism of the cells. The first prospective study to show uptake of ^{18}F-FDG in atherosclerotic lesions was published by Rudd and colleagues in 2002. Uptake was observed in symptomatic carotid plaque, and the finding was confirmed by autoradiography (ARG) showing co-localization of tritiated deoxyglucose and macrophages (Rudd et al. 2002). Already before that, a retrospective study showed the association of ^{18}F-FDG uptake in vessels and cardiovascular risk factor (Yun et al. 2002). ^{18}F-FDG uptake has been shown to correlate with lesion macrophages in animal models (Ogawa et al. 2004; Zhang et al. 2006; Hyafil et al. 2009; Davies et al. 2010; Hag et al. 2012; Wenning et al. 2014) and in patients undergoing ^{18}F-FDG PET/CT imaging and endarterectomy for histological correlations (Tawakol et al. 2006; Jezovnik et al. 2014; Liu et al. 2016). Increased vascular ^{18}F-FDG uptake has been linked to diabetes and metabolic syndrome (Tahara et al. 2007; Bucerius et al. 2012) and even to risk of

future cardiovascular events (Rominger et al. 2009; Figueroa et al. 2013). ^{18}F-FDG imaging of atherosclerotic plaques can be seen as the "gold standard" to assess the inflammation *in vivo*, although the direct mechanisms of intake in inflammatory cells need further characterization.

Imaging of atherosclerotic plaque inflammation provides an interesting new tool to measure the effects of therapies. ^{18}F-FDG is a sensitive marker of plaque inflammation, and several studies have proven its usability in assessing therapy responses, both in pre-clinical and clinical settings (Table 2). Imaging of atherosclerosis with ^{18}F-FDG in has shown high reproducibility, which even more improves its value for assessing therapy responses (Rudd et al. 2007; Rudd et al. 2008). Therefore, ^{18}F-FDG imaging is today commonly used in clinical trials as a surrogate marker for plaque inflammation. Proof-of-concept studies have shown the effects of statins in lowering ^{18}F-FDG uptake (Tahara et al. 2006; Ishii et al. 2010; Wu et al. 2012; Tawakol et al. 2013; Watanabe et al. 2015), and trials for anti-inflammatory therapies for atherosclerosis often utilize this method (Fayad et al. 2011; Gaztanaga et al. 2015).

Despite the advantages of ^{18}F-FDG, such as high sensitivity and reproducibility, it also has some disadvantages and limitations. Not all studies have shown uptake of ^{18}F-FDG in atherosclerotic arteries (Laurberg et al. 2007) or correlation to macrophages (Myers et al. 2012). In addition, ^{18}F-FDG is not specific for inflammation, and it has high physiological uptake in the myocardium. This limits coronary artery imaging, although it is possible to diminish it by fasting or with low-carbohydrate diet. High blood glucose (> 7mmol/l) can also diminish the uptake in vessels (Bucerius et al. 2016) and therefore imaging in diabetic patients might be compromised. There is also debate on the factors affecting ^{18}F-FDG uptake in plaque macrophages. Macrophages, as well as other myeloid cells, have high glycolytic energy metabolism, which is even more up-regulated in cellular activation. The glucose utilization of macrophages is, however, highly dependent on their polarization. According to the current paradigm, the M1-polarized macrophages, especially those induced by LPS, have higher glucose uptake and consumption than M2-polarized macrophages (Rodríguez-Prados et al. 2010; Satomi et al. 2013; Tavakoli et al. 2013). There are, however, some studies suggesting that hypoxia might be more prominent determinant of macrophage glucose utilization than the polarization state (Folco et al. 2011; Tawakol et al. 2015). For these reasons, new, more specific PET tracers would be needed.

Table 2. The effects of different pharmacological treatments to ^{18}F-FDG uptake in arteries.

Treatment and duration	Drug type or mechanism of action	Experimental setting/ patient group	Quantitation of tracer uptake	Drug effect on atherosclerosis and biomarkers	Drug effect on tracer uptake	Reference
Studies in animal models						
Atorvastatin 3 months	HMG-CoA reductase inhibitor	Rabbit (NZW, balloon injury)	SUV_{max}; SUV_{mean}	Mφ ↓, ApoB ↓, oxPL ↔, SMA ↔, neovascularization ↔, vessel wall area ↔	↔	(Vucic et al. 2012)
Atorvastatin+ diet 6 months	HMG-CoA reductase inhibitor	Rabbit (NZW, balloon injury)	SUV_{mean}	Mφ ↓	↓ 39 %	(Millon et al. 2013)
Prednisolone liposome Single dose, imaging at day 7	Glucocorticoid	Rabbit (NZW, balloon injury)	SUV_{mean}	Mφ ↓, MCP-1 ↓	↓ ~30 %	(Lobatto et al. 2010)
Pioglitazone 3 months	Thiazolidinedione, PPARγ agonist	Rabbit (NZW, balloon injury)	SUV_{max}; SUV_{mean}	Mφ ↓, ApoB ↔, oxPL ↓, SMA ↔, neovascularization ↔, vessel wall area ↔	↔	(Vucic et al. 2011)
Probucol 6 months	Antioxidant	Rabbit (Watanabe)	SUV	Mφ ↓	↓ ~30 %	(Ogawa et al. 2006)
R211945 3 months	LXR agonist	Rabbit (NZW, balloon injury)	SUV_{max}; SUV_{mean}	Mφ ↓, ApoB ↓, oxPL ↓, SMA ↔, neovascularization ↔, vessel wall area ↔	↓ ~15 %	(Vucic et al. 2012)
Clinical studies						
Simvastatin 3 months	HMG-CoA reductase inhibitor	Voluntary participants with ^{18}F-FDG uptake in arteries	SUV	LDL ↓, HDL ↑	↓ ~10 %	(Tahara et al. 2006)
Atorvastatin 6 months	HMG-CoA reductase inhibitor	Patients with stable angina and no current lipid treatment	TBR_{mean}	LDL ↓, MDA-LDL ↓, hsCRP↓, TG↓	↓ ~9 %	(Ishii et al. 2010)
Atorvastatin 3 months	HMG-CoA reductase inhibitor	Patients with history of atherosclerosis	TBR_{mean}; TBR_{max}	LDL ↓, hsCRP↓, TG↓, FABP4 ↓, MMP-9 ↓, follistatin ↓, MCP-1 ↓	↓ 20 %	(Wu et al. 2012)
Atorvastatin 3 months	HMG-CoA reductase inhibitor	Patients with history of atherosclerosis, T2DM, obesity or high LDL cholesterol	TBR_{max}	LDL ↓, CRP↓, TG↓	↓ 14 % high-dose; ↔ low-dose	(Tawakol et al. 2013)
Pitavastatin 6 months	HMG-CoA reductase inhibitor	Patients with hyperlipidemia, high risk of atherosclerosis, atrial fibrillation or valvular disease	TBR_{max}	LDL ↓, HDL ↔, hsCRP ↔, TG ↔, IMT ↓	↓ 19 %	(Watanabe et al. 2015)
Pravastatin 6 months	HMG-CoA reductase inhibitor	Patients with hyperlipidemia, high risk of atherosclerosis, atrial fibrillation or valvular disease	TBR_{max}	LDL ↓, HDL ↔, hsCRP ↔, TG ↔, IMT ↑	↔	(Watanabe et al. 2015)
Pioglitazone 4 months	Thiazolidinedione, PPARγ agonist	Patients with T2DM or IGT and atherosclerosis	TBR	hsCRP↓, HDL ↑, LDL ↔, TG ↔	↓ 10 %	(Mizoguchi et al. 2011)
Glimepiride 4 months	Sulfonylurea	Patients with T2DM or IGT and atherosclerosis	TBR	hsCRP↑, HDL ↔, LDL ↔, TG ↔	↔	(Mizoguchi et al. 2011)
Dalcetrapib 6/24 months	CETP inhibitor	Patients with known CAD or high risk for CAD	TBR	hsCRP↑, HDL ↑, LDL ↔, TG ↔, lesion area ↓ (vs. placebo)	↔ (↓ 7 % vs. placebo)	(Fayad et al. 2011)
Losmapimod 3 months	p38 mitogen-activated protein kinase inhibitor	Patients with history of atherosclerosis and on statin therapy	TBR	Low dose: hsCRP ↔ High dose: hsCRP ↓	↓ 7 %	(Elkhawad et al. 2012)
VIA-2291 6 months (addition to statin)	5-lipoxygenase inhibitor	Patients with ACS 1-3 months prior to randomization	TBR_{mean}; TBR_{max}	↔	↔	(Gaztanaga et al. 2015)

2.4.3 PET imaging with other tracers

Besides ^{18}F-FDG, a number of PET tracers have been evaluated for the imaging of inflammation in atherosclerotic lesions. Commonly, the tracers are adapted from other fields, such as oncology, and are not developed specifically for vascular imaging purposes. The PET tracers for imaging of plaque inflammation are presented in Table 3.

Tracers of choline metabolism

Choline is an essential nutrient which is needed in the formation of phospholipids and neurotransmitter acetylcholine. Choline metabolism is altered in cancer cells, and imaging of prostate and breast cancers have been studied with radiolabelled choline analogues (DeGrado et al. 2001). In addition to cancer cells, increased uptake of choline analogues has been observed in inflammatory conditions, where the macrophages take up choline. Increased uptake of choline analogues has also been observed in atherosclerosis. In pre-clinical models, uptake of ^{11}C-choline and ^{18}F-fluoromethylcholine (^{18}F-FMCH) was seen in macrophage-rich atherosclerotic lesions (Matter et al. 2006; Laitinen et al. 2010). Only a few clinical studies of atherosclerosis imaging with choline analogues have been performed. Bucerius and colleagues showed uptake of ^{18}F-FMCH in vessel wall alterations (Bucerius et al. 2008). In another clinical study, uptake of ^{11}C-choline was seen in atherosclerotic plaques, mainly in non-calcified lesions, and its uptake in myocardium was lower than that of ^{18}F-FDG (Kato et al. 2009). However, the sample sizes in these studies were limited, and further studies are needed to confirm the value of choline analogues in the imaging of inflammation in atherosclerosis.

TSPO-targeting tracers

18 kDa translocator protein (TSPO), formerly called peripheral benzodiazepine receptor, is a mitochondrial membrane protein involved in numerous cellular functions. TSPO is highly expressed in cells of monocytic lineage, and it has been evaluated as a drug target for enhancing cholesterol efflux from macrophages (Lecanu et al. 2013; Taylor et al. 2014). TSPO-targeted imaging has been mainly studied in neuroinflammatory diseases, where the activated glial cells overexpress TSPO. Imaging of vascular inflammation has also been studied with TSPO-targeting tracer ^{11}C-PK11195, mainly in imaging vasculitis (Pugliese et al. 2010; Lamare et al. 2011). In an autoradiographic study, increased uptake of ^{3}H-PK11195 was correlated with macrophages in human carotid plaques (Fujimura et al. 2008). *In vivo* imaging of atherosclerotic plaque inflammation with ^{11}C-PK11195 has been shown to be feasible (Gaemperli et al. 2012). New ^{18}F-labelled TSPO ligands have been developed, and they might overcome the limitations of ^{11}C-PK11195, such as the short physical half-life and low target-to-background ratio (Chauveau et al. 2009).

Tracers targeting somatostatin receptors

Somatostatin receptors (SSTR) are overexpressed in neuroendocrine tumors as well as in activated macrophages. Although the focus in SSTR imaging has been in oncology, some studies on atherosclerosis imaging with SSTR-2-targeting tracer ^{68}Ga-DOTATATE have been performed. In a preclinical ApoE$^{-/-}$ model, uptake of ^{68}Ga-DOTATATE was correlated with macrophage-rich areas (Li et al. 2013). Uptake of the same tracer in atherosclerotic vessels has also been observed in retrospective clinical studies in cancer patients. Rominger and colleagues detected uptake in coronary vessels, whereas the study by Li and colleagues focused on large arteries (carotid, aortic and iliac). ^{68}Ga-DOTATATE uptake correlated with calcifications as well as with cardiovascular risk factors, such as age and hypertension (Rominger et al. 2010; Li et al. 2012). Similar results were also observed with ^{64}Cu-DOTATATE (Malmberg et al. 2015). In a prospective study in patients undergoing ^{64}Cu-DOTATATE imaging and endarterectomy, tracer uptake was detected in symptomatic carotid artery and the uptake correlated with macrophage markers CD68 and CD163 (Pedersen et al. 2015). Based on these studies, somatostatin receptors are a promising target for imaging macrophage infiltration in atherosclerotic lesions.

Tracers targeting other macrophage surface molecules

Mannose receptors are expressed especially in M2 polarized macrophages. ^{18}F-fluorodeoxymannose (^{18}F-FDM) is taken up in cells via GLUTs, but also via MR. Therefore, ^{18}F-FDM might show higher specificity by targeting especially M2 macrophages. ^{18}F-FDM showed high uptake in macrophages *in vitro* and similar imaging properties as ^{18}F-FDG in rabbit model of atherosclerosis (Tahara et al. 2014).

Cellular surface protein p32 is highly expressed in tumor cells and tumor-associated macrophages. p32 protein is also present in macrophages in atherosclerotic plaques, and has been targeted for imaging with ^{18}F- and ^{64}Cu-labelled peptides. ^{18}F-FBA-LyP-1 showed increased uptake in the aortas of ApoE$^{-/-}$ mice compared to healthy controls. However, the remaining tracer radioactivity in blood was almost as high as in the aorta (Hamzah et al. 2011). ^{64}Cu-LyP1 dendrimer showed better aorta-to-blood ratio at the same 3-hour time point in the same mouse model, but the study lacked comparison to healthy controls (Seo et al. 2014).

Viral macrophage inflammatory protein II targets several chemokine receptors, and has been labelled with ^{64}Cu for imaging. The tracer ^{64}Cu-DOTA-vMIP-II has been studied as a single molecule (Liu et al. 2013) and as a comb-like nanoparticle (Luehmann et al. 2016), and it has shown increased uptake in injury-associated atherosclerosis compared to a non-injured site. Blood clearance was also rapid. ^{64}Cu-DOTA-DAPTA-comb targets only chemokine receptor 5, which is expressed in T cells and macrophages (Luehmann et al. 2014). The tracer shows increasing uptake in the lesion area over time, but the radioactivity in blood circulation remains high even at 48 hours post-injection.

Table 3. Tracers for imaging inflammation in atherosclerosis.

Target	Tracer	Tracer type	Species and strain	Vascular bed	References
Metabolic activity					
Glucose metabolism	^{18}F-FDG	Small molecule	Mouse (ApoE$^{-/-}$; LDLR$^{-/-}$ApoB$^{100/100}$)	Aorta	(Laitinen et al. 2006; Silvola et al. 2011b; Hag et al. 2012)
			Rabbit (Watanabe)	Aorta	(Ogawa et al. 2004; Ishino et al. 2014)
			Rabbit (NZW, balloon injury)	Aorta	(Tawakol et al. 2005; Zhang et al. 2006; Hyafil et al. 2009; Davies et al. 2010)
			Swine (STZ-diabetes + high-fat diet)	Coronary	(Tarkia et al. 2015)
Phospholipid metabolism	^{18}F-FMCH	Small molecule	Mouse (ApoE$^{-/-}$)	Aorta	(Matter et al. 2006)
	^{11}C-Choline	Small molecule	Mouse (LDLR$^{-/-}$ ApoB$^{100/100}$)	Aorta	(Laitinen et al. 2010)
Cell proliferation	^{18}F-FLT	Nucleotide analogue	Mouse (ApoE$^{-/-}$), rabbit (NZW, wire injury), human	Aorta, carotid	(Ye et al. 2015)
Macrophage phagocytosis	^{64}Cu-TNP	Nanoparticle	Mouse (ApoE$^{-/-}$)	Aorta	(Nahrendorf et al. 2008)
Macrophage surface proteins					
Translocator protein	^{11}C-PK11195	Small molecule	Mouse (LDLR$^{-/-}$ ApoB$^{100/100}$)	Aorta	(Laitinen et al. 2009a)
Somatostatin receptors	^{68}Ga-DOTATATE	Peptide	Mouse (ApoE$^{-/-}$)	Aorta	(Li et al. 2013)
Mannose receptor	^{18}F-FDM	Small molecule	Rabbit (NZW, balloon injury)	Aorta	(Tahara et al. 2014)
p32 protein	^{18}F-FBA-LyP-1	Peptide	Mouse (ApoE$^{-/-}$)	Aorta	(Hamzah et al. 2011)
	^{64}Cu-LyP1 dendrimer	Peptide dendrimer	Mouse (ApoE$^{-/-}$)	Aorta	(Seo et al. 2014)
Chemokine receptors	^{64}Cu-DOTA-vMIP-II	Peptide nanoparticle	Mouse (ApoE$^{-/-}$, wire injury)	Femoral	(Liu et al. 2013; Luehmann et al. 2016)
Chemokine receptor 5	^{64}Cu-DOTA-DAPTA-comb	Peptide nanoparticle	Mouse (ApoE$^{-/-}$, wire injury)	Femoral	(Luehmann et al. 2014)
Integrins and adhesion molecules					
αvβ3-integrin	^{18}F-Flotegatide	Peptide	Mouse (ApoE$^{-/-}$)	Aorta	(Su et al. 2014)
	^{18}F-Galacto-RGD	Peptide	Mouse (LDLR$^{-/-}$ ApoB$^{100/100}$)	Aorta	(Laitinen et al. 2009b; Saraste et al. 2012)
	^{68}Ga-NOTA-RGD	Peptide	Mouse (ApoE$^{-/-}$)	Aorta	(Paeng et al. 2013)
	^{68}Ga-DOTA-RGD	Peptide	Mouse (LDLR$^{-/-}$ ApoB$^{100/100}$)	Aorta	(Haukkala et al. 2009)
VCAM-1	^{18}F-4V	Peptide	Mouse (ApoE$^{-/-}$)	Aorta	(Nahrendorf et al. 2009)
	^{18}F-FB-anti-VCAM-1 Nb	Nanobody	Mouse (ApoE$^{-/-}$)	Aorta	(Bala et al. 2016)
P-selectin	^{64}Cu-DOTA-anti-P-selectin mAb	Monoclonal antibody	Mouse (LDLR$^{-/-}$)	Aorta	(Nakamura et al. 2013)

Tracers targeting integrins and adhesion molecules

Integrins are molecules associated with cell-cell-interactions. $\alpha_v\beta_3$-integrins are present in endothelial cells as well as in macrophages, and therefore they could provide a target for imaging both inflammation and neovascularization (Brooks et al. 1994; Hoshiga et al. 1995; Antonov et al. 2004). $\alpha_v\beta_3$-integrin targeting tracers contain the RGD (arginine-glycine-aspartate) motif, which binds to the integrin. RGD tracers have been studied mainly in cancer imaging, since many

tumors overexpress $\alpha_v\beta_3$-integrins. However, $\alpha_v\beta_3$-integrin-targeting PET tracers ^{18}F-Galacto-RGD and ^{68}Ga-NOTA-RGD been shown to be feasible in detecting inflamed atherosclerotic plaques in mouse model as well as in human carotid arteries (Laitinen et al. 2009b; Paeng et al. 2013; Beer et al. 2014). ^{18}F-Galacto-RGD showed uptake in stenotic areas of human carotid arteries and the uptake correlated with the expression of $\alpha_v\beta_3$-integrin. The tracer uptake, however, did not show significant correlation to macrophages or endothelial cells. ^{68}Ga-NOTA-RGD also showed uptake in human atherosclerotic arteries, but low spatial resolution limited the imaging, compared to ^{18}F-FDG (Paeng et al. 2013). The value of $\alpha_v\beta_3$–targeted PET imaging in atherosclerotic plaque imaging remains to be studied further.

Adhesion molecules mediate the interactions between endothelial cells and cells in the circulation. They are up-regulated in inflammation, and are therefore a possible target for imaging. VCAM-1-targeting tracers ^{18}F-4V and ^{18}F-FB-anti-VCAM-1 nanobody have shown promising results. ^{18}F-4V showed uptake in plaques in ApoE$^{-/-}$ mice, and the uptake correlated with VCAM-1 expression, and was diminished with atorvastatin treatment (Nahrendorf et al. 2009). ^{18}F-FB-anti-VCAM-1nanobody showed specific uptake in ApoE$^{-/-}$ mouse aortas and the degree of uptake was associated with disease severity (Bala et al. 2016). Another adhesion molecule, P-selectin, has been targeted for imaging with monoclonal antibody (^{64}Cu-DOTA-anti-P-selectin mAb). The tracer showed increased uptake in LDLR$^{-/-}$ mice fed with high-fat diet, compared to chow-fed mice of the same strain, but the study lacked the analysis of P-selectin expression in these mice (Nakamura et al. 2013).

Macrophage proliferation and phagocytosis

It was long considered that macrophages do not proliferate, and the only source of new macrophages in atherosclerotic plaques are the tissue-penetrating blood monocytes. Only recently has it been shown that macrophages do proliferate in atherosclerotic lesions and the proliferation is actually the predominant source of lesion macrophages (Robbins et al. 2013). The proliferation process in atherosclerotic lesions has been targeted with thymidine analogue ^{18}F-FLT (Ye et al. 2015). The tracer showed increased uptake in atherosclerotic ApoE$^{-/-}$ aortas, compared to healthy ones, although the SUV values in aortas were relatively low. Similar results were also observed in rabbits. The uptake also showed relatively weak correlation with ^{18}F-FDG uptake. Elevated ^{18}F-FLT accumulation was also observed in aorta and carotid arteries in patients with high risk of atherosclerosis, compared to subjects with low risk score.

The macrophage phagocytosis has also been studied as imaging target. Dextran-coated nanoparticle tracer, ^{64}Cu-TNP, is internalized by macrophages and can be visualized with *in vivo* PET in ApoE$^{-/-}$ mice. The uptake of ^{64}Cu-TNP was shown to be even higher than that of ^{18}F-FDG. The tracer contains also iron oxide core and fluorescent reporter, and it can therefore be utilized in imaging also with other modalities. (Nahrendorf et al. 2008)

3 AIMS OF THE STUDY

The purpose of this study was to evaluate macrophage-targeting PET tracers (Figure 2) for the imaging of inflammation in atherosclerosis in hypercholesterolemic mouse models. Another aim was to study the effects of interventions on plaque inflammation by utilizing an established tracer, ^{18}F-FDG.

The specific aims of this study were:

1. To assess the feasibility of somatostatin receptor-targeting PET tracers in detecting atherosclerotic plaque inflammation.
2. To investigate the uptake of ^{18}F-FMCH into inflamed atherosclerotic plaques in mice with or without type 2 diabetes, in comparison to ^{18}F-FDG.
3. To evaluate 18-kDa translocator protein-targeting tracer ^{18}F-FEMPA in detecting atherosclerotic plaque inflammation.
4. To study the effects of atorvastatin and diet interventions on aortic inflammation and ^{18}F-FDG uptake in LDLR$^{-/-}$ApoB$^{100/100}$ mice.

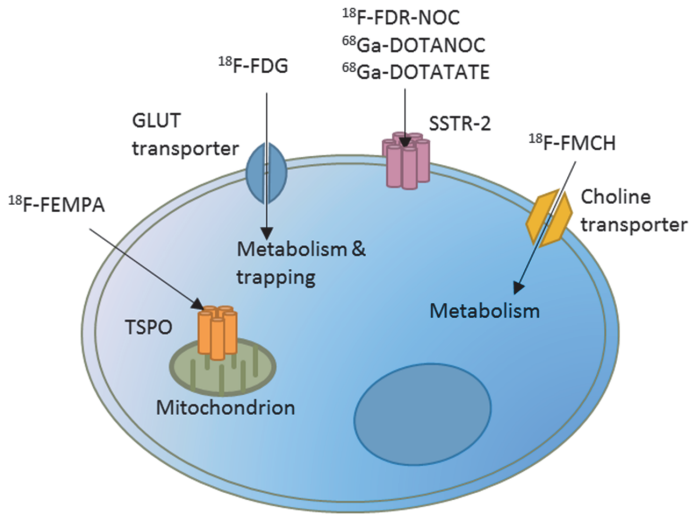

Figure 2. The targets of the studied tracers in macrophage cells. SSTR-2: Somatostatin receptor type 2, GLUT: glucose transporter, TSPO: 18-kDa translocator protein.

4 MATERIALS AND METHODS

4.1 Experimental animals

Two strains of hypercholesterolemic mice were utilized in the studies: LDLR$^{-/-}$ApoB$^{100/100}$ (Jackson Laboratories, Bar Harbor, ME, USA) (Powell-Braxton et al. 1998) and IGF-II/LDLR$^{-/-}$ApoB$^{100/100}$ (A.I. Virtanen Institute of Molecular Sciences, University of Eastern Finland, Kuopio, Finland) (Heinonen et al. 2007). The mice were fed with high-fat diet (TD.88137 Adjusted Calories Diet, Harlan Teklad, 42 % of calories from fat, 0.2 % total cholesterol, no sodium cholate, Harlan Laboratories, Madison, WI, USA) in order to accelerate the development of atherosclerosis. Healthy C57BL/6N mice were utilized as control animals, and they were fed normal chow diet (CRM [E], product code 801730, 9.1 % of calories from fat, Special Diet Services, Essex, United Kingdom). The C57BL/6N mouse strain was chosen for control, since both the hypercholesterolemic strains are cross-bred to C57BL/6N background. The numbers of animals in each study are listed in Table 4.

The mice were bred and housed in standardized conditions in University of Turku Central Animal Laboratory with a 12h/12h dark/light cycle and they had access to water and food *ad libitum*. All of the animal experiments were performed in accordance with the relevant European Union Directive and approved by Regional State Administrative Agency for Southern Finland (Licence numbers ESLH-2009-06012/Ym-23, ESAVI/1583/04.10.03/2012 and ESAVI/2163/04.10.07/2015).

4.2 General study design

The macrophage-targeting PET tracers were evaluated in mouse models of atherosclerosis. The tracer distribution and uptake in aorta was analyzed by *in vivo* PET/CT imaging, *ex vivo* biodistribution and autoradiography (ARG) after intravenous (i.v.) tracer injection to mouse tail vein. The *in vivo* stability of the tracers was also studied. The features of atherosclerotic plaques, such as the presence of macrophages and tracer target molecules were studied by histology and immunohistochemistry of aortic tissue sections. Various biomarkers were measured from the plasma of mice. The general study design is depicted in Figure 3A.

4.2.1 Interventional protocol (IV)

In study IV, the effects of diet and atorvastatin interventions on plaques, biomarkers and the uptake of an established tracer, ^{18}F-FDG, was studied. The hypercholesterolemic LDLR$^{-/-}$ApoB$^{100/100}$ mice were on chow diet (CRM [E], product code 801730, 9.1 % of calories from fat, Special Diet Services, Essex, United Kingdom) for the first 2 months and then 3 months on high-fat diet (TD.88137 Adjusted Calories Diet, Harlan Teklad, 42 % of calories from fat, 0.2

% total cholesterol, no sodium cholate, Harlan Laboratories, Madison, WI, USA). The first blood samples were taken at this point. The interventional groups were then allocated to either continue on high-fat diet (HFD), switch to chow diet (Chow) or to high-fat+atorvastatin diet (TD.88137 diet with 0.1 mg/g of food-added atorvastatin and modified starch for better pellet quality) (HFD+A). After a three-month interventional period, the mice underwent ^{18}F-FDG PET/CT imaging, *ex vivo* biodistribution and ARG. Second plasma samples were taken for biomarker measurements, and aortic roots were obtained for histological analyses. The interventional protocol is shown in Figure 3B.

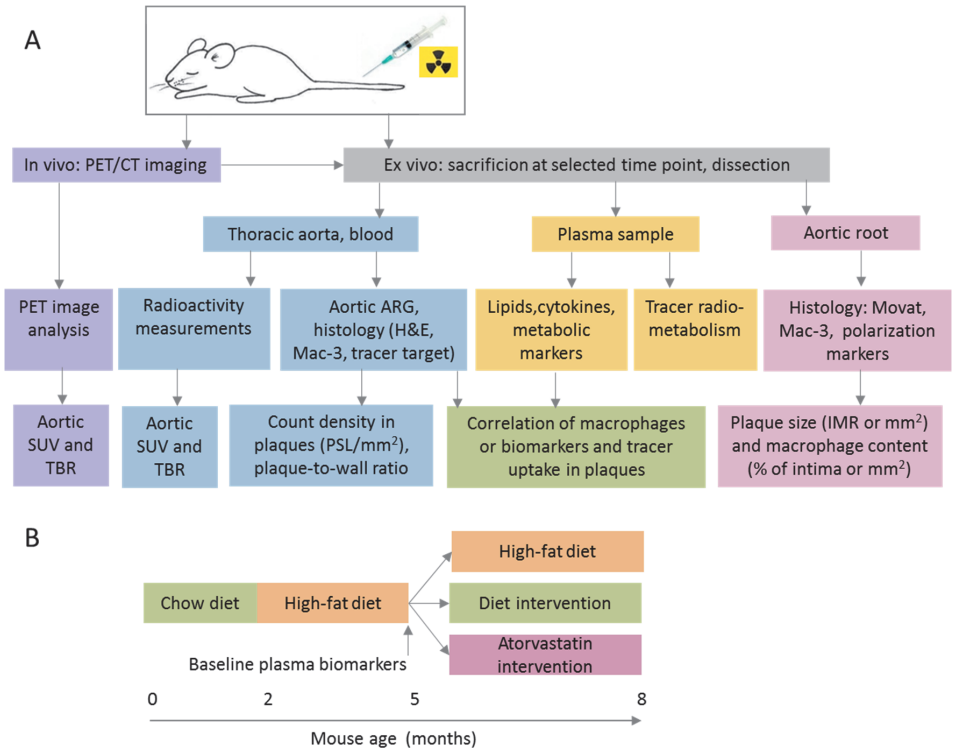

Figure 3. The general study design. A: Protocol in studies I-III. Not all measurements were conducted in every study. B: The interventional protocol in study IV. After the intervention, the mice were studied with ^{18}F-FDG according to the protocol described in A.

4.3 Tracer radiosyntheses

Most of the radiotracers utilized in this study were synthesized in the Radiopharmaceutical Chemistry Laboratory of Turku PET Centre. ^{18}F-FMCH batches were purchased from MAP Medical Technologies Oy (Helsinki, Finland). The radiochemical purity exceeded 95 % in every batch. ^{18}F-FDR-NOC syntheses were conducted either at Turku PET Centre or in the Laboratory of Radiochemistry, Department of Chemistry, University of Helsinki, Helsinki, Finland. ^{18}F-FDG was synthesized in the radiopharmaceutical laboratory of Turku PET Centre according to previously described protocols (Hamacher et al. 1986).

Somatostatin receptor targeting tracers

The radiosynthesis of ^{68}Ga-DOTANOC was performed with an automated synthesis device (Modular Lab, Eckert & Ziegler Eurotope GmbH, Berlin, Germany). The tracer ^{18}F-FDR-NOC was synthetized utilizing 5-deoxy-5-[^{18}F]-fluororibose (^{18}F-FDR) as a prosthetic group. [^{18}F]FDR was conjugated to the somatostatin analogue NOC peptide (0.3 mM, ABX GmbH, Radeberg, Germany) in anilinium buffer (0.3 M, pH 4.6). The reaction mixture was purified with high-performance liquid chromatography (HPLC) with a Jupiter Proteo C18 column (250×10 mm, Phenomenex Inc, Torrance, CA, USA), and ^{18}F-FDR-NOC was formulated in phosphate-buffered saline (PBS). For the ^{68}Ga labelling of DOTATATE, ^{68}Ga was obtained from a ^{68}Ge/^{68}Ga generator (Eckert& Ziegler, CA, USA) by elution with 0.1 M HCl. ^{68}Ga eluate (500 µl) was mixed with HEPES (120 mg) to give a pH of approximately 5 and thereafter DOTATATE peptide (1 mM, Peptide Specialty Laboratories GmbH, Heidelberg, Germany) was added to the mixture. The reaction mixture was then heated at 100 °C for 10 min. Radiochemical purity was > 99 % for ^{68}Ga-DOTANOC and ^{18}F-FDR-NOC and > 96 % for ^{68}Ga-DOTATATE. The specific radioactivities of the tracers were 30.8, 39.6–40.5 and 30.3–33.0 GBq/µmol, respectively.

^{18}F-FEMPA

^{18}F-fluoride ion was produced with a cyclotron (Efremov Institute of Elektrophysical Apparatuses, St Petersburg, Russia). ^{18}F-FEMPA was synthesized by nucleophilic fluorination of FEMPA-mesylate precursor (Bayer Schering Pharma/Piramal Imaging SA, Matran, Switzerland). The labeled product was separated and purified by HPLC and a solid phase extraction C18 cartridge. The sterile end product was formulated in PBS (pH 7.4) containing 10 % ethanol. The radiochemical purity of ^{18}F-FEMPA was > 99 % and the specific radioactivity > 91 GBq/ µmol.

4.4 *In vivo* tracer stability measurements

The *in vivo* stability of ^{18}F-FDR-NOC, ^{18}F-FMCH and ^{18}F-FEMPA was analyzed in studies I-III. The analyses were performed with the radio-HPLC method. Blood samples were obtained from cardiac puncture, plasma was separated with centrifugation and proteins were precipitated with acetonitrile.

The columns utilized in the analyses were Partisil 10 µm SCX, 250 × 4.6 mm (Phenomenex, Torrance, CA, USA), Jupiter Proteo HPLC, 250 × 10 mm (Phenomenex, Torrance, CA, USA) and a µ-Bondapak-C18, 300 × 7.8 mm, 10 µm (Waters, Milford, MA, USA), for ^{18}F-FDR-NOC, ^{18}F-FMCH and ^{18}F-FEMPA, respectively. The respective buffers for elution were gradient of 0.1 % trifluoroacetic acid (TFA)/acetonitrile + 0.1 % TFA (Kiviniemi et al. 2014), sodium dihydrogen phosphate pH 4.8 and acetonitrile (90:10) (Roivainen et al. 2000) and acetonitrile/10 mM phosphoric acid gradient (Varrone et al. 2015). The intact tracer and radiometabolites were detected by radiodetector.

4.5 PET/CT imaging

In studies I and IV, *in vivo* PET/CT imaging was performed for a subset of mice before the *ex vivo* measurements, whereas in studies II and III, separate mice were utilized in the *in vivo* imaging (Table 4). The imaging was performed with Inveon Multimodality PET/CT scanner (Siemens Medical Solutions, Knoxville, TN, USA). The mice were under isoflurane anesthesia (1.5-2 %, oxygen as carrier) during the imaging, and a catheter was placed in the tail vein for the injections. Tracer doses were measured with a dose calibrator (VDC-202., Veenstra Instruments, Joure, The Netherlands). CT for attenuation correction was performed before PET imaging. Dynamic PET imaging starting at the radiotracer injection was performed in studies I (30 minutes) II (30 minutes) and III (40 minutes), and static 20-minute PET starting at 50 minutes post-injection in study IV. Contrast-enhanced CT was performed after PET in all studies. 100-200 µl of i.v. contrast agent (eXia 160XL, Binitio Biomedical, Ottawa, Canada) was injected via tail vein catheter before CT in order to visualize the large blood vessels. The PET images were reconstructed with 2-dimensional ordered-subsets expectation maximization algorithm and CT images with a Feldkamp-based algorithm.

Table 4. The details of the study animals and studies performed for each group.

Study	Tracer	Number of animals (m/f)	Studies performed[a]	Age (months)	High-fat diet (months)	Weight (g)
LDLR$^{-/-}$ApoB$^{100/100}$						
II	^{18}F-FMCH	11 (7/4)	B + A	6-7	4	33 ± 6
	^{18}F-FMCH	9 (4/5)	B + A	8-10	6	35 ± 7
	^{18}F-FMCH[b]	3 (3/0)	B	6	4	38 ± 1
	^{18}F-FDG	12 (8/4)	B + A	6-7	4	36 ± 9
III	^{18}F-FEMPA	10 (6/4)	B + A	6-7	4-5	39 ± 8
	^{18}F-FEMPA	3 (3/0)	PET	6-7	4-5	44 ± 7
IV	^{18}F-FDG	36 (15/21)	PET (n=31) + B + A	8	3+3[c]	30 ± 7
IGF-II/LDLR$^{-/-}$ApoB$^{100/100}$						
I	^{68}Ga-DOTANOC	16 (8/8)	PET (n=2) + B + A	6-9	4-5	32 ± 7
	^{18}F-FDR-NOC	9 (8/1)	PET (n=4) + B + A	6-7	4-5	34 ± 8
	^{68}Ga-DOTATATE[d]	6 (0/6)	PET + B + A	6	4-5	24 ± 3
II	^{18}F-FMCH	11 (6/5)	B + A (n=8) or *Ex vivo* PET (n=3)	6-7	4	32 ± 7
	^{18}F-FMCH	3 (0/3)	PET	5	3	25 ± 3
	^{18}F-FDG	11 (6/5)	B + A	6-7	4	35 ± 8
C57BL/6N						
I	^{68}Ga-DOTANOC	11 (7/4)	PET (n=2) + B + A	2-7	-	27 ± 6
	^{18}F-FDR-NOC	6 (6/0)	PET (n=4) + B + A	7	-	40 ± 4
	^{68}Ga-DOTATATE[d]	4 (0/4)	PET + B + A	4	-	23 ± 2
II	^{18}F-FMCH	13 (9/4)	B + A (n=6) or *Ex vivo* PET (n=3)	5-11	-	38 ± 8
III	^{18}F-FEMPA	7 (7/0)	B + A	7	-	40 ± 4
	^{18}F-FEMPA	4 (4/0)	PET	3	-	28 ± 2

[a]B: ex vivo biodistribution, A: ex vivo autoradiography, PET: in vivo PET/CT imaging.
[b]After 4-hour fast
[c]3 months of high-fat diet + 3 months of high-fat, chow or high-fat+atorvastatin diet
[d] The same mice were imaged with ^{68}Ga-DOTANOC earlier (head-to-head comparison)

The analysis of *in vivo* PET/CT images was performed with Carimas software (Carimas 2.8 or 2.9, Turku PET Centre, Turku, Finland). All of the radioactivities were decay-corrected to the injection time, and the tracer dose remaining in the tail was subtracted. PET and CT images were co-registered with an automated algorithm of the software and confirmed visually based on the anatomical landmarks. Regions of interest (ROI) were defined in tissues based on the contrast-enhanced CT. ROI for aorta was defined in the aortic arch, and blood pool radioactivity was measured from *vena cava*. The results were extracted as standardized uptake values (SUV) calculated as (radioactivity in tissue/injected radioactivity) / (tissue volume/mouse weight). TBR values were calculated by dividing the aortic SUVs by the blood pool SUVs.

Ex vivo PET for aorta and heart (II)

For a subset of mice, *ex vivo* PET imaging of aorta and heart was performed. The mice were sacrificed at 20 minutes post-injection, tissues were dissected and measured for radioactivity, and placed in a tube containing ultrasonography gel. The tube was placed in the PET/CT device, and 40-minute static PET was performed. The PET images were reconstructed with a 3-dimensional ordered-subsets expectation maximization algorithm.

4.6 *Ex vivo* biodistribution

The mice were anesthetized with isoflurane (1.5-2.5 %, air as a carrier) and kept on a heating pad during the *ex vivo* biodistribution studies. The studied radiotracers were injected into the tail vein of the mice via a catheter. Tracer doses were measured with a dose calibrator (VDC-202., Veenstra Instruments, Joure, The Netherlands). At a certain time point after injection (Table 5), mice were euthanized by cardiac puncture and cervical dislocation in deep anesthesia. Tissue samples were dissected, weighed and measured for radioactivity with a gamma counter (Triathler 425-010, Hidex, Turku, Finland or 1480 Wizard 3″ Gamma Counter, PerkinElmer/Wallac, Turku, Finland). Blood and plasma samples were also included in the measurements. All of the measured radioactivities were decay-corrected to the injection time, and the radioactivity concentrations in tissues were calculated as standardized uptake values (SUV, I, III, IV) or as percentage of injected radioactivity per gram of tissue (%IA/g, II). The SUVs were calculated as (radioactivity in tissue/tissue weight) / (injected radioactivity/mouse weight). For the aorta, TBR was calculated by dividing the aortic SUV by blood SUV.

Table 5. Details of the *ex vivo* protocols for each studied tracer.

Study	Tracer	Feeding prior to study	Injected radioactivity (MBq)	Time point (min)
I	^{68}Ga-DOTANOC	4-hour fast	7.4 ± 1.5	60
	^{18}F-FDR-NOC	4-hour fast	10.2 ± 0.9	60
	^{68}Ga-DOTATATE	4-hour fast	6.9 ± 0.2	60
II	^{18}F-FMCH	Ad libitum	10.2 ± 1.6	20
	^{18}F-FDG	4-hour fast	11.0 ± 1.6	90
III	^{18}F-FEMPA	Ad libitum	10.3 ± 1.4	20
IV	^{18}F-FDG	4-hour fast	10.6 ± 1.0	90

4.7 Autoradiography studies

Ex vivo autoradiography (I-IV)

The more detailed tracer distribution within the aortic tissue was determined with ARG. After the radioactivity measurement described in the previous chapter, the aortas were embedded, frozen in cooled isopentane and cut into serial 20- and 8-µm sections longitudinally with a cryomicrotome. The sections were thaw-mounted to microscope slides, air-dried and placed under a radiation-sensitive imaging plate (Fuji Imaging Plate BAS-TR2025, Fuji Photo Film Co., Ltd., Tokyo, Japan). The ARG exposure times were 4 h in studies I, III and IV and overnight in study II. At the end of the exposure, the plates were scanned with a phosphoimager (Fuji Analyzer BAS-5000, internal resolution of 25 µm or Fuji FLA-5100, internal resolution 10 µm) to obtain digital ARG data images. The sections were stored in -70 °C and stained later with histological or immunohistochemical methods (see chapter 4.8).

The ARG was analyzed from 6 to 10 sections per animal with Tina 2.1 software (Raytest Isotopemessgeräte, GmbH, Straubenhardt, Germany). The outlines of sections were carefully co-registered with the ARG images, and ROIs were defined in plaques (excluding media and calcifications), normal vessel wall (media without visually detectable lesion formation) and adventitia (vessel-surrounding brown adipose tissue). The data from ARG analysis was obtained as count density (photo-stimulated luminescence per square millimeter, PSL/mm^2). The background was subtracted, and the PSL/mm^2 values were normalized for injected dose per gram of mouse weight and the proportion of radioactivity decay during exposure. An example of ARG analysis is shown in Figure 4.

In studies II and III, the count densities were compared in plaques with different degrees of Mac-3-positive staining, i.e. the amount of macrophages in the respective plaque. In II, the ROIs were defined in areas of visually high or low Mac-3-positive staining. The degree of macrophage infiltration was quantified with ImageJ software (Fiji, National Institutes of Health, Bethesda, MD, USA), and the plaque areas were classified as low, intermediate or high macrophage density based on the percentage of Mac-3-positive staining. In III, the ROIs were

defined in plaque areas with different macrophage densities. The macrophage densities in plaque areas were visually graded as (0) no macrophages, (1) low (occasional macrophages), (2) intermediate (scattered groups of macrophages) or (3) high (confluent areas of macrophages). The mean PSL/mm^2 values were calculated for each grading group.

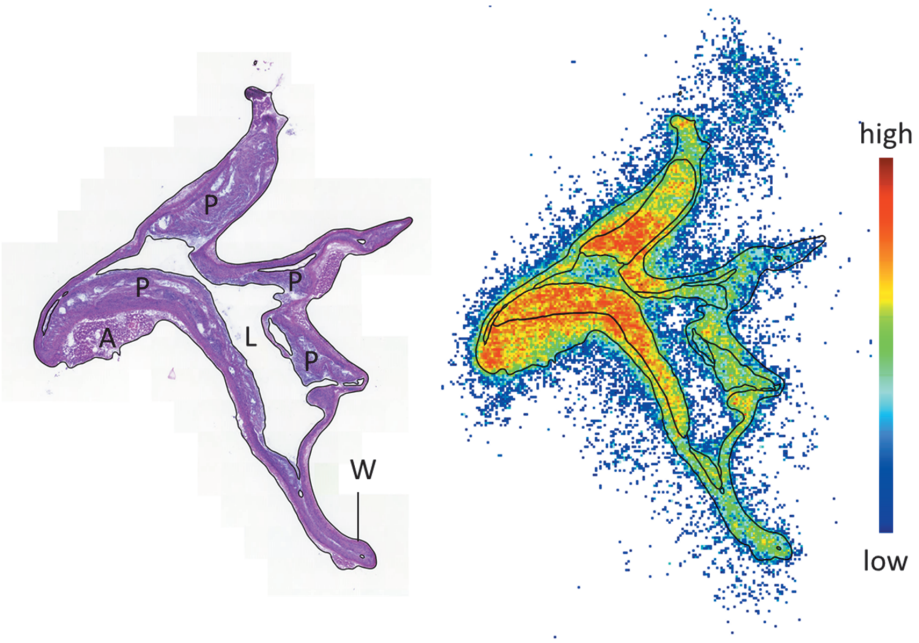

Figure 4. An example of autoradiography. Hematoxylin-eosin stained section of aortic arch on the left and corresponding ^{18}F-FDG autoradiograph on the right. The regions of interest were defined as adventitia (A), plaque (P) and normal vessel wall (W). L represents the lumen. The plaques are circled, and the high uptake (red) can be seen in some of the plaques, whereas the normal vessel wall uptake is relatively low.

In vitro autoradiography (III)

In vitro ARG in the presence and absence of unlabeled competitive TSPO binder (PK11195) was performed to show the specificity of ^{18}F-FEMPA binding. Both mouse aortic sections (LDLR$^{-/-}$ApoB$^{100/100}$, n = 3 and C57BL/6N, n = 2) and human carotid plaque samples (n = 4) were utilized. The human carotid plaques were from endarterectomy surgery of patients with recent ischemic symptoms. The patient study protocol was accepted by the ethics committee of the Hospital District of Southwest Finland and the study was conducted according to the Declaration of Helsinki. Sections were incubated in Tris-HCl buffer containing 0.040 MBq/ml ^{18}F-FEMPA with or without 50 nM unlabeled PK11195 (C0424, Sigma-Aldrich, St. Louis, MO). ARG was performed similarly as in the *ex vivo* ARG, with the exception that exposure was 2.5 hours. In the human carotid plaque sections, ROIs were defined in areas positive for macrophages (CD68) or smooth muscle cells (alpha-smooth muscle actin, α-SMA), and in murine aortic sections, ROIs were defined in plaque and wall.

4.8 Histology and immunohistochemistry

The 20-µm aortic cryosections were stained with hematoxylin and eosin (H&E) for basic histology and 8-µm sections were stained for macrophages (Mac-3, also known as CD107b and lysosome-associated membrane protein 2) in all studies. The sections were melted and fixed with 4 % formaldehyde, followed by boiling in 10 mM citrate buffer. The sections were incubated with primary antibody (rat anti-mouse Mac-3, clone M3/84, 1:5000, BD Pharmingen, Franklin Lakes, NJ, USA). Polyclonal rabbit anti-rat antibody (DakoCytomation E0468, 1:200) was utilized as secondary and EnVision+ System- horseradish peroxidase (HRP) -labelled goat anti-rabbit antibody (DakoCytomation EnVision anti-rabbit K4003) as tertiary antibody. Detection was performed with 3,3' diaminobenzidine tetrahydrochloride hydrate (DAB) and substrate (DakoCytomation K3468), and Mayer's haematoxylin was used for counterstaining. The Mac-3 stained aortic cryosections were utilized in quantitative ARG analyses in studies II and III, and as a visual estimate of the presence of macrophages in studies I and IV.

Staining for somatostatin receptors (I)

SSTR-2 immunohistochemical stainings were performed on the 8-µm mouse aortic cryosections and human carotid endarterectomy sample cryosection. The human sample was obtained from a patient with a recent ischemic stroke. The slides were fixed in cold acetone and incubated with a SSTR-2 monoclonal antibody (clone UMB-1, 1:100, Abcam, Cambridge, UK) using a LabVision autostainer with BrightVision detection kit (Immunologic, Duiven, the Netherlands). Negative control stainings were performed without the primary antibody.

Detection of dividing cells (II)

In order to detect the dividing cells, Ki-67 stainings were performed on longitudinally cut aortic cryosections. The sections were fixed in 10 % formalin and pre-incubated in 10 mM boiling citric acid. The primary antibody (monoclonal rat anti-mouse clone TEC-3, M7249, 1:1000, DakoCytomation, Glostrup, Denmark) was incubated overnight. Polyclonal rabbit anti-rat E0468 (1:200, DakoCytomation, Glostrup, Denmark) was utilized as a secondary antibody and EnVision anti-rabbit (K4003, DakoCytomation, Glostrup, Denmark) as a tertiary antibody. The detection and counterstaining was performed with Rat-on-Mouse HRP-polymer RT 517 kit (Biocare Medical, Concord, CA, USA), followed by chromogen (DAB, K3468, DakoCytomation, Glostrup, Denmark) and counterstaining with Mayer's hematoxylin.

Determination of plaque size and the amount of macrophages (II, IV)

The plaque size and the amount of positive staining for macrophages were analyzed from aortic root sections. The formalin-fixed aortic roots were

embedded in paraffin and sectioned at the level of coronary ostia. Basic histology of aortic roots was determined from modified Movat's pentachrome staining. Adjacent sections were stained for macrophages (Mac-3). Stainings for macrophage M1 and M2 polarization markers iNOS and MRC-1, as well as macrophage scavenger receptor CD36 were stained in study II. For the Mac-3 staining, the sections were incubated with primary antibody (Anti-Mac-3 M3/84, 1:500, BD Pharmingen, Franklin Lakes, NJ, USA). Next, Rat-on-Mouse HRP-polymer RT 517 kit (Biocare Medical, Concord, CA, USA) was utilized, followed by chromogen (DAB, Dako K3468) and counterstaining with Mayer's hematoxylin. For the iNOS and mannose receptor C type 1 (MRC-1) stainings, the sections were pre-incubated in 10 mM citric acid followed by the primary antibody (anti-iNOS ab15323, 1:200, or anti-MRC-1 ab64693, 1:500, Abcam, Cambridge, UK). Secondary antibody (Dako EnVision anti-rabbit K4003) was incubated, followed by chromogen and counterstaining as described above. For CD36, the protocol was similar, except for the pre-incubation by boiling in 10 mM tris-EDTA buffer. The primary antibody was anti-CD36 ab80978, 1:500, (Abcam, Cambridge, UK).

The plaque size was assessed as intima-to-media ratio (IMR) in study II and as the absolute area of intima (mm^2) in aortic root sections in study IV. The amount of positive staining for Mac-3 (II and IV) and iNOS, MRC-1 and CD36 (study II) was also analyzed. The analysis of area was performed by outlining the intima and media with an image processing software (GIMP2), based on the histology, in three parallel sections. The area of intima and media was defined with ImageJ software (Fiji, National Institutes of Health, Bethesda, MD, USA). The area positive for Mac-3, iNOS, MRC-1 or CD36 was also assessed with ImageJ by color deconvolution method detecting the DAB-stained areas. The amount of staining was expressed as percentage of total intimal area in study II and as absolute area (mm^2) in IV.

Detection of TSPO (III)

Aortic roots of three $LDLR^{-/-}ApoB^{100/100}$ and two C57BL/6N mice were prepared and stained with anti-TSPO antibody. Adjacent sections were stained for macrophages (Mac-3) as described above. The formalin-fixed, paraffin-embedded sections were pre-incubated in 10 mM citrate buffer followed by incubation with the primary antibody (NBP1-95674, 1:10000, Novus Biologicals). HRP-conjugated secondary antibody (Dako EnVision+ System HRP goat anti-rabbit K4003) was added, and detection was performed with DAB and substrate (DakoCytomation K3468). Mayer's hematoxylin was used for counterstaining. Negative control stainings were performed without the primary antibody.

Detection of macrophages and smooth muscle cells in human samples (III)

Human carotid plaque sections were stained for macrophages with anti-CD68 antibody (clone PG-MI, 1:200, DakoCytomation, Glostrup, Denmark) and for

smooth muscle cells with anti-α-SMA antibody (1:15000, clone 1A4, Sigma-Aldrich, St. Louis, MO). The frozen sections were thawed and fixed in acetone (CD68) or with 4 % formaldehyde (α-SMA). The primary antibody was incubated overnight. Biotinylated anti-mouse IgG was utilized as secondary antibody (Vectastain ABC-kit, Vector Laboratories Inc., Burlingame, CA, USA), and detection was performed with ABC-reagent (Vectastain-kit) and DAB. The sections were counterstained with hematoxylin.

4.9 Measurement of plasma biomarkers (I, II, IV)

Glucose

In the mice studied with ^{18}F-FDG (studies II and IV), the blood glucose values were measured from whole blood with a glucometer (One Touch UltraEasy, LifeScan, Inc., Milpitas, CA, USA [II] or Bayer Contour, Bayer AG, Leverkusen, Germany [IV]) before radiotracer injections. For the mice studied with ^{18}F-FMCH in the study II, the glucose levels were measured with a glucose analyzer (GM9, Analox Instruments, London, UK) from the plasma obtained at the end of the study.

Cytokines and metabolic markers

Blood samples were taken from the mice by cardiac puncture. Plasma was separated by centrifugation and samples were stored at -70 ˚C before the analyses. Plasma levels of cytokines and metabolic markers were measured with Luminex assays (MILLIPLEX, MMHMAG-44K and MCYTOMAG-70K, Magnetic Bead Panel, Merck Millipore, Billerica, MA, USA). The analytes IL-6, monocyte chemotactic protein 1 (MCP-1), insulin, and leptin were measured in studies I, II and IV. Additionally, RANTES and C-peptide levels were measured in studies I and II, and IL-1β, IFN-γ and glucagon in study II. The minimum detectable concentrations (picogram per milliliter) for the analytes were 3.2 (IFN-γ), 3.5 (IL-1β), 1.1 (IL-6), 6.7 (MCP-1), 2.7 (RANTES), 20 (C-peptide), 7 (glucagon), 14 (insulin), and 19 (leptin). The correlation of plasma cytokines and metabolic markers to aortic PET tracer uptake was analyzed in studies I, II and IV. Additionally, levels of markers were compared between interventional groups in study IV.

Lipids and lipid-related proteins (II, IV)

Total cholesterol levels were measured using the Cholesterol CHOD-PAP kit (Roche Diagnostics, Basel, Switzerland) and triglycerides with the Triglycerides GPO-PAP kit (Roche Diagnostics, Basel, Switzerland). In study II, phospholipids were analyzed using the Phospholipids B kit (Wako Chemicals, Neuss, Germany) or Pureauto S PL kit (Daiichi Pure Chemicals, Tokyo, Japan). The activity of phospholipid transfer protein (PLTP) was measured with a radiometric

method, as described previously by Jauhiainen and Ehnholm (2005). Paraoxonase-1 (PON-1) activity (μmol/min) was measured with a chromogenic method (Kleemola et al. 2002). The levels of lipids and lipid-related proteins were compared with the ^{18}F-FMCH uptake in plaques by correlation analysis in study II. In study IV, the levels of total cholesterol and triglycerides were compared with the ^{18}F-FDG uptake.

4.10 Statistical analyses

The statistical analyses were conducted with IBM SPSS Statistics 21 (IBM Corp., Armonk, NY, USA) (II-IV) or GraphPad Prism 5 (GraphPad Software, Inc., La Jolla, CA, USA) (I, graphs in I-IV). The results are expressed as mean ± standard deviation (SD) unless otherwise specified. Shapiro-Wilk test was utilized as a normality test, and Levene's test was utilized in determining the equality of variances. Independent-sample *t*-test was utilized to calculate the differences between two independent groups. If three or more groups were compared, the differences were analyzed with one-way ANOVA. The post-hoc correction methods for ANOVA were Bonferroni or Holm-Sidak (Study I), Tukey (III) and Tukey or Tamhane (II and IV). In study I, one-sample *t*-test was conducted to test the deviation of plaque-to-wall and plaque-to-adventitia ratios from a hypothetical value of 1.0. The analyses of paired data, such as different measurements from same animals, were conducted with paired *t*-tests. The correlations (I, II and IV) were assessed with Pearson's coefficient (*r*). *P*-values less than 0.05 were regarded as statistically significant.

5 RESULTS

5.1 Characterization of mouse models

5.1.1 Histology and immunohistochemistry

Determination of plaque size and the amount of macrophages (II, IV)

All LDLR$^{-/-}$ApoB$^{100/100}$ and IGF-II/LDLR$^{-/-}$ApoB$^{100/100}$ mice in the studies developed atherosclerotic plaques, whereas no atherosclerotic lesions were observed in the C57BL/6N mice. The plaques were mainly fibroatheroma-type lesions with lipids, collagen and cells. In study II, the IMR was 2.7 ± 0.88 and 1.8 ± 0.51 in 6-month-old LDLR$^{-/-}$ApoB$^{100/100}$ and IGF-II/LDLR$^{-/-}$ApoB$^{100/100}$ mice, respectively. The aged (8-10-month-old) IGF-II/LDLR$^{-/-}$ApoB$^{100/100}$ mice exhibited larger plaques (IMR 4.3 ± 0.49, $p < 0.001$ than 6-month-old mice).

All the analyzed plaques had at least occasional macrophages. As measured from the aortic roots, the percentage of Mac-3-positive area in the intima was 15 ± 2.3 and 17 ± 0.98 in LDLR$^{-/-}$ApoB$^{100/100}$ and IGF-II/LDLR$^{-/-}$ApoB$^{100/100}$ mice, respectively. iNOS and MRC-1 stainings were utilized to detect the M1- and M2-polarized macrophages, respectively. The areal percentages of M1 and M2 macrophages in the intima were similar in LDLR$^{-/-}$ApoB$^{100/100}$ (14 ± 1.3 and 30 ± 1.3) and IGF-II/LDLR$^{-/-}$ApoB$^{100/100}$ (14 ± 1.7 and 32 ± 1.2) mice.

In study IV, the plaque burden and amount of macrophages were measured as absolute areas (mm^2). The Chow group presented 34 % smaller area of intima, compared to HFD (0.76 ± 0.27 vs. 1.1 ± 0.39 mm^2, $p = 0.031$). In addition, the Mac-3-positive area was 61 % smaller (0.049 ± 0.029 vs. 0.13 ± 0.039 mm^2, $p < 0.001$). The intimal and Mac-3-positive areas were similar in HFD+A group (0.96 ± 0.11 mm^2 and 0.11 ± 0.039 mm^2) compared to the HFD group.

SSTR-2, dividing cells and TSPO (I, II and III)

SSTR-2-positive cells were observed both in mouse plaques and in the human endarterectomy sample. In the mouse aorta, the staining was localized mainly in the fibrous cap areas of plaque, and no staining was observed in the vessel wall. In the human endarterectomy sample, positive staining was seen in areas with high nuclear density as seen with H&E staining.

Only occasional Ki-67-positive cells were observed in aortic sections. This suggests a low rate of cellular proliferation in the plaques.

TSPO mainly co-localized with Mac-3-positive macrophages in the plaque intima. Some areas showed positivity for TSPO but not for Mac-3. Vessel walls of both atherosclerotic and healthy mice were positive for TSPO.

Detection of macrophages and smooth muscle cells in human samples (III)

The human carotid endarterectomy plaque sections showed CD68-positive areas in all but one sample, which was fibrotic and calcified tissue without apparent macrophage infiltration. Smooth muscle cells were present in all of the studied samples.

5.1.2 Plasma biomarkers

In study II, both LDLR$^{-/-}$ApoB$^{100/100}$ and IGF-II/LDLR$^{-/-}$ApoB$^{100/100}$ mice presented high total cholesterol levels after high-fat diet (31 ± 4.3 and 36 ± 12 mmol/l, respectively). In healthy C57BL/6N mice, the cholesterol levels were 1.8 ± 0.3 mmol/l. The blood fasting glucose levels were also similar between the strains (7.8 ± 1.0 in LDLR$^{-/-}$ApoB$^{100/100}$ and 9.1 ± 3.1 in IGF-II/LDLR$^{-/-}$ApoB$^{100/100}$ mice). The glucose values measured without fasting, at 20 minutes post-injection, were also similar between LDLR$^{-/-}$ApoB$^{100/100}$, IGF-II/LDLR$^{-/-}$ApoB$^{100/100}$ and C57BL/6N mice.

Of the other biomarkers measured, there was a tendency towards higher plasma concentrations of insulin, C-peptide and IL-6 in IGF-II/LDLR$^{-/-}$ApoB$^{100/100}$ mice than in LDLR$^{-/-}$ApoB$^{100/100}$ mice.

Effects of interventions on plasma biomarkers (IV)

Both Chow and HFD+A interventions lowered the total cholesterol levels, compared to the baseline or to the HFD group. The levels at the end of the study were 70 % lower (10 ± 3.2 mmol/l) in Chow and 34 % lower (23 ± 4.9 mmol/l) in HFD+A groups than in the HFD group (34 ± 9.2 mmol/l) ($p < 0.001$ between all groups).

Chow intervention led to lower leptin levels, compared to the HFD group (2.1 ± 1.9 vs. 7.3 ± 5.9 ng/ml, $p = 0.037$). The leptin levels in HFD+A group (4.0 ± 3.4 ng/ml) did not significantly differ from the other groups. There was a tendency for lower triglycerides, IL-6 and MCP-1 in the Chow group than in the HFD group, but no significant differences between the groups were observed. The levels of other measured markers were similar between the groups.

5.2 *In vivo* stability of the tracers (I-III)

The *in vivo* stability of ^{18}F-FDR-NOC, ^{18}F-FMCH and ^{18}F-FEMPA was studied. Of these tracers, ^{18}F-FDR-NOC showed the highest *in vivo* stability, with approximately 83 % of intact tracer in plasma at 60 minutes post-injection. Both ^{18}F-FMCH and ^{18}F-FEMPA showed rapid *in vivo* metabolism, since only 8 % and 10 % of the tracer was intact at 20 minutes post-injection, respectively. ^{18}F-FDR-NOC and ^{18}F-FMCH were both excreted to urine in both intact and metabolized form. The detailed results of *in vivo* stability are shown in Table 6.

Table 6. *In vivo* stability of ^{18}F-FDR-NOC, ^{18}F-FMCH and ^{18}F-FEMPA.

Study	Tracer	Time point (min)	Mouse strain	Number of samples	% Intact tracer
Plasma					
I	^{18}F-FDR-NOC	60	IGF-II/LDLR$^{-/-}$ApoB$^{100/100}$	4	82.5 ± 5.2
	^{18}F-FDR-NOC	60	C57BL/6N	5	83.6 ± 2.1
II	^{18}F-FMCH	20	IGF-II/LDLR$^{-/-}$ApoB$^{100/100}$	8	7.5 ± 2.4
	^{18}F-FMCH	20	LDLR$^{-/-}$ApoB$^{100/100}$	8	8.5 ± 3.5
	^{18}F-FMCH	20	C57BL/6N	5	7.6 ± 5.6
III	^{18}F-FEMPA	10	C57BL/6N	3	27.7 ± 11.1
	^{18}F-FEMPA	20	C57BL/6N	3	10.0 ± 4.6
Urine					
I	^{18}F-FDR-NOC	60	LDLR$^{-/-}$ApoB$^{100/100}$	4	59.2 ± 13.7
	^{18}F-FDR-NOC	60	C57BL/6N	5	67.5 ± 9.7
II	^{18}F-FMCH	20	LDLR$^{-/-}$ApoB$^{100/100}$	3	43.3 ± 2.5
	^{18}F-FMCH	20	C57BL/6N	3	40.8 ± 3.6

5.3 PET/CT imaging

^{68}Ga-DOTANOC and ^{68}Ga-DOTATATE TBR values at 30 minutes post-injection were higher in IGF-II/LDLR$^{-/-}$ApoB$^{100/100}$ mice than in C57BL/6N mice, whereas ^{18}F-FDR-NOC showed no difference in uptake between IGF-II/LDLR$^{-/-}$ApoB$^{100/100}$ and C57BL/6N mice. In the head-to-head comparison, the same IGF-II/LDLR$^{-/-}$ApoB$^{100/100}$ mice were imaged with ^{68}Ga-DOTANOC and ^{68}Ga-DOTATATE. ^{68}Ga-DOTANOC showed higher aortic uptake than ^{68}Ga-DOTATATE (TBR values 0.83 ± 0.07 vs. 0.67 ± 0.04), $p = 0.0015$.

^{18}F-FEMPA uptake in the aortic arch was studied at 40 minutes post-injection in LDLR$^{-/-}$ApoB$^{100/100}$ and C57BL/6N mice. No significant differences were observed between the strains in aortic uptake or TBR values. ^{18}F-FMCH imaging was performed only on a small group of young IGF-II/LDLR$^{-/-}$ApoB$^{100/100}$ mice, and the uptake was measured at 20 minutes post-injection. The TBR was 0.85 ± 0.27. The studied mice represented only small atherosclerotic plaques (IMR 0.72 ± 0.13). All of the *in vivo* imaging results on aortic uptake are described in Table 7 and examples of PET/CT images are shown in Figure 5.

Ex vivo PET for aorta and heart (II)

The *ex vivo* PET imaging of aorta and heart with ^{18}F-FMCH PET showed focal areas of high tracer uptake in the aortic arch of LDLR$^{-/-}$ApoB$^{100/100}$ mice. In the C57BL/6N mice, uptake in the aortas was lower and homogeneous.

Effects of interventions on ^{18}F-FDG aortic uptake in vivo (IV)

The ^{18}F-FDG uptake in the aorta, measured as SUV at 50-70 minutes post-injection, was similar between the groups (Table 7). However, when comparing the TBR values, the Chow group showed significantly lower TBR than the HFD group (p = 0.018). The TBR in the HFD+A group did not differ from the HFD group.

Table 7. The results of *in vivo* PET/CT imaging expressed as standardized uptake values (SUV) and target-to-background ratios (TBR)

Study	Tracer (IV: group)	Mouse strain	SUV	TBR	TBR p value[a]
I	^{68}Ga-DOTANOC	IGF-II/LDLR$^{-/-}$ApoB$^{100/100}$	1.0 ± 0.06	0.9 ± 0.03	0.049
	^{68}Ga-DOTANOC	C57BL/6N	0.6 ± 0.1	0.6 ± 0.01	
	^{18}F-FDR-NOC	IGF-II/LDLR$^{-/-}$ApoB$^{100/100}$	1.5 ± 0.1	0.6 ± 0.09	0.89
	^{18}F-FDR-NOC	C57BL/6N	1.7 ± 0.1	0.6 ± 0.07	
	^{68}Ga-DOTATATE	IGF-II/LDLR$^{-/-}$ApoB$^{100/100}$	0.5 ± 0.02	0.7 ± 0.04	<0.001
	^{68}Ga-DOTATATE	C57BL/6N	0.3 ± 0.03	0.5 ± 0.05	
II	^{18}F-FMCH	IGF-II/LDLR$^{-/-}$ApoB$^{100/100}$	0.8 ± 0.2	0.9 ± 0.3	
III	^{18}F-FEMPA	LDLR$^{-/-}$ApoB$^{100/100}$	0.8 ± 0.1	0.6 ± 0.05	0.30
	^{18}F-FEMPA	C57BL/6N	0.9 ± 0.1	0.6 ± 0.1	
IV	^{18}F-FDG (HFD)	LDLR$^{-/-}$ApoB$^{100/100}$	0.9 ± 0.1	2.1 ± 0.2	
	^{18}F-FDG (Chow)	LDLR$^{-/-}$ApoB$^{100/100}$	0.9 ± 0.2	1.7 ± 0.2	0.018
	^{18}F-FDG (HFD+A)	LDLR$^{-/-}$ApoB$^{100/100}$	1.1 ± 0.2	2.1 ± 0.4	1.0

[a]I and III: vs. C57BL/6N mice, IV: vs. HFD group

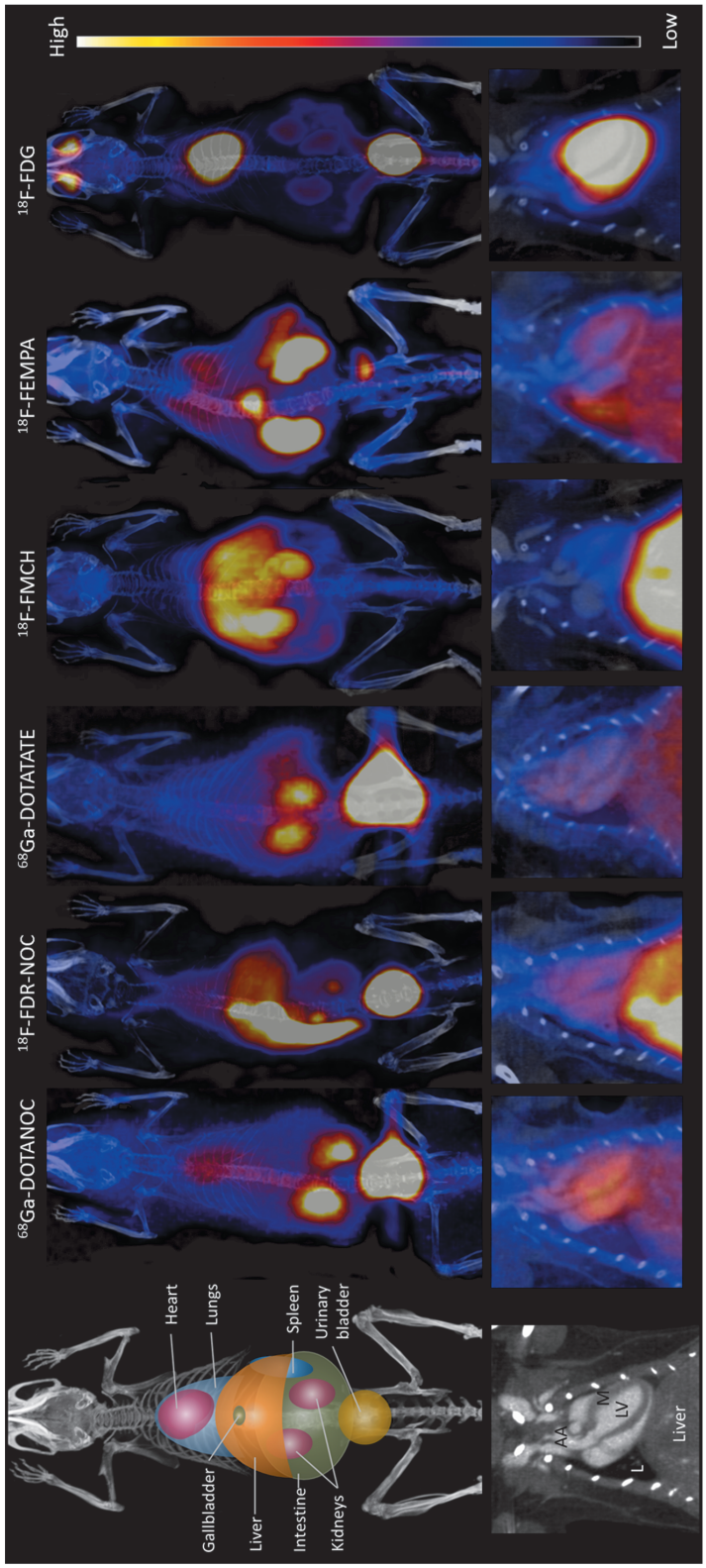

Figure 5. *In vivo* biodistribution of the studied tracers. The whole-body distribution is shown as a three-dimensional image in the upper panel and detailed distribution in the mouse thorax area in the lower panel. The schematic view of the organs is shown on the left. AA: aortic arch, L: lungs, LV: left ventricle, M: myocardium.

5.4 *Ex vivo* biodistribution

In study I, the uptake of ^{68}Ga-DOTANOC was higher in the aortas of IGF-II/LDLR$^{-/-}$ApoB$^{100/100}$ mice than of C57BL/6N mice when measured as SUV, whereas the higher blood radioactivity in IGF-II/LDLR$^{-/-}$ApoB$^{100/100}$ mice led to similar TBR values between the strains (Table 8). ^{18}F-FDR-NOC uptake was similar in both mouse strains. Similarly to ^{68}Ga-DOTANOC, ^{68}Ga-DOTATATE showed increased aortic uptake in IGF-II/LDLR$^{-/-}$ApoB$^{100/100}$ mice compared to in C57BL/6N mice when measured as SUV, but no difference was seen in the TBR values.

In study II, ^{18}F-FMCH showed higher uptake in the aortas of IGF-II/LDLR$^{-/-}$ApoB$^{100/100}$ mice than of C57BL/6N or LDLR$^{-/-}$ApoB$^{100/100}$ mice, measured both as SUV or TBR. ^{18}F-FMCH TBR was similar to ^{18}F-FDG TBR in IGF-II/LDLR$^{-/-}$ApoB$^{100/100}$ mice, but lower in LDLR$^{-/-}$ApoB$^{100/100}$ mice. Uptake in the myocardium was lower with ^{18}F-FMCH than with ^{18}F-FDG in all mice.

In study III, ^{18}F-FEMPA showed higher uptake in the aortas of LDLR$^{-/-}$ApoB$^{100/100}$ mice than of C57BL/6N controls. The remaining radioactivity in blood was very low, leading to high TBR values, especially in LDLR$^{-/-}$ApoB$^{100/100}$ mice. All of the biodistribution results of aortic SUV and TBR values are shown in Table 8.

Table 8. The results of *ex vivo* biodistribution (standardized uptake value, SUV and target-to-background ratio, TBR) and ARG (count density, PSL/mm^2 and plaque-to-wall ratio).

			***Ex vivo* biodistribution**			**Autoradiography**	
Study	**Tracer (IV: group)**	**Mouse strain**	**Aorta SUV**	**TBR**	**TBR *p*-value[a]**	**PSL/mm^2**	**P/W Ratio**
I	^{68}Ga-DOTANOC	IGF-II/LDLR$^{-/-}$ApoB$^{100/100}$	1.0 ± 0.3	1.2 ± 0.3	0.14	48 ± 16	1.7 ± 0.3
	^{68}Ga-DOTANOC	C57BL/6N	0.4 ± 0.2	1.3 ± 0.3		-	-
	^{18}F-FDR-NOC	IGF-II/LDLR$^{-/-}$ApoB$^{100/100}$	1.5 ± 0.5	1.0 ± 0.2	0.38	259 ± 87	1.2 ± 0.2
	^{18}F-FDR-NOC	C57BL/6N	1.8 ± 0.4	1.2 ± 0.6		-	-
	^{68}Ga-DOTATATE	IGF-II/LDLR$^{-/-}$ApoB$^{100/100}$	0.2 ± 0.03	0.5 ± 0.1	0.11	14 ± 2	2.1 ± 0.5
	^{68}Ga-DOTATATE	C57BL/6N	0.1 ± 0.01	0.6 ± 0.1		-	-
II	^{18}F-FMCH	LDLR$^{-/-}$ApoB$^{100/100}$	0.5 ± 0.1	1.6 ± 0.5	1.0	186 ± 31	2.5 ± 0.3
	^{18}F-FMCH	IGF-II/LDLR$^{-/-}$ApoB$^{100/100}$	0.6 ± 0.1	3.9 ± 1.9	0.016	236 ± 67	2.6 ± 0.3
	^{18}F-FMCH	C57BL/6N	0.5 ± 0.1	1.7 ± 0.4	-	-	-
	^{18}F-FDG	LDLR$^{-/-}$ApoB$^{100/100}$	1.8 ± 0.7	4.9 ± 2.2	-	315 ± 103	2.1 ± 0.6
	^{18}F-FDG	IGF-II/LDLR$^{-/-}$ApoB$^{100/100}$	1.6 ± 0.4	3.6 ± 1.5	-	288 ± 65	2.1 ± 0.5
III	^{18}F-FEMPA	LDLR$^{-/-}$ApoB$^{100/100}$	2.4 ± 0.6	4.9 ± 1.3	0.30	266 ± 85	0.5 ± 0.1
	^{18}F-FEMPA	C57BL/6N	1.9 ± 0.2	3.6 ± 0.7		-	-
IV	^{18}F-FDG (HFD)	LDLR$^{-/-}$ApoB$^{100/100}$	1.3 ± 0.4	5.2 ± 2.3		209 ± 92	1.6 ± 0.3
	^{18}F-FDG (Chow)	LDLR$^{-/-}$ApoB$^{100/100}$	0.7 ± 0.2	2.8 ± 0.9	0.011	104 ± 70	1.6 ± 0.2
	^{18}F-FDG (HFD+A)	LDLR$^{-/-}$ApoB$^{100/100}$	1.0 ± 0.4	3.9 ± 1.8	0.37	155 ± 88	1.4 ± 0.3

[a]I-III: vs. C57BL/6N mice, IV: vs. HFD group

Effects of interventions on ^{18}F-FDG biodistribution (IV)

Similarly to the *in vivo* measurements, *ex vivo* ^{18}F-FDG uptake in the aortas (both SUV and TBR) was lower in the Chow group than in the HFD group ($p < 0.001$ and $p = 0.011$). HFD+A group did not differ from HFD or Chow group in SUV or TBR values.

5.5 Autoradiography studies

Ex vivo autoradiography

The uptake of tracers in plaque, normal vessel wall and vessel-surrounding adventitia was analyzed as count density in digital ARG. The count densities were normalized to injected dose/mouse weight and the proportion of radioactivity decayed during the ARG exposure.

^{68}Ga-DOTANOC and ^{68}Ga-DOTATATE showed significantly higher uptake in plaques than in normal vessel wall, but for ^{18}F-FDR-NOC, the plaque uptake was only marginally higher than in wall. Uptake in adventitia was lower than the plaque uptake in all tracers.

^{18}F-FMCH uptake in plaques was high in both LDLR$^{-/-}$ApoB$^{100/100}$ and IGF-II/LDLR$^{-/-}$ApoB$^{100/100}$ mice, leading to high plaque-to-wall ratio (2.5 and 2.6, respectively). The plaque uptake also exceeded the adventitial uptake in both strains. ^{18}F-FDG uptake showed a similar pattern, but in IGF-II/LDLR$^{-/-}$ ApoB$^{100/100}$ mice, the plaque-to-wall ratio was lower than that of ^{18}F-FMCH.

^{18}F-FEMPA was an exception out of the studied tracers, since its uptake was more pronounced in the normal vessel wall than in plaques. The plaque uptake was, however, higher than that of adventitia. All of the ARG results are listed in Table 8.

Effects of interventions on autoradiography (IV)

The Chow intervention led to lower uptake in plaque, wall and adventitia, as compared to the HFD group. The respective uptakes in the HFD+A group did not significantly differ from the HFD group or the Chow group. The plaque-to-wall ratios were equal between all the groups.

Comparison of tracer uptake and macrophage content in plaques (II, III)

Both ^{18}F-FMCH and ^{18}F-FEMPA showed higher uptake in macrophage-rich plaque areas than in areas with low macrophage content. ^{18}F-FMCH showed significantly higher count densities in areas with high than low macrophage density (110 ± 5.3 vs. 81 ± 4.5 PSL/mm^2, $p = 0.0027$). ^{18}F-FEMPA showed highest uptake in macrophage-rich plaques. The count densities were 40 ± 13, 67 ± 22, 140 ± 30, and 190 ± 54 PSL/mm^2 in areas of no macrophages, low,

intermediate and high macrophage density, respectively. Compared to areas with no macrophages, uptake was significantly higher in the plaques with intermediate ($p = 0.0017$) or high macrophage density ($p < 0.001$). The data on comparison of tracer uptake and macrophage content in plaque is shown in Figure 6.

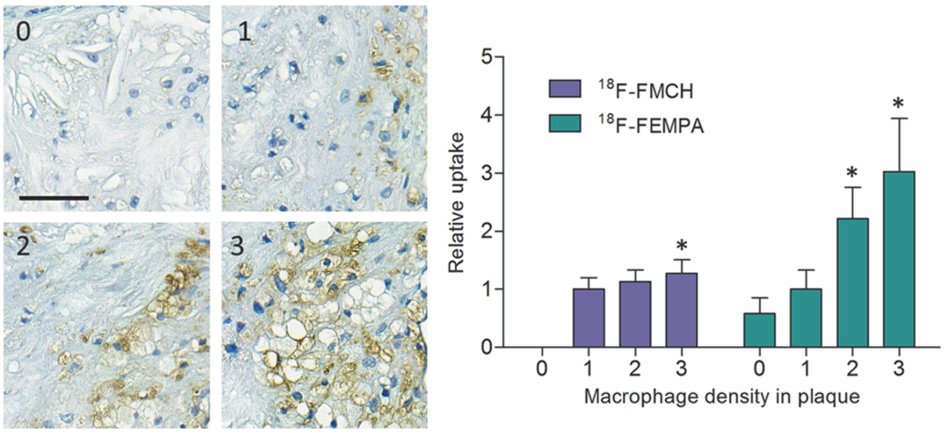

Figure 6. Comparison of ^{18}F-FMCH and ^{18}F-FEMPA plaque uptake in autoradiography and macrophage density in plaques. The macrophage density in plaques (brown color in histological stainings) is classified as 0: no macrophages, 1: low (occasional macrophages), 2: intermediate (scattered groups of macrophages) and 3: high (confluent areas of macrophages). Scale bar: 50 µm. Tracer uptake is presented relative to the uptake in plaques with macrophage density class 1, both tracers separately. *Significant difference to the lowest macrophage density class ($p < 0.05$).

In vitro autoradiography (III)

The specificity of ^{18}F-FEMPA binding to plaques was studied by *in vitro* ARG study with a competitive TSPO binder, PK11195. ^{18}F-FEMPA binding tended to be higher in CD68-positive areas (760 ± 520 PSL/mm^2) than in the α-SMA-positive areas (230 ± 220 PSL/mm^2, $p = 0.091$). The count densities were lowered by 75 % in the CD68 positive areas and by 79 % in the α-SMA-positive areas in the presence of 100 × molar excess of PK11195. In the mouse aortic sections, blocking with PK11195 lowered the count densities by 79 % in the plaques ($p = 0.0058$) and 84 % in the vessel wall of atherosclerotic mice ($p < 0.001$).

5.6 Correlation of plasma biomarkers and tracer uptake (I, II, IV)

In study I, the uptake of ^{68}Ga-DOTANOC and ^{18}F-FDR-NOC in plaques (measured as plaque-to-wall ratio) was compared with plasma levels of IL-6, MCP-1, RANTES, C-peptide, insulin, and leptin. The ^{68}Ga-DOTANOC uptake was directly correlated with plasma IL-6, insulin and leptin levels and tended to correlate with MCP-1, whereas ^{18}F-FDR-NOC uptake showed no correlations with cytokines or metabolic markers.

The uptake of ^{18}F-FMCH uptake in plaques (count density, PSL/mm^2, pooled data from LDLR$^{-/-}$ApoB$^{100/100}$ and IGF-II/LDLR$^{-/-}$ApoB$^{100/100}$ mice) was compared to plasma levels of total cholesterol, phospholipids, triglycerides, PLTP, PON-1, glucagon, glucose, C-peptide, insulin, leptin, IFN-γ, IL-6, MCP-1 and RANTES. The plaque ^{18}F-FMCH uptake showed positive correlation with total cholesterol, PLTP, C-peptide, insulin and leptin. A trend towards positive correlation was observed with plasma PON-1activity, IL-6 and RANTES. No correlation was observed with other measured markers.

The interventional groups were pooled for the correlation analysis. ^{18}F-FDG uptake, measured as *in vivo* and *ex vivo* TBR and plaque uptake in ARG, was compared with levels of plasma total cholesterol, triglycerides, IL-6, MCP-1, insulin and leptin. Plasma total cholesterol levels were positively correlated with TBR *in vivo* ($r = 0.38$, $p = 0.037$), *ex vivo* ($r = 0.46$, $p = 0.005$) and plaque uptake in ARG ($r = 0.47$, $p = 0.005$). Plaque uptake in ARG also showed positive correlation with leptin levels ($r = 0.52$, $p = 0.002$).

6 DISCUSSION

6.1 Animal models

The mice were bred and housed in the University of Turku Central Animal Laboratory and they were generally in good health. Some mice had inflamed skin xanthomas, which are typical for these strains especially on high-fat diet. In study IV, five mice were sacrificed before the end of the study due to severe xanthomas or weight loss. The coincidental findings in the apparently healthy mice included one aortic aneurysm, one kidney cyst, a few tumors and cases of cirrhotic livers. IGF-II/LDLR$^{-/-}$ApoB$^{100/100}$ mice also exhibited cases of eye problems, such as half-blindness.

The mouse models utilized in this thesis, LDLR$^{-/-}$ApoB$^{100/100}$and IGF-II/LDLR$^{-/-}$ApoB$^{100/100}$, are not utilized as widely as ApoE$^{-/-}$ and LDLR$^{-/-}$ mice. Especially the IGF-II/LDLR$^{-/-}$ApoB$^{100/100}$ mouse model has not been thoroughly characterized, since only a few studies have been published (Heinonen et al. 2007; Heinonen et al. 2011; Silvola et al. 2011b; Kinnunen et al. 2013; Laplante et al. 2013). These models have a lipid profile which is closer to that in human FH, especially compared to the ApoE$^{-/-}$ model. This is an advantage especially in translational studies. These two mouse models also enable studies on the effects of type II diabetes on atherosclerosis, since both strains have similar lipid levels but IGF-II/LDLR$^{-/-}$ApoB$^{100/100}$ mice also exhibit insulin resistance and mildly-elevated glucose levels (Heinonen et al. 2007). Despite the similar plasma lipid levels, IGF-II/LDLR$^{-/-}$ApoB$^{100/100}$ mice may present higher inflammatory activity in plaques (Heinonen et al. 2007), which was also supported by our results in study II, although the amounts of M1 and M2 macrophages were similar between the strains.

Despite the lipid profiles in the mice resembling human FH, the mouse models do not depict the whole spectrum of human atherosclerosis. In the two models utilized in this thesis, plaques develop mainly in the aorta, whereas the human disease focuses on coronary arteries. Plaque ruptures in mice are also extremely rare. In addition, neoangiogenesis and the presence of smooth muscle cells in the intima is nearly absent in mice. In mice, the inflammatory process in plaques tends to diminish with increasing age, whereas in humans the plaques progress throughout the lifespan. The experimental mice also live in very clean facilities, and they generally do not encounter infections during their lifetimes, which may affect the disease development.

In preclinical imaging studies, it is self-evident, that the target of the imaging agent must be present in the animal model in order to get reliable results. Nevertheless, lack of other features of the disease, such as plaque ruptures, might not be a concern in this application. Regarding the use of mice in testing new therapies for atherosclerosis, it must be taken into account that mice do not respond to treatments similarly as men, and that the choice of mouse model may affect the treatment response. Again, the target of the drug to be tested should be

present in the model. The mouse models utilized in this thesis were suitable for their purpose, since they presented large numbers of macrophages in the plaques. In addition, the limited responsiveness to statins in $LDLR^{-/-}ApoB^{100/100}$ mice was part of the study design in study IV. (Zadelaar et al. 2007; Getz and Reardon 2012; Hag et al. 2013)

6.2 Experimental methods

6.2.1 In vivo imaging

In vivo PET imaging in mice is always compromised because of the small size of the animals. This is even more pronounced in imaging small targets, such as atherosclerotic plaques. Partial volume and spillover effects need to be carefully considered in the analysis. In the studies presented in this thesis, the tracer uptake in the aorta was analyzed from the aortic arch and the background radioactivity from vena cava. The analysis was performed after a careful co-registration of images, and the ROIs were drawn to avoid spillover from adjacent organs. Despite the careful analysis, the TBR values measured from the *in vivo* images (at average 0.99 in all studied groups of mice) are lower than the TBR values from the *ex vivo* measurements (at average 2.4). In all of the studies, the aortic uptake analyzed from the *in vivo* images was lower than measured *ex vivo*.

6.2.2 Autoradiography

Ex vivo ARG was performed in all of the studies to confirm the distribution of tracer uptake within the aortic tissue. The method has been shown to be reproducible (Haukkala et al. 2009). The ARG was performed on longitudinal aortic sections in order to cover the whole aortic arch, branches and descending aorta. The analysis was done on several (six to ten) sections per mouse. In some cases, parts of the aorta were missing due to failed dissection or sectioning. This might affect the results, since tracer uptake is not necessarily similar in all plaques.

The ARG data was normalized to injected dose/mouse weight and the proportion of radioactivity decayed during exposure. The normalization was performed to each study separately, so the PSL/mm^2 values are not comparable between studies, but should be that within each study. However, in study I, there were tracers with different isotopes, and these are not comparable to each other. The PSL/mm^2 values were normalized separately for ^{18}F-FDR-NOC and ^{68}Ga tracers. One limitation of the ARG in the studies is the lack of data conversion to Becquerel values. For that, a standard with known radioactivity should have been included in each ARG exposure.

The digital ARG has a wide dynamic range. It might, however, underestimate the count density in very thin structures such as vessel wall, since the radiation scatters from its origin to the surrounds, especially with ^{68}Ga-labelled tracers due

to higher positron energy. The vessel wall ROIs were placed in areas where the media is free of plaque formation and surrounding adventitia, and the ROI is very narrow. In the analyzed larger areas, such as plaques or adventitia, the scatter effect is not as strong.

6.2.3 Detection of macrophages and assessing plaque burden

Macrophage antigen Mac-3 was utilized in all studies as a universal macrophage marker. Mac-3 is a glycoprotein, which is expressed in macrophages, but not in monocytes or lymphoid cells (Ho and Springer 1983). Mac-3 staining was chosen mainly because the staining protocols were already established and worked well. However, Mac-3 might not be the best option for detecting macrophages, since fibroblast cells may also express Mac-3 (Inoue et al. 2005). In addition to Mac-3, F4/80 and CD68 are commonly-utilized macrophage markers. Whilst CD68 staining is a highly specific and sensitive marker for macrophages in humans, F4/80 might be the best option in mice, since it has no cross-reactions with other cell types (Inoue et al. 2005).

The choice of M1 and M2 markers was a challenging task, since there are multiple different markers utilized. iNOS was chosen since it is induced in the pro-inflammatory activation and is restricted to M1-polarized macrophages. The production of NO in macrophages is mediated by iNOS and it is required for anti-microbial functions. It is an intracellular enzyme, and therefore a better choice for immunohistochemistry than secreted proteins. MRC-1 is a surface receptor, which is up-regulated in M2 polarization, and is one of the classical M2 markers. MRC-1 expression is, however, not restricted in M2. It may also be expressed in other types of macrophages. The division of M1- and M2-specific molecules is not strict, since these two polarization states are more the ends of a continuum rather that two distinct and separate cell types. Differences between species may also occur. Therefore, there are no perfect markers, but these give an estimation of the subsets. (Martinez et al. 2006)

The quantitation of histology is a topic undergoing debate. There are always differences in the stainings done at separate occasions, even if it is carried out in exactly the same way each time. The antibodies represent different characteristics, and for example, in study II, the areal percentage of MRC-1-positive M2 macrophages in aortic root intima was higher than the area of Mac-3-positive macrophages, which are supposed to represent the whole macrophage population. The detection of DAB, a brown color in immunohistochemical stains, is dependent on the computational algorithms. The quantitation divides the analyzed areas into DAB-positive or -negative areas and it might over- or underestimate the DAB-positive area depending on the quality of staining. However, the computer-based algorithms give observer-independent and quantitative results, which are of great use for the analyses.

There are a large number of options for assessing the plaque burden. The most often-utilized methods include *en face* analysis of the aorta and analysis of the

aortic root sections from the level of aortic sinus. Analysis from other vascular beds, such as the brachiocephalic artery or aorta at the level of renal arteries, is also possible, but rarely used (Daugherty and Rateri 2005). In this thesis, the plaque burden was measured from the aortic root sections at the level of coronary ostia. This level differs slightly from the level of aortic sinus, since the valve leaflets are not fully present in all sections. However, all the sections were performed similarly, and should therefore provide reliable results on plaque burden. The *en face* analysis was not feasible in this study, since the aortas were sectioned for ARG.

6.2.4 Plasma biomarker measurements

The measurement of biomarkers was mainly performed from the plasma samples obtained when the mouse was sacrificed. Therefore, the mice have been under anesthesia, and if fasting was not included in the study protocol, the samples are derived in fed state. Therefore, the results must be interpreted with caution. The cytokine and metabolic marker measurements were performed with Luminex kits. The results exhibited great variation between animals, resulting in non-significant differences between the strains. The kits are very convenient, since multiple markers can be measured simultaneously, but the reliability of the results remains an open question.

6.3 Evaluation of the tracers for imaging atherosclerotic plaque inflammation

6.3.1 SSTR-2-targeting tracers

Somatostatin is a regulatory neuropeptide which is produced by multiple different cell types, such as neurons and inflammatory cells. It inhibits the effects of growth hormone, thyroid-stimulating hormone, as well as the production of gastrointestinal hormones such as insulin and glucagon. It also suppresses angiogenesis and cell proliferation and has a role in mediating effects between neuroendocrine and inflammatory systems. The effects of somatostatin are mediated by SSTRs (SSTR1-5), which are G-protein coupled receptors. These receptors are expressed in highest numbers in the central nervous system, pituitary gland, gastrointestinal tract and pancreas. Expression is also common in many tumors as well as inflammatory cells. SSTR-2 are expressed in macrophages, especially in the activated state. (Dalm et al. 2003; Pintér et al. 2006; Armani et al. 2007; Ameri and Ferone 2012)

SSTR-imaging has been commonly utilized in the imaging of neuroendocrine tumors, but it has been studied in the imaging of atherosclerosis. In retrospective studies on cancer patients, SSTR-2-targeting PET tracers ^{68}Ga- and ^{64}Cu-DOTATATE have shown uptake in atherosclerotic arteries and correlation with cardiovascular risk factors (Rominger et al. 2010; Li et al. 2012). Another SSTR-

targeting tracer, ^{68}Ga-DOTATOC, however, did not correlate with risk factors for atherosclerosis (Malmberg et al. 2015).

Our study showed increased uptake of two SSTR-2-targeting tracers, ^{68}Ga-DOTANOC and ^{68}Ga-DOTATATE, in atherosclerotic aortas and plaques, compared to in healthy aortas or normal vessel wall, respectively. However, the aorta-to-blood ratios did not differ between the atherosclerotic and healthy mice in the *in vivo* or *ex vivo* measurements, since blood radioactivity was also elevated in the atherosclerotic mice. The third tracer studied, ^{18}F-FDR-NOC, showed similar uptake in atherosclerotic and healthy aortas, and the count densities in plaques and normal vessel wall had only minimal difference. The cause for this is not known, since both ^{68}Ga-DOTANOC and ^{18}F-FDR-NOC share the same NOC peptide, which is responsible for the SSTR-binding. The glycosylation might affect the biodistribution and pharmacokinetic properties of the novel tracer.

^{68}Ga-DOTANOC showed superior characteristics to ^{68}Ga-DOTATATE. The results showed consistently higher ^{68}Ga-DOTANOC uptake, as measured *in vivo*, *ex vivo* or in ARG. ^{68}Ga-DOTANOC also showed higher aorta-to-blood ratio in the head-to-head *in vivo* comparison. The correlation of ^{68}Ga-DOTANOC uptake in plaques with plasma IL-6 and the tendency to correlate with MCP-1 also link the uptake with higher systemic inflammatory activity. Correlation was also observed to insulin and leptin, which are both associated with increased risk of cardiovascular events (Ducimetiere et al. 1980; Koh et al. 2008). We did not analyze the correlation of macrophages and ^{68}Ga-DOTANOC uptake, but in the ARG they were visually co-localized. In a previous study, ^{64}Cu-DOTATATE uptake was shown to better correlate with CD163-positive macrophages than general macrophage marker CD68, indicating preferential uptake by M2 macrophages (Pedersen et al. 2015).

The remaining ^{68}Ga-DOTANOC radioactivity in blood was at the same level as in the aortas, leading to an aorta-to-blood ratio of 1.2 *ex vivo*. This might limit the utility of the tracer in clinical imaging. However, in the *ex vivo* biodistribution measurements, the aorta also includes the normal vessel wall and adventitia, which have significantly less tracer uptake as measured in the ARG. Therefore, the plaque-to-blood ratio, which would be the measurement in the case of clinical imaging, would be higher.

The concept of atherosclerosis imaging with SSTR-targeting tracers is still new and under investigation. Although there is only a limited amount of data on the correlation of histopathology and tracer uptake, the consensus is that SSTR-targeted imaging might be an important tool in assessing plaque inflammation. The potential of it in assessing the effects of inflammation has shown promise, but needs larger studies to be confirmed (Schatka et al. 2013). All in all, the results of this study support the utilization of SSTR-2-targeted imaging in the detection of inflamed atherosclerotic plaques. To our knowledge, ^{68}Ga-DOTANOC has not yet been studied in clinical imaging of atherosclerosis, and

therefore further studies in other pre-clinical models and in clinical settings are needed to establish the value of ^{68}Ga-DOTANOC.

6.3.2 ^{18}F-FMCH

Choline is an essential nutrient which is needed for the formation of phosphatidylcholine for cell membranes and for acetylcholine for neurotransmission. Phosphatidylcholines are phospholipids which contain choline in the hydrophilic head, whereas phosphorylcholine refers to the choline-containing head. Choline is taken into cells via choline transporters, which are present in all nucleated cells. The uptake of choline in cells is mediated by specific choline transporters and choline transporter-like proteins. Uptake is also mediated by other molecules, such as organic cation transporters. The metabolism of choline includes three routes: phosphorylation, oxidation and acetylation, leading to formation of phosphorylcholine, betaine and acetylcholine, respectively. (Li and Vance 2008)

Increased uptake and metabolism of choline is observed in cancer cells and activated macrophages (Boggs et al. 1995; Katz-Brull et al. 2002). Radiolabelled derivatives of choline are currently utilized in the imaging of prostate cancer and other malignant diseases (DeGrado et al. 2001; Treglia et al. 2012). Studies have also shown tracer uptake associated with inflammatory processes, such as joint inflammation in rheumatoid arthritis (Roivainen et al. 2003) and soft tissue infection (Wyss et al. 2004). A couple of animal studies and small-scale clinical studies have shown uptake of ^{11}C-choline and ^{18}F-FMCH in atherosclerotic arteries in patients (Matter et al. 2006; Bucerius et al. 2008; Kato et al. 2009; Laitinen et al. 2010).

In study II, ^{18}F-FMCH showed increased uptake in diabetic atherosclerosis, compared to non-diabetic mice, and the uptake was associated with a higher amount of macrophages in the lesions. The reasons for these remain unknown. Increased choline transport has been suggested to be responsible for the uptake in macrophages. The choline kinase levels have shown no differences between atherosclerotic and healthy aortas suggesting similar choline metabolism (Matter et al. 2006). Hypoxia or LPS stimulation do not increase choline uptake, whereas they both significantly increase ^{18}F-FDG uptake (Hara et al. 2006; Schwarz et al. 2016). There seems to be differences in choline metabolism associated with diabetes (Floegel et al. 2013; Svingen et al. 2016). However, the underlying mechanisms are not well known. We observed correlation of ^{18}F-FMCH uptake with total cholesterol, insulin and leptin, which are all associated with increased risk of atherosclerosis (Ducimetiere et al. 1980; Stamler et al. 1986; Koh et al. 2008). There was also a tendency of correlation with IL-6, which was higher in the IGF-II/LDLR$^{-/-}$ApoB$^{100/100}$ mice than in LDLR$^{-/-}$ApoB$^{100/100}$ mice. The clearance of ^{18}F-FMCH from the blood to tissues was also more efficient, since the tracer was less present in blood and urine in diabetic mice. Although the choline uptake is generally associated with cell proliferation, this might not be the case in atherosclerosis. The cells do proliferate in plaques, but not at as high a

rate as in tumors. We observed only a few occasional Ki-67 positive cells in plaques, so the proliferation does not explain the uptake.

^{18}F-FMCH was superior to ^{18}F-FDG in the diabetic mice, measured as plaque-to-wall ratio, and the aorta-to-blood ratio was similar. The myocardial uptake of ^{18}F-FMCH is lower than that of ^{18}F-FDG, which might facilitate coronary artery imaging. However, the myocardial uptake was still lower than aortic uptake, which might limit coronary artery imaging. In patient studies, no significant myocardial uptake of choline-based PET tracers has been observed, so this might not eventually limit the imaging of coronary atherosclerosis. As the imaging of diabetic patients with ^{18}F-FDG might be problematic because of competing glucose in the bloodstream (Bucerius et al. 2012; Bucerius et al. 2014), ^{18}F-FMCH might be a good option for this purpose. Based on the promising results on ^{18}F-FMCH imaging in diabetic atherosclerosis, a clinical study is being planned.

6.3.3 ^{18}F-FEMPA

TSPO is a mitochondrial membrane protein which has multiple functions. It was first recognized as a peripheral benzodiazepine receptor, but was later re-named to better depict its function (Papadopoulos et al. 2006). It is mainly localized in the outer mitochondrial membrane as a complex with a voltage-dependent anion channel and adenine nucleotide transporter. Its most important functions include cholesterol transport for steroid biosynthesis as well as transport of proteins and porphyrin. TSPO is expressed ubiquitously, but in highest numbers in tissues involved in steroid biosynthesis. The expression of TSPO is 20-fold higher in human macrophages than in VSMCs (Bird et al. 2010). However, species differences have been observed, since rat VSMCs express high levels of TSPO (French and Matlib 1988).

TSPO has been studied as a drug target for multiple diseases, including atherosclerosis. TSPO has a role in cholesterol efflux from the cells, and therefore it is an interesting target for mediating lipid removal from the lesions. TSPO overexpression increases cholesterol efflux from macrophages and reduces macrophage foam cell formation. The cholesterol efflux can also be achieved with treatment with TSPO ligands, implicating potential for atherosclerosis treatment (Taylor et al. 2014). Reduction of blood cholesterol is also observed if cholesterol-binding domain of TSPO is given as a peptide treatment (Lecanu et al. 2013). TSPO ligands may also have anti-inflammatory effects mediated by inhibition of NLRP3 inflammasome (Lee et al. 2016).

There is quite limited amount of information on TSPO expression in different macrophage polarization states. In a study conducted in a mouse model of intracerebral hemorrhage, TSPO expression was observed in both M1 and M2 macrophages/microglia (Bonsack et al. 2016). TSPO-targeting tracer ^{11}C-PBR28 has shown increased uptake in LPS-treated cultured macrophages, compared to in non-activated macrophages. However, the increase was modest (35 %)

compared to the increase of ^{18}F-FDG uptake following LPS stimulation (175 %) (English et al. 2014).

TSPO is commonly utilized as an imaging target for neuroinflammatory diseases. There are multiple different ligands for TSPO radiolabelled for PET imaging, starting from the prototypic ^{11}C-PK11195 to a number of second-generation ligands. The utilization of TSPO-targeting tracers for the imaging of atherosclerosis is significantly less studied, but shows promise, although hindered by low target-to-background ratio. ^{11}C-PK11195 has shown uptake in atherosclerotic lesions, but the target-to-background ratio has been low. (Gaemperli et al. 2012)

In our study, the PET tracer ^{18}F-FEMPA showed fast blood clearance and uptake in atherosclerotic plaques, but uptake was also observed in the healthy vessel wall. The uptake in atherosclerotic plaques was associated with the amount of macrophages and was shown to be specific. The uptake of ^{18}F-FEMPA in vascular walls of mice was pronounced and specific, since the VSMCs were positive for TSPO, and the tracer accumulation could be blocked *in vitro* with unlabeled PK11195. However, in the human sections, the tracer accumulation was more pronounced in the macrophage-positive areas than in VSMCs. Therefore, uptake in vascular wall might be limited to rodents, which reflects the species differences observed earlier (French and Matlib 1988; Mak and Barnes 1990).

In the *in vivo* imaging, the aorta-to-blood ratio was low and did not show differences between atherosclerotic and healthy mice. The low aorta-to-blood ratio *in vivo* might be due to underestimation of aortic uptake, overestimation of blood uptake, or most probably, both. The partial volume effects may affect the analyzed aortic uptake, as well as inclusion of blood with low radioactivity in the ROI, leading to underestimated SUV values. The blood SUV was higher as measured *in vivo* than *ex vivo*, and this might be caused by spillover from the high uptake in vascular wall or other surrounding tissues.

^{18}F-FEMPA showed potential in the imaging of atherosclerosis, but the observed low target-to-background ratio is a disadvantage. The high uptake in normal vessel wall and relatively high uptake in the myocardium and lungs might limit its use in clinical imaging of atherosclerosis, but imaging of more intense arterial inflammation, such as in vasculitis, could be more feasible.

6.3.4 Diet and atorvastatin interventions and ^{18}F-FDG

Statins inhibit the HMG-CoA reductase enzyme, which catalyzes the endogenous cholesterol biosynthesis (Istvan and Deisenhofer 2001). This leads to enhanced LDLR expression in hepatocytes, which increases the cellular cholesterol intake and thus lowers blood cholesterol. The effects of statins in mice without LDLR are therefore compromised. However, the intake of cholesterol to hepatocytes may be mediated by LRPs or receptor-independent mechanisms in the absence of LDLR (Véniant et al. 1998). Statins may also have effects independent of

cholesterol lowering, including lowering of inflammation (Schwartz et al. 2001; Cannon et al. 2004; Collins et al. 2004; Blum and Shamburek 2009).

In our study, the diet intervention efficiently lowered the total cholesterol levels. The atorvastatin intervention also led to significantly lower cholesterol levels, although the decrease was less than with diet intervention. The lipoprotein clearance mechanisms in LDLR$^{-/-}$ApoB$^{100/100}$ mouse model are defective, since both the LDLR-mediated and LRP-mediated clearance are impaired (Véniant et al. 1998; Powell-Braxton et al. 1998). The intracellular cholesterol levels in hepatocytes might paradoxically be low due to the impaired cellular intake. Therefore, cholesterol biosynthesis might still be active in this mouse model regardless of the high cholesterol levels in bloodstream (Bisgaier et al. 1997). The inhibition of endogenous cholesterol biosynthesis by statins might therefore lower the plasma cholesterol levels. The cholesterol intake from bloodstream to hepatocytes might also be mediated by receptor-independent mechanisms.

Diet intervention resulted in lower plaque burden and amount of macrophages in the aortic root, which was expected based on previous study (Saraste et al. 2012). Atorvastatin treatment did not affect the plaque size, which is inconsistent with previous studies on LDLR$^{-/-}$ mice, since statin treatment has resulted in smaller lesion size in multiple studies (Wang et al. 2002; Chen 2002; Zadelaar et al. 2007; Eussen et al. 2011). In addition, the atorvastatin treatment did not show effects on the amount of macrophages in plaques.

The ^{18}F-FDG PET/CT imaging, *ex vivo* measurements and ARG showed consistent results, which also reflected the histology. The Chow group represented the lowest and the HFD group the highest aortic ^{18}F-FDG TBR both *in vivo* and *ex vivo*. The atorvastatin intervention did not have significant effects on aortic ^{18}F-FDG uptake, compared to the HFD group. Thus, no cholesterol-independent effects of atorvastatin were observed, since also the amount of macrophages was unchanged, compared to the HFD group, despite the lower plasma cholesterol values. ^{18}F-FDG uptake was also positively correlated with plasma cholesterol levels, which was not the case in a previous clinical study (Tawakol et al. 2013).

The plaque uptake in ARG reflected the ^{18}F-FDG TBR values. However, the plaque-to-wall ratio showed no differences between the interventional groups and did not correlate with the measured TBR values. This was unexpected, since the plaque-to-wall ratio has been a standard way to assess the plaque uptake. The reasons why ^{18}F-FDG uptake in the apparently normal vessel wall was also affected by the interventions are not known.

As can be seen in Figure 5, myocardial ^{18}F-FDG uptake in the study was intense, although the mice were fasted for 4 hours prior to tracer injection. One major reason for this is the anesthesia, since isoflurane intensively increases the myocardial uptake of ^{18}F-FDG. Myocardial uptake could be suppressed by utilizing other types of anesthesia, such as ketamine-xylazine, or by performing tracer injection and distribution without anesthesia (Thackeray et al. 2015). This

should be taken into account when planning *in vivo* imaging of atherosclerosis in small animals.

In vivo ^{18}F-FDG PET/CT was sensitive in detecting plaque inflammation, although the differences between groups in the *in vivo* imaging were subtle, compared to the *ex vivo* measurements and ARG. Therefore, the *in vivo* PET/CT imaging of atherosclerotic plaque inflammation in mice cannot replace the *ex vivo* analyses, but might give additional value due to its repeatability. Further studies are needed to evaluate the value of *in vivo* PET/CT imaging of atherosclerosis in mice.

6.4 Future aspects

PET imaging of inflammation in atherosclerosis has evolved tremendously during the last decade, starting from the observation of ^{18}F-FDG uptake in the arteries in 2002 (Rudd et al. 2002). Imaging devices have evolved from separate PET and anatomical imaging to multimodal PET/CT and PET/MRI cameras, which are more and more available around the world. Numerous new tracers have been identified and evaluated. The role of imaging has moved from detecting the rupture-prone plaques to evaluating therapy responses and studying the pathobiology of the disease.

The development of PET, CT and MRI techniques and their combinations has majorly impacted the vascular imaging. Especially PET/MRI has potential to be developed further, since MRI brings more versatility over CT. Lack of radiation dose to patient is also an advantage. The increased versatility include, for example, the variety of different MRI sequences for better soft-tissue contrast (Rischpler et al. 2013) and use of dual-modality tracers (Nahrendorf et al. 2008). In preclinical imaging, the size of blood vessels especially in mice is a limitation; therefore, the high spatial resolution of MRI is an advantage. There are, however, some limitations. The PET/MRI combination is a challenge itself, since the magnetic field of MRI unit may cause interference for PET detectors. In addition, the MRI-based attenuation correction methods need further evaluation. Although the motion correction for breathing and corrections for partial volume effects are possible, they would require development, especially in preclinical applications. The longer imaging times with MRI compared to CT may also limit the wider use of PET/MRI. For these reasons, it is unlikely that PET/MRI would completely replace PET/CT; however, it most likely will be increasingly utilized in selected applications. The use of PET/MRI in preclinical evaluation of PET tracers for imaging plaque inflammation will probably increase. More evidence and guidelines for PET/MR imaging are needed for the increased use in clinical practice. (Catana et al. 2013; Rischpler et al. 2013; Bailey et al. 2016)

In addition to ^{18}F-FDG, new tracers for identifying inflamed or rupture-prone plaques have emerged. In the future, employment of other tracers than ^{18}F-FDG as a tool to assess vascular inflammation in atherosclerosis is likely. One imaging agent that has gained much attention has been ^{18}F-NaF, which accumulates in

sites of active calcification process and detects also very small calcifications which are not detected by traditional calcium score scanning (Joshi et al. 2014; Irkle et al. 2015). Clinical prospective studies on ^{18}F-NaF imaging to identify high-risk plaques are ongoing (Tarkin et al. 2016). Another new potential tracer for imaging inflammation in atherosclerosis is ^{18}F-FDM, which might have more specific uptake to macrophages than ^{18}F-FDG (Tahara et al. 2014). One new aspect in the imaging of inflammation is the whole-body view instead of looking only the inflammation in individual plaques (Nahrendorf et al. 2015). Increased knowledge on macrophage cellular biology has also been employed in imaging. The polarization state of macrophages as well as the local proliferation in lesions have been recognized as important imaging aspects (Satomi et al. 2013; Tavakoli et al. 2013; Ye et al. 2015). In this thesis, ^{18}F-FMCH was identified as a promising tracer especially for detecting atherosclerotic plaque inflammation in the presence of diabetes. Clinical studies are being planned based on the results.

There are a number of practical issues that limit the use of PET imaging. The costs of PET/CT or PET/MRI imaging are high, and the access to imaging devices or certain tracers might also limit imaging. Therefore it is likely, that PET imaging of inflammation in atherosclerosis will remain more as a research tool than as a risk assessment method used in clinical practice. However, the availability of commercial PET tracers has increased, and imaging devices are implemented in use around the world, which facilitates the increasing use in research purposes. The ^{68}Ga-labelled tracers are produced from generator-derived ^{68}Ga and no on-site cyclotron is needed, which facilitates imaging in hospitals and research centers without access to a radiochemistry laboratory. ^{18}F-labelled tracers can also be transported from one facility to another, as long as the transport time is short enough.

All in all, imaging of inflammation in atherosclerosis is a field with active and innovative ongoing research. The development of technology and new findings in basic research drive the imaging field forward. Advances in creating more refined animal models will probably increase the reliability of result translation to humans. Especially novel models combining aspects of cardiovascular and metabolic disease are of major importance (Heinonen et al. 2015). The use of PET/CT and PET/MRI imaging will be an important part of atherosclerosis research in the future. The focus of research will probably move from evaluating new PET tracers to other aspects. Imaging can give a new sight to disease pathobiology and be useful in characterizing new preclinical models. In addition, the use of imaging in assessing therapy responses in preclinical and clinical drug development will probably expand. These areas of research will be increasingly studied in the coming years.

7 SUMMARY AND CONCLUSIONS

Altogether, six PET tracers targeting macrophages in atherosclerotic plaques were evaluated in mouse models. In summary, the main findings were that:

1. Somatostatin receptor-targeting tracer ^{68}Ga-DOTANOC was superior to ^{18}F-FDR-NOC and ^{68}Ga-DOTATATE in the detection of inflamed atherosclerotic plaques.

2. The aortic ^{18}F-FMCH uptake was increased by type 2 diabetes and reflected the plaque inflammation. Comparison with ^{18}F-FDG suggested potential for ^{18}F-FMCH in the imaging of vascular inflammation in diabetes.

3. ^{18}F-FEMPA showed rapid blood clearance and uptake in the aorta. The tracer uptake in plaques correlated with the amount of macrophages, but the high uptake in normal vessel wall might limit its utility.

4. Atorvastatin therapy did not show effects on inflammation in atherosclerotic lesions in mice, determined by histology and aortic ^{18}F-FDG uptake, whereas diet intervention was effective.

Of the studied tracers, ^{18}F-FMCH showed the highest potential in the imaging of inflammation in atherosclerosis in addition to ^{18}F-FDG. The other studied tracers, except for ^{18}F-FDR-NOC, also showed suitable characteristics for *in vivo* imaging, but had some specific limitations.

8 ACKNOWLEDGEMENTS

This study was conducted during the years 2010-2016 in Turku PET Centre, Institute of Clinical Medicine, Department of Clinical Physiology and Nuclear Medicine, Turku University Hospital and University of Turku, Turku, Finland. I express my appreciation to Professor Jaakko Hartiala, the head of Department of Clinical Physiology and Nuclear Medicine and Professor Juhani Knuuti, the Director of Turku PET Centre (and head of Department of Clinical Physiology and Nuclear Medicine since May 2016), for providing the excellent facilities for research.

I want to warmly thank my supervisors, Professor Anne Roivainen and Associate Professor Antti Saraste. Without your help and valuable guidance this thesis would not be here. In addition to the scientific issues, I have also been able to rely on the financing of the studies, which is a crucial aspect in research. In addition to Anne and Antti, Juhani is also thanked for acquiring the research funds. Anne, you have given critical expertise in preclinical studies, and it has always been easy to come to your office with any questions or worries. Antti, your knowledge in clinical imaging and cardiology has been most valuable, and your effort in editing the manuscripts has been essential.

I wish to thank the official reviewers of my thesis: Adjunct Professor Katariina Öörni and Doctor Fabien Hyafil. I appreciate your valuable constructive comments and suggestions. I warmly thank my supervisory board members, Professor Emeritus Pekka Saukko, Academy Research Fellow Eriika Savontaus and Professor Juhani Knuuti for giving directions and support. The Director of FinPharma Doctoral Programme, Mika Scheinin, and Director of Drug Research Doctoral Programme, University of Turku, Markku Koulu, are most warmly thanked. The coordinator of DRDP, Eeva Valve, also is acknowledged for such great organization of all DRDP events and giving the all necessary information related to the doctoral programme.

I wish to thank the staff of Central Animal Laboratory of University of Turku. Director Ulla-Marjut Jaakkola, the office staff Aila Saari and Nina Kulmala as well as veterinarians Rafael Frias and Emrah Yatkin are warmly thanked. The animal technicians, especially Seija Lindqvist, Riina Valtonen, Nea Konttinen, Terhi Hiltula-Maisala and Anitta Niittymäki (in memoriam) deserve great thanks for taking care of all the mice. Regarding the histotechnology, the technicians have been essential. Liisa Lempiäinen, Erica Nyman, Marja-Riitta Kajaala, Taija Leinonen, Duyen Le, Minna Grönroos and Sinikka Collanus are warmly thanked. Timo Kattelus is acknowledged for skilled image processing and Ville Aalto for help with statistics.

Turku PET Centre personnel, both past and present, are warmly thanked for all help and for providing such a great atmosphere for work. Mirja Jyrkinen, Laura Jaakkola and Sinikka Lehtola are thanked for secretarial matters and Tarja Marttila for taking care of university project finances. Marko Tättäläinen and Rami Mikkola are acknowledged for their assistance in all IT issues and the

Carimas team for creating and improving the PET analysis software. I wish to thank the laboratory technicians, especially Sanna Suominen, Eija Salo, Heidi Partanen and Hanna Liukko-Sipi, for all the help with PET laboratory issues, helping with Wizard and making glucose measurements. Tarja Keskitalo is thanked for taking care of dosimeters and Minna Aatsinki for scheduling. Mika Teräs, Marko Tirri and Tuula Tolvanen are acknowledged for all the help with PET technology and managing radiation safety. Päivi Marjamäki is warmly thanked for the kind and skillful assistance especially in the *in vitro* studies. Aake Honkaniemi and Leena Tokoi-Eklund have been essential in the animal imaging, thank you for that! Anni Ukkonen and Marja Jeskanen are acknowledged for their valuable summer work and Tuija Orre for HPLC analyses. All the members of CoE, Anne's Gallium group and cardiac projects group are also warmly thanked for their keen interest in science and nice discussions. Thanks also for all the conversations around the coffee table, especially to Virva and Marita.

The co-authors and collaborators have been crucial for this study. Seppo Ylä-Herttuala from University of Eastern Finland is acknowledged for essential collaboration within the CoE. Matti Jauhiainen, Jari Metso and Sari Nuutinen from National Institute of Health and Welfare are warmly thanked for providing lipid measurements and expertise on those topics. Matti, your knowledge and enthusiasm in the lipid research is inspiring! Anu Airaksinen and Kerttuli Helariutta from University of Helsinki are acknowledged for fruitful collaboration regarding ^{18}F-FDR-NOC. Andrea Thiele, Anja Hoffman and their colleagues from Bayer are acknowledged for contribution in planning and writing of ^{18}F-FEMPA-study. Pirjo Nuutila is warmly thanked for contribution in the issues regarding diabetes and metabolism and also for providing financial support by the SUMMIT/ENSO projects. I wish to thank Pekka Saukko, Jukka Laine and Maria Gardberg for expertise in pathology and Harri Hakovirta for providing essential artery samples for research. The radiochemists are warmly thanked: Without the tracer syntheses, no studies could have been done. Thank you Olli Eskola, Meeri Käkelä, Xiang-Guo Li, Pauliina Luoto, Olli Metsälä, Nina Sarja, Tapio Viljanen and all other personnel involved in the cyclotron operation and radiochemistry for producing the tracers. Petteri Rinne deserves special thanks for putting the pieces together and forming a cohesive article from all the NOC-studies (that truly helped tremendously). Johanna Silvola is thanked for the guidance in everything: from breeding the mice to lab work, data analysis and writing. Heidi Liljenbäck, Suvi Sippola and Jenni Virta, your involvement in the animal studies has been essential. Especially Heidi deserves thanks for the skillful animal handling and keeping the lab in order. Max Kiugel and Mia Ståhle are thanked for skilled assistance and nice company during the long days in the lab (and outside the lab as well).

Our group members during the years have been one key factor in the process. Special thanks to Iina Laitinen for giving me the first introduction to PET and atherosclerotic mouse studies. Thank you for being the 1st generation plaque researcher and setting up all the methods, it was easy for the next generations to follow! Anu, Helena, Johanna, Juho, Maria, Max, Mia, Miikka, Petri, Reija and Riikka: without all you, this work would have been impossible to cope with.

Thanks for sharing the experience (and the office) and providing me support and fun company. The moments shared in the office, lab and in congress trips will never be forgotten. Teamwork is the best!

The friends from my M.Sc. studies ("päiväkahviseura") – especially Iida, Anu, Annemari, Henkka and Joonas – thank you for the nice gatherings around the coffee table or elsewhere. The Salo girls, Soile, Emmi, Henna, Tiia and Salla: you deserve great thanks for long-lasting friendship. Andrei, thank you for the help with Minni and staying friends for all these years. Samu, you have been a great support during this process, thank you for the friendship and all the help. I also wish to thank my cousin Heidi, you have been a dear friend to me all these years. Vauhtisammakon juoksukoulu is also warmly thanked for giving me the opportunity to get exercise, nice company and fresh air for my brain all in one.

Finally, I wish to thank my parents Liisa and Jukka and my brothers Janne and Jarno for all the support. Kiitos.

The study was conducted within the Finnish Centre of Excellence in Cardiovascular and Metabolic Diseases supported by the Academy of Finland, University of Turku, Turku University Hospital and Åbo Akademi University. Funding was received from FinPharma Doctoral Programme and Drug Research Doctoral Programme, University of Turku Graduate School. Grants for this research were obtained from Finnish Cultural Foundation, Varsinais-Suomi Regional Fund, Turku University Foundation, Ida Montin's Foundation, Aarne Koskelo Foundation, Emil Aaltonen Foundation, Sigrid Jusélius Foundation and Finnish Foundation for Cardiovascular Research.

Turku, December 2016

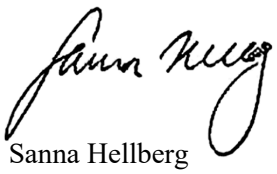

Sanna Hellberg

9 REFERENCES

Abela GS, Aziz K (2006) Cholesterol crystals rupture biological membranes and human plaques during acute cardiovascular events-a novel insight into plaque rupture by scanning electron microscopy. Scanning 28:1–10.

Aikawa E (2015) Cardiovascular imaging: Arterial and aortic valve inflammation and calcification. Springer. pp 12–26.

Ameri P, Ferone D (2012) Diffuse endocrine system, neuroendocrine tumors and immunity: what's new? Neuroendocrinology 95:267–276.

Antonov AS, Kolodgie FD, Munn DH, Gerrity RG (2004) Regulation of macrophage foam cell formation by αVβ3 integrin. Am J Pathol 165:247–258.

Armani C, Catalani E, Balbarini A, et al (2007) Expression, pharmacology, and functional role of somatostatin receptor subtypes 1 and 2 in human macrophages. J Leukoc Biol 81:845–855.

Baigent C, Keech A, Kearney P, et al (2005) Efficacy and safety of cholesterol-lowering treatment: prospective meta-analysis of data from 90 056 participants in 14 randomised trials of statins. Lancet 366:1267–1278.

Bailey DL, Pichler BJ, Gückel B, et al (2016) Combined PET/MRI: from status quo to status go. Summary report of the fifth international workshop on PET/MR imaging; February 15-19, 2016; Tübingen, Germany. Mol Imaging Biol 18:637–650.

Bala G, Blykers A, Xavier C, et al (2016) Targeting of vascular cell adhesion molecule-1 by ^{18}F-labelled nanobodies for PET/CT imaging of inflamed atherosclerotic plaques. Eur Heart J Cardiovasc Imaging 17:1001-1008.

Barter PJ, Caulfield M, Eriksson M, et al (2007) Effects of torcetrapib in patients at high risk for coronary events. N Engl J Med 357:2109–2122.

Beer AJ, Pelisek J, Heider P, et al (2014) PET/CT imaging of integrin αvβ3 expression in human carotid atherosclerosis. JACC Cardiovasc Imaging 7:178–187.

Bird JLE, Izquierdo-Garcia D, Davies JR, et al (2010) Evaluation of translocator protein quantification as a tool for characterising macrophage burden in human carotid atherosclerosis. Atherosclerosis 210:388–391.

Bisgaier CL, Essenburg AD, Auerbach BJ, et al (1997) Attenuation of plasma low density lipoprotein cholesterol by select 3-hydroxy-3-methylglutaryl coenzyme A reductase inhibitors in mice devoid of low density lipoprotein receptors. J Lipid Res 38:2502–2515.

Blum A, Shamburek R (2009) The pleiotropic effects of statins on endothelial function, vascular inflammation, immunomodulation and thrombogenesis. Atherosclerosis 203:325–330.

Boggs KP, Rock CO, Jackowski S (1995) Lysophosphatidylcholine and 1-O-octadecyl-2-O-methyl-rac-glycero-3- phosphocholine inhibit the CDP-choline pathway of phosphatidylcholine synthesis at the CTP:phosphocholine cytidylyltransferase step. J. Biol. Chem. 270:7757–7764.

Bonsack F, Alleyne CH, Sukumari-Ramesh S (2016) Augmented expression of TSPO after intracerebral hemorrhage: a role in inflammation? J Neuroinflammation 13:151.

Bot I, Shi G-P, Kovanen PT (2015) Mast cells as effectors in atherosclerosis. Arterioscler Thromb Vasc Biol 35:265–271.

Brooks PC, Clark RA, Cheresh DA (1994) Requirement of vascular integrin alpha v beta 3 for angiogenesis. Science 264:569–571.

Bucerius J, Hyafil F, Verberne HJ, et al (2016) Position paper of the Cardiovascular committee of the European association of nuclear medicine (EANM) on PET imaging of atherosclerosis. Eur J Nucl Med Mol Imaging. 43(4):780-792.

Bucerius J, Mani V, Moncrieff C, et al (2012) Impact of noninsulin-dependent type 2 diabetes on carotid wall ^{18}F-fluorodeoxyglucose positron emission tomography uptake. J Am Coll Cardiol 59:2080–2088.

Bucerius J, Mani V, Moncrieff C, et al (2014) Optimizing ^{18}F-FDG PET/CT imaging of vessel wall inflammation: the impact of ^{18}F-FDG circulation time, injected dose, uptake parameters, and fasting blood glucose levels. Eur J Nucl Med Mol Imaging 41:369–383.

Bucerius J, Schmaljohann J, Böhm I, et al (2008) Feasibility of ^{18}F-fluoromethylcholine PET/CT for imaging of vessel wall alterations in humans - first results. Eur J Nucl Med Mol Imaging 35:815–820.

Bulgarelli A, Leite ACA, Dias AAM, Maranhão RC (2013) Anti-atherogenic effects of methotrexate carried by a lipid nanoemulsion that binds to ldl receptors in cholesterol-fed rabbits. Cardiovasc Drugs Ther 27:531–539.

Bulgarelli A, Martins Dias AA, Caramelli B, Maranhão RC (2012) Treatment with methotrexate inhibits atherogenesis in cholesterol-fed rabbits. J Cardiovasc Pharmacol 59:308–314.

Buono C, Binder CJ, Stavrakis G, et al (2005) T-bet deficiency reduces atherosclerosis and alters plaque antigen-specific immune responses. Proc Natl Acad Sci U S A 102:1596–1601.

Bäck M, Hansson GK (2015) Anti-inflammatory therapies for atherosclerosis. Nat Rev Cardiol 12:199–211.

Cannon CP, Braunwald E, McCabe CH, et al (2004) Intensive versus moderate lipid lowering with statins after acute coronary syndromes. N Engl J Med 350:1495–1504.

Catana C, Guimaraes AR, Rosen BR (2013) PET and MR imaging: the odd couple or a match made in heaven? J Nucl Med 54:815–824.

Chauveau F, Van Camp N, Dollé F, et al (2009) Comparative evaluation of the translocator protein radioligands ^{11}C-DPA-713, ^{18}F-DPA-714, and ^{11}C-PK11195 in a rat model of acute neuroinflammation. J Nucl Med 50:468–476.

Chen Z (2002) Simvastatin reduces neointimal thickening in low-density lipoprotein receptor-deficient mice after experimental angioplasty without changing plasma lipids. Circulation 106:20–23.

Chistiakov DA, Bobryshev Y V, Nikiforov NG, et al (2015) Macrophage phenotypic plasticity in atherosclerosis: the associated features and the peculiarities of the expression of inflammatory genes. Int J Cardiol 184:436–445.

Chiu J-J, Chien S (2011) Effects of disturbed flow on vascular endothelium: pathophysiological basis and clinical perspectives. Physiol Rev 91:327–387.

Cines DB, Pollak ES, Buck CA, et al (1998) Endothelial cells in physiology and in the pathophysiology of vascular disorders. Blood 91:3527–3561.

Cochain C, Zernecke A (2015) Macrophages and immune cells in atherosclerosis: recent advances and novel concepts. Basic Res Cardiol 110:34.

Colin S, Chinetti-Gbaguidi G, Staels B (2014) Macrophage phenotypes in atherosclerosis. Immunol Rev 262:153–166.

Collins R, Armitage J, Parish S, et al (2004) Effects of cholesterol-lowering with simvastatin on stroke and other major vascular events in 20 536 people with cerebrovascular disease or other high-risk conditions. Lancet 363:757–767.

Cormode DP, Roessl E, Thran A, et al (2010) Atherosclerotic plaque composition: analysis with multicolor CT and targeted gold nanoparticles. Radiology 256:774–782.

Cybulsky M, Iiyama K, Li H, et al (2001) A major role for VCAM-1, but not ICAM-1, in early atherosclerosis. J Clin Invest 107:1255–1262.

Dalm VASH, van Hagen PM, van Koetsveld PM, et al (2003) Expression of somatostatin, cortistatin, and somatostatin receptors in human monocytes, macrophages, and dendritic cells. Am J Physiol Endocrinol Metab 285:E344–E353.

Daugherty A, Rateri DL (2005) Development of experimental designs for atherosclerosis studies in mice. Methods 36:129–138.

Davies JR, Izquierdo-Garcia D, Rudd JHF, et al (2010) FDG-PET can distinguish inflamed from non-inflamed plaque in an animal model of atherosclerosis. Int J Cardiovasc Imaging 26:41–48.

De Meyer GRY, De Cleen DMM, Cooper S, et al (2002) Platelet phagocytosis and processing of β-amyloid precursor protein as a mechanism of macrophage activation in atherosclerosis. Circ Res 90:1197–1204.

DeGrado TR, Baldwin SW, Wang S, et al (2001) Synthesis and evaluation of ^{18}F-labeled choline analogs as oncologic PET tracers. J Nucl Med 42:1805–1814.

Di Angelantonio E, Sarwar N, Perry P, et al (2009) Major lipids, apolipoproteins, and risk of vascular disease. JAMA 302:1993–2000.

Drechsler M, Megens RTA, Van Zandvoort M, et al (2010) Hyperlipidemia-triggered neutrophilia promotes early atherosclerosis. Circulation 122:1837–1845.

Ducimetiere P, Eschwege E, Papoz L, et al (1980) Relationship of plasma insulin levels to the incidence of myocardial infarction and coronary heart disease mortality in a middle-aged population. Diabetologia 19:205–210.

Duewell P, Kono H, Rayner KJ, et al (2010) NLRP3 inflammasomes are required for

atherogenesis and activated by cholesterol crystals. Nature 464:1357–1361.

Ehara S, Kobayashi Y, Yoshiyama M, et al (2004) Spotty calcification typifies the culprit plaque in patients with acute myocardial infarction: an intravascular ultrasound study. Circulation 110:3424–3429.

Ehlgen A, Bylock A, Kreuzer J, et al (2015) Clinical imaging in anti-atherosclerosis drug development. Drug Discov Today 20:1317–1327.

Elhage R, Maret A, Pieraggi M-T, et al (1998) Differential effects of interleukin-1 receptor antagonist and tumor necrosis factor binding protein on fatty-streak formation in apolipoprotein E–deficient mice. Circulation 97:242–244.

Elkhawad M, Rudd JHF, Sarov-Blat L, et al (2012) Effects of p38 mitogen-activated protein kinase inhibition on vascular and systemic inflammation in patients with atherosclerosis. JACC Cardiovasc Imaging 5:911–922.

Elmaleh DR, Fischman AJ, Tawakol A, et al (2006) Detection of inflamed atherosclerotic lesions with diadenosine-5',5'''-P1,P4-tetraphosphate (Ap4A) and positron-emission tomography. Proc Natl Acad Sci U S A 103:15992–15996.

English SJ, Diaz JA, Shao X, et al (2014) Utility of ^{18}F-FDG and ^{11}C-PBR28 microPET for the assessment of rat aortic aneurysm inflammation. EJNMMI Res 4:20.

Eussen SRBM, Rompelberg CJM, Andersson KE, et al (2011) Simultaneous intake of oat bran and atorvastatin reduces their efficacy to lower lipid levels and atherosclerosis in LDLr-/- mice. Pharmacol Res 64:36–43.

Everett BM, Pradhan AD, Solomon DH, et al (2013) Rationale and design of the Cardiovascular inflammation reduction trial: a test of the inflammatory hypothesis of atherothrombosis. Am Heart J 166:199–207.

Fayad ZA, Mani V, Woodward M, et al (2011) Safety and efficacy of dalcetrapib on atherosclerotic disease using novel non-invasive multimodality imaging (dal-PLAQUE): A randomised clinical trial. Lancet 378:1547–1559

Feil S, Fehrenbacher B, Lukowski R, et al (2014) Transdifferentiation of vascular smooth muscle cells to macrophage-like cells during atherogenesis. Circ Res 115:662–667.

Figueroa AL, Abdelbaky A, Truong QA, et al (2013) Measurement of arterial activity on routine FDG PET/CT images improves prediction of risk of future CV events. JACC Cardiovasc Imaging 6:1250–1259.

Floegel A, Stefan N, Yu Z, et al (2013) Identification of serum metabolites associated with risk of type 2 diabetes using a targeted metabolomic approach. Diabetes 62:639–648.

Folco EJ, Sheikine Y, Rocha VZ, et al (2011) Hypoxia but not inflammation augments glucose uptake in human macrophages: Implications for imaging atherosclerosis with ^{18}fluorine-labeled 2-deoxy-D-glucose positron emission tomography. J Am Coll Cardiol 58:603–614.

French JF, Matlib MA (1988) Identification of a high-affinity peripheral-type benzodiazepine binding site in rat aortic smooth muscle membranes. J Pharmacol Exp Ther 247:23–28.

Fujimura Y, Hwang PM, Trout H, et al (2008) Increased peripheral benzodiazepine receptors in arterial plaque of patients with atherosclerosis: An autoradiographic study with [^{3}H]PK11195. Atherosclerosis 201:108–111.

Gaemperli O, Shalhoub J, Owen DRJ, et al (2012) Imaging intraplaque inflammation in carotid atherosclerosis with ^{11}C-PK11195 positron emission tomography/computed tomography. Eur Heart J 33:1902–1910.

Gaztanaga J, Farkouh M, Rudd JHF, et al (2015) A phase 2 randomized, double-blind, placebo-controlled study of the effect of VIA-2291, a 5-lipoxygenase inhibitor, on vascular inflammation in patients after an acute coronary syndrome. Atherosclerosis 240:53–60.

GBD 2013 Mortality and Causes of Death Collaborators (2015) Global, regional, and national age-sex specific all-cause and cause-specific mortality for 240 causes of death, 1990-2013: A systematic analysis for the Global Burden of Disease Study 2013. Lancet 385:117–171.

Getz GS, Reardon CA. (2012) Animal models of atherosclerosis. Arterioscler Thromb Vasc Biol 32:1104–1115.

Ginhoux F, Jung S (2014) Monocytes and macrophages: developmental pathways and tissue homeostasis. Nat Rev Immunol 14:392–404.

Gleissner CA, Shaked I, Little KM, Ley K (2010) CXC chemokine ligand 4 induces a unique

transcriptome in monocyte-derived macrophages. J Immunol 184:4810–4818.

Habib A, Finn AV. (2014) The role of iron metabolism as a mediator of macrophage inflammation and lipid handling in atherosclerosis. Front Pharmacol 5:1–6.

Hag AMF, Pedersen SF, Christoffersen C, et al (2012) ^{18}F-FDG PET imaging of murine atherosclerosis: association with gene expression of key molecular markers. PLoS One 7:e50908.

Hag AMF, Ripa RS, Pedersen SF, et al (2013) Small animal positron emission tomography imaging and in vivo studies of atherosclerosis. Clin Physiol Funct Imaging 33:173–85.

Hamacher K, Coenen HH, Stöcklin G (1986) Efficient stereospecific synthesis of no-carrier-added 2-[^{18}F]-fluoro-2-deoxy-D-glucose using aminopolyether supported nucleophilic substitution. J Nucl Med 27:235–238.

Hamzah J, Kotamraju VR, Seo JW, et al (2011) Specific penetration and accumulation of a homing peptide within atherosclerotic plaques of apolipoprotein E-deficient mice. Proc Natl Acad Sci U S A 108:7154–7159.

Hansson GK, Hermansson A (2011) The immune system in atherosclerosis. Nat Immunol 12:204–212.

Hansson GK, Libby P (2006) The immune response in atherosclerosis: a double-edged sword. Nat Rev Immunol 6:508–519.

Hara T, Bansal A, DeGrado TR (2006) Effect of hypoxia on the uptake of [methyl-^{3}H]choline, [1-^{14}C] acetate and [^{18}F]FDG in cultured prostate cancer cells. Nucl Med Biol 33:977–984.

Haukkala J, Laitinen I, Luoto P, et al (2009) ^{68}Ga-DOTA-RGD peptide: biodistribution and binding into atherosclerotic plaques in mice. Eur J Nucl Med Mol Imaging 36:2058–2067.

Heinonen SE, Genové G, Bengtsson E, et al (2015) Animal models of diabetic macrovascular complications: key players in the development of new therapeutic Approaches. J Diabetes Res 2015:404085.

Heinonen SE, Leppänen P, Kholová I, et al (2007) Increased atherosclerotic lesion calcification in a novel mouse model combining insulin resistance, hyperglycemia, and hypercholesterolemia. Circ Res 101:1058–1067.

Heinonen SE, Merentie M, Hedman M, et al (2011) Left ventricular dysfunction with reduced functional cardiac reserve in diabetic and non-diabetic LDL-receptor deficient apolipoprotein B100-only mice. Cardiovasc Diabetol 10:59.

Herrington W, Lacey B, Sherliker P, et al (2016) Epidemiology of atherosclerosis and the potential to reduce the global burden of atherothrombotic disease. Circ Res 118:535–546.

Hilgendorf I, Swirski FK (2012) Making a difference: Monocyte heterogeneity in cardiovascular disease. Curr Atheroscler Rep 14:450–459.

Hirano K, Young SG, Farese RV, et al (1996) Targeted disruption of the mouse apobec-1 gene abolishes apolipoprotein B mRNA editing and eliminates apolipoprotein B48. J Biol Chem 271:9887–9890.

Ho MK, Springer TA. (1983) Tissue distribution, structural characterization, and biosynthesis of Mac-3, a macrophage surface glycoprotein exhibiting molecular weight heterogeneity. J Biol Chem 258:636–642.

Hoshiga M, Alpers CE, Smith LL, et al (1995) Alpha-v beta-3 integrin expression in normal and atherosclerotic artery. Circ Res 77:1129–1135.

Hsieh H-J, Liu C-A, Huang B, et al (2014) Shear-induced endothelial mechanotransduction: the interplay between reactive oxygen species (ROS) and nitric oxide (NO) and the pathophysiological implications. J Biomed Sci 21:3.

Huber SA, Sakkinen P, David C, et al (2001) T helper-cell phenotype regulates atherosclerosis in mice under conditions of mild hypercholesterolemia. Circulation 103:2610–2616.

Hyafil F, Cornily J-C, Feig JE, et al (2007) Noninvasive detection of macrophages using a nanoparticulate contrast agent for computed tomography. Nat Med 13:636–641.

Hyafil F, Cornily J-C, Rudd JHF, et al (2009) Quantification of inflammation within rabbit atherosclerotic plaques using the macrophage-specific CT contrast agent N1177: a comparison with ^{18}F-FDG PET/CT and histology. J Nucl Med 50:959–965.

Inoue T, Plieth D, Venkov CD, et al (2005) Antibodies against macrophages that overlap in specificity with fibroblasts. Kidney Int 67:2488–2493.

Irkle A, Vesey AT, Lewis DY, et al (2015) Identifying active vascular microcalcification

by ^{18}F-sodium fluoride positron emission tomography. Nat Commun 6:7495.

Ishibashi S, Brown MS, Goldstein JL, et al (1993) Hypercholesterolemia in low density lipoprotein receptor knockout mice and its reversal by adenovirus-mediated gene delivery. J Clin Invest 92:883–893.

Ishii H, Nishio M, Takahashi H, et al (2010) Comparison of atorvastatin 5 and 20 mg/d for reducing F-18 fuorodeoxyglucose uptake in atherosclerotic plaques on positron emission tomography/computed tomography: a randomized, investigator-blinded, open-label, 6-month study in Japanese adults scheduled for percutaneous coronary Intervention. Clin Ther 32:2337–2347.

Ishino S, Ogawa M, Mori I, et al (2014) 18F-FDG PET and intravascular ultrasonography (IVUS) images compared with histology of atherosclerotic plaques: ^{18}F-FDG accumulates in foamy macrophages. Eur J Nucl Med Mol Imaging 41:624–633.

Istvan ES, Deisenhofer J (2001) Structural mechanism for statin inhibition of HMG-CoA reductase. Science 292:1160–1164.

Jacobsson LTH, Turesson C, Gülfe A, et al (2005) Treatment with tumor necrosis factor blockers is associated with a lower incidence of first cardiovascular events in patients with rheumatoid arthritis. J Rheumatol 32:1213–1218.

Janoudi A, Shamoun FE, Kalavakunta JK, Abela GS (2016) Cholesterol crystal induced arterial inflammation and destabilization of atherosclerotic plaque. Eur Heart J. 37:1959-1967.

Jauhiainen M, Ehnholm C (2005) Determination of human plasma phospholipid transfer protein mass and activity. Methods 36:97–101.

Jezovnik MK, Zidar N, Lezaic L, et al (2014) Identification of inflamed atherosclerotic lesions in vivo using PET-CT. Inflammation 37:426–434.

Johnson RC, Chapman SM, Dong ZM, et al (1997) Absence of P-selectin delays fatty streak formation in mice. J Clin Invest 99:1037–1043.

Joshi NV, Vesey AT, Williams MC, et al (2014) ^{18}F-fluoride positron emission tomography for identification of ruptured and high-risk coronary atherosclerotic plaques: a prospective clinical trial. Lancet 383:705–713.

Kadl A, Meher AK, Sharma PR, et al (2010) Identification of a novel macrophage phenotype that develops in response to atherogenic phospholipids via Nrf2. Circ Res 107:737–746.

Kato K, Schober O, Ikeda M, et al (2009) Evaluation and comparison of ^{11}C-choline uptake and calcification in aortic and common carotid arterial walls with combined PET/CT. Eur J Nucl Med Mol Imaging 36:1622–1628.

Katz-Brull R, Seger D, Rivenson-Segal D, et al (2002) Metabolic markers of breast cancer: Enhanced choline metabolism and reduced choline-ether-phospholipid synthesis. Cancer Res 62:1966–1970.

Kinnunen K, Heinonen SE, Kalesnykas G, et al (2013) LDLR$^{-/-}$ApoB$^{100/100}$ mice with insulin-like growth factor II overexpression reveal a novel form of retinopathy with photoreceptor atrophy and altered morphology of the retina. Mol Vis 19:1723–1733.

Kiviniemi A, Gardberg M, Autio A, et al (2014) Feasibility of experimental BT4C glioma models for somatostatin receptor 2-targeted therapies. Acta Oncol 53:1125–1134.

Kleemola P, Freese R, Jauhiainen M, et al (2002) Dietary determinants of serum paraoxonase activity in healthy humans. Atherosclerosis 160:425–432.

Koh KK, Park SM, Quon MJ (2008) Leptin and cardiovascular disease: response to therapeutic interventions. Circulation 117:3238–3249.

Laitinen I, Marjamäki P, Haaparanta M, et al (2006) Non-specific binding of [^{18}F]FDG to calcifications in atherosclerotic plaques: Experimental study of mouse and human arteries. Eur J Nucl Med Mol Imaging 33:1461–1467.

Laitinen I, Marjamäki P, Någren K, et al (2009a) Uptake of inflammatory cell marker [^{11}C]PK11195 into mouse atherosclerotic plaques. Eur J Nucl Med Mol Imaging 36:73–80.

Laitinen I, Saraste A, Weidl E, et al (2009b) Evaluation of αvβ3 integrin-targeted positron emission tomography tracer ^{18}F-galacto-RGD for imaging of vascular inflammation in atherosclerotic mice. Circ Cardiovasc Imaging 2:331–338.

Laitinen IEK, Luoto P, Någren K, et al (2010) Uptake of ^{11}C-choline in mouse atherosclerotic plaques. J Nucl Med 51:798–802.

Lamare F, Hinz R, Gaemperli O, et al (2011) Detection and quantification of large-vessel inflammation with ^{11}C-(R)-PK11195 PET/CT. J Nucl Med 52:33–39.

Laplante M-A, Charbonneau A, Avramoglu RK, et al (2013) Distinct metabolic and vascular effects of dietary triglycerides and cholesterol in atherosclerotic and diabetic mouse models. Am J Physiol Endocrinol Metab 305:E573–84.

Laurberg JM, Olsen AK, Hansen SB, et al (2007) Imaging of vulnerable atherosclerotic plaques with FDG-microPET: No FDG accumulation. Atherosclerosis 192:275–282.

Lecanu L, Yao ZX, McCourty A, et al (2013) Control of hypercholesterolemia and atherosclerosis using the cholesterol recognition/interaction amino acid sequence of the translocator protein TSPO. Steroids 78:137–146.

Lee J-W, Kim LE, Shim H-J, et al (2016) A translocator protein 18 kDa ligand, Ro5-4864, inhibits ATP-induced NLRP3 inflammasome activation. Biochem Biophys Res Commun 474:587–593.

Li X, Bauer W, Kreissl MC, et al (2013) Specific somatostatin receptor II expression in arterial plaque: ^{68}Ga-DOTATATE autoradiographic, immunohistochemical and flow cytometric studies in apoE-deficient mice. Atherosclerosis 230:33–39.

Li X, Samnick S, Lapa C, et al (2012) ^{68}Ga-DOTATATE PET/CT for the detection of inflammation of large arteries: correlation with18F-FDG, calcium burden and risk factors. EJNMMI Res 2:52.

Li Z, Vance DE (2008) Phosphatidylcholine and choline homeostasis. J Lipid Res 49:1187–1194.

Libby P (2002) Inflammation in atherosclerosis. Nature 420:868–874.

Libby P, Theroux P (2005) Pathophysiology of coronary artery disease. Circulation 111:3481–3488.

Lindner JR (2009) Molecular imaging of cardiovascular disease with contrast-enhanced ultrasonography. Nat Rev Cardiol 6:475–81.

Liu J, Kerwin WS, Caldwell JH, et al (2016) High resolution FDG-microPET of carotid atherosclerosis: plaque components underlying enhanced FDG uptake. Int J Cardiovasc Imaging 32:145–152.

Liu Y, Pierce R, Luehmann HP, et al (2013) PET Imaging of chemokine receptors in vascular injury–accelerated atherosclerosis. J Nucl Med 54:1135-1141.

Liuzzo G, Goronzy JJ, Yang H, et al (2000) Monoclonal T-cell proliferation and plaque instability in acute coronary syndromes. Circulation 101:2883–2888.

Lobatto ME, Fayad ZA, Silvera S, et al (2010) Multimodal clinical imaging to longitudinally assess a nanomedical anti-inflammatory treatment in experimental atherosclerosis. Mol Pharm 7:2020–2029.

Luehmann HP, Detering L, Fors BP, et al (2016) PET/CT Imaging of chemokine receptors in inflammatory atherosclerosis using targeted nanoparticles. J Nucl Med. 57:1124-1129.

Luehmann HP, Pressly ED, Detering L, et al (2014) PET/CT Imaging of chemokine receptor CCR5 in vascular injury model using targeted nanoparticle. J Nucl Med 55:629–634.

Mak JCW, Barnes PJ (1990) Peripheral type benzodiazepine receptors in human and guinea pig lung: characterization and sutoradiographic mapping. J Pharmacol Exp Ther 252:880–885.

Malmberg C, Ripa RS, Johnbeck CB, et al (2015) Atherosclerosis in large arteries and its correlation with risk factors: head-to-head comparison with ^{68}Ga-DOTATOC in 60 Patients. J Nucl Med 56:1895–1900.

Mankoff DA (2007) A definition of molecular imaging. J Nucl Med 48:18N- 21N.

Mantovani A, Garlanda C, Locati M (2009) Macrophage diversity and polarization in atherosclerosis: a question of balance. Arterioscler Thromb Vasc Biol 29:1419–1423.

Martinez FO, Gordon S, Locati M, Mantovani A (2006) Transcriptional profiling of the human monocyte-to-macrophage differentiation and polarization: new molecules and patterns of gene expression. J Immunol 177:7303–7311.

Mateo J, Izquierdo-Garcia D, Badimon JJ, et al (2014) Noninvasive assessment of hypoxia in rabbit advanced atherosclerosis using ^{18}F-fluoromisonidazole positron emission tomographic imaging. Circ Cardiovasc Imaging 7:312–320.

Matter CM, Wyss MT, Meier P, et al (2006) ^{18}F-choline images murine atherosclerotic plaques ex vivo. Arterioscler Thromb Vasc Biol 26:584–589.

McEvoy JW, Blaha MJ, DeFilippis AP, et al (2010) Coronary artery calcium progression: an important clinical measurement? J Am Coll Cardiol 56:1613–1622.

Millon A, Dickson SD, Klink A, et al (2013) Monitoring plaque inflammation in atherosclerotic rabbits with an iron oxide (P904) and ^{18}F-FDG using a combined

PET/MR scanner. Atherosclerosis 228:339–345.

Mizoguchi M, Tahara N, Tahara A, et al (2011) Pioglitazone attenuates atherosclerotic plaque inflammation in patients with impaired glucose tolerance or diabetes: a prospective, randomized, comparator-controlled study using serial FDG PET/CT imaging study of carotid artery and ascending aorta. JACC Cardiovasc Imaging 4:1110–1118.

Moore KJ, Tabas I (2011) Macrophages in the pathogenesis of atherosclerosis. Cell 145:341–355.

Mosser DM, Edwards JP (2008) Exploring the full spectrum of macrophage activation. Nat Rev Immunol 8:958–969.

Mueller RL, Sanborn TA (1995) The history of interventional cardiology: cardiac catheterization, angioplasty, and related interventions. Am Heart J 129:146–172.

Myers KS, Rudd JHF, Hailman EP, et al (2012) Correlation between arterial FDG uptake and biomarkers in peripheral artery disease. JACC Cardiovasc Imaging 5:38–45.

Nahrendorf M, Frantz S, Swirski FK, et al (2015) Imaging systemic inflammatory networks in ischemic heart disease. J Am Coll Cardiol 65:1583–1591.

Nahrendorf M, Keliher E, Panizzi P, et al (2009) 18F-4V for PET-CT imaging of VCAM-1 expression in atherosclerosis. JACC Cardiovasc Imaging 2:1213–1222.

Nahrendorf M, Zhang H, Hembrador S, et al (2008) Nanoparticle PET-CT imaging of macrophages in inflammatory atherosclerosis. Circulation 117:379–387.

Nakamura I, Hasegawa K, Wada Y, et al (2013) Detection of early stage atherosclerotic plaques using PET and CT fusion imaging targeting P-selectin in low density lipoprotein receptor-deficient mice. Biochem Biophys Res Commun 433:47–51.

Nakashima Y, Raines EW, Plump AS, et al (1998) Upregulation of VCAM-1 and ICAM-1 at atherosclerosis-prone sites on the endothelium in the ApoE-deficient mouse. Arterioscler Thromb Vasc Biol 18:842–851.

Narula J, Garg P, Achenbach S, et al (2008) Arithmetic of vulnerable plaques for noninvasive imaging. Nat Clin Pract Cardiovasc Med 5 Suppl 2:S2–S10.

Nicholls SJ, Kastelein JJP, Schwartz GG, et al (2014) Varespladib and cardiovascular events in patients with an acute coronary syndrome: the VISTA-16 randomized clinical trial. JAMA 311:252–262.

Nidorf SM, Eikelboom JW, Budgeon CA, Thompson PL (2013) Low-dose colchicine for secondary prevention of cardiovascular disease. J Am Coll Cardiol 61:404–406.

Nissen SE, Tuzcu M, Schoenhagen P, et al (2005) Statin Therapy, LDL cholesterol, C-reactive protein, and coronary artery disease. N Engl J Med 352:29–38.

Ogawa M, Ishino S, Mukai T, et al (2004) ^{18}F-FDG accumulation in atherosclerotic plaques: immunohistochemical and PET imaging study. J Nucl Med 45:1245–1250.

Ogawa M, Magata Y, Kato T, et al (2006) Application of ^{18}F-FDG PET for monitoring the therapeutic effect of antiinflammatory drugs on stabilization of vulnerable atherosclerotic plaques. J Nucl Med 47:1845–1850.

Paeng JC, Lee YS, Lee JS, et al (2013) Feasibility and kinetic characteristics of ^{68}Ga-NOTA-RGD PET for in vivo atherosclerosis imaging. Ann Nucl Med 27:847–854.

Paigen B, Morrow A, Brandon C, et al (1985) Variation in susceptibility to atherosclerosis among inbred strains of mice. Atherosclerosis 57:65–73.

Papadopoulos V, Baraldi M, Guilarte TR, et al (2006) Translocator protein (18 kDa): new nomenclature for the peripheral-type benzodiazepine receptor based on its structure and molecular function. Trends Pharmacol Sci 27:402–409.

Pasterkamp G (2013) Methods of accelerated atherosclerosis in diabetic patients. Heart 99:743–749.

Patel SS, Thiagarajan R, Willerson JT, Yeh ET (1998) Inhibition of alpha4 integrin and ICAM-1 markedly attenuate macrophage homing to atherosclerotic plaques in ApoE-deficient mice. Circulation 97:75–81.

Pedersen SF, Sandholt BV, Keller SH, et al (2015) ^{64}Cu-DOTATATE PET/MRI for detection of activated macrophages in carotid atherosclerotic plaques: studies in patients undergoing endarterectomy. Arterioscler Thromb Vasc Biol 35:1696–1703.

Piedrahita JA, Zhang SH, Hagaman JR, et al (1992) Generation of mice carrying a mutant apolipoprotein E gene inactivated by gene targeting in embryonic stem cells. Proc Natl Acad Sci U S A 89:4471–4475.

Pintér E, Helyes Z, Szolcsányi J (2006) Inhibitory effect of somatostatin on inflammation and nociception. Pharmacol Ther 112:440–456.

Plump AS, Masucci-Magoulas L, Bruce C, et al (1999) Increased atherosclerosis in ApoE and LDL receptor gene knock-out mice as a result of human cholesteryl ester transfer protein transgene expression. Arterioscler Thromb Vasc Biol 19:1105–1110.

Plump AS, Smith JD, Hayek T, et al (1992) Severe hypercholesterolemia and atherosclerosis in apolipoprotein E-deficient mice created by homologous recombination in ES cells. Cell 71:343–353.

Powell-Braxton L, Véniant M, Latvala RD, et al (1998) A mouse model of human familial hypercholesterolemia: markedly elevated low density lipoprotein cholesterol levels and severe atherosclerosis on a low-fat chow diet. Nat Med 4:934–948.

Pugliese F, Gaemperli O, Kinderlerer AR, et al (2010) Imaging of vascular inflammation with [^{11}C]-PK11195 and positron emission tomography/computed tomography angiography. J Am Coll Cardiol 56:653–661.

Rader DJ, Cohen J, Hobbs HH (2003) Monogenic hypercholesterolemia : new insights in pathogenesis and treatment. J Clin Invest. 111:1795–1803.

Rajamäki K, Lappalainen J, Öörni K, et al (2010) Cholesterol crystals activate the NLRP3 inflammasome in human macrophages: a novel link between cholesterol metabolism and inflammation. PLoS One 5:e11765.

Reardon CA, Blachowicz L, White T, et al (2001) Effect of immune deficiency on lipoproteins and atherosclerosis in male apolipoprotein E-deficient mice. Arterioscler Thromb Vasc Biol 21:1011–1016.

Reiss AB, Carsons SE, Anwar K, et al (2008) Atheroprotective effects of methotrexate on reverse cholesterol transport proteins and foam cell transformation in human THP-1 monocyte/macrophages. Arthritis Rheum 58:3675–3683.

Ridker PM, Danielson E, Fonseca FA, et al (2009) Reduction in C-reactive protein and LDL cholesterol and cardiovascular event rates after initiation of rosuvastatin: a prospective study of the JUPITER trial. Lancet 373:1175–1182.

Ridker PM, Thuren T, Zalewski A, Libby P (2011) Interleukin-1β inhibition and the prevention of recurrent cardiovascular events: Rationale and design of the Canakinumab Anti-inflammatory Thrombosis Outcomes Study (CANTOS). Am Heart J 162:597–605.

Rischpler C, Nekolla SG, Dregely I, Schwaiger M (2013) Hybrid PET/MR imaging of the heart: potential, initial experiences, and future prospects. J Nucl Med 54:402–415.

Robbins CS, Hilgendorf I, Weber GF, et al (2013) Local proliferation dominates lesional macrophage accumulation in atherosclerosis. Nat Med 19:1166–1172.

Rodríguez-Prados J-C, Través PG, Cuenca J, et al (2010) Substrate fate in activated macrophages: a comparison between innate, classic, and alternative activation. J Immunol 185:605–614.

Roivainen A, Forsback S, Grönroos T, et al (2000) Blood metabolism of [methyl-^{11}C]choline; implications for in vivo imaging with positron emission tomography. Eur J Nucl Med 27:25–32.

Roivainen A, Parkkola R, Yli-Kerttula T, et al (2003) Use of positron emission tomography with methyl-^{11}C-choline and 2-^{18}F-fluoro-2-deoxy-D-glucose in comparison with magnetic resonance imaging for the assessment of inflammatory proliferation of synovium. Arthritis Rheum 48:3077–3084.

Rominger A, Saam T, Vogl E, et al (2010) In vivo imaging of macrophage activity in the coronary arteries using ^{68}Ga-DOTATATE PET/CT: correlation with coronary calcium burden and risk factors. J Nucl Med 51:193–197.

Rominger A, Saam T, Wolpers S, et al (2009) ^{18}F-FDG PET/CT identifies patients at risk for future vascular events in an otherwise asymptomatic cohort with neoplastic disease. J Nucl Med 50:1611–1620.

Rong JX, Shapiro M, Trogan E, Fisher EA (2003) Transdifferentiation of mouse aortic smooth muscle cells to a macrophage-like state after cholesterol loading. Proc Natl Acad Sci U S A 100:13531–13536.

Ross R, Glomset JA (1976a) The pathogenesis of atherosclerosis (first of two parts). N Engl J Med 295:369–377.

Ross R, Glomset JA (1976b) The pathogenesis of atherosclerosis (second of two parts). N Engl J Med 295:420–425.

Roubille F, Busseuil D, Shi Y, et al (2014) The interleukin-1β modulator gevokizumab reduces neointimal proliferation and improves reendothelialization in a rat carotid denudation model. Atherosclerosis 236:277–285.

Rudd JHF, Myers KS, Bansilal S, et al (2008) Atherosclerosis inflammation imaging with ^{18}F-FDG PET: Carotid, iliac, and femoral uptake reproducibility, quantification methods, and recommendations. J Nucl Med 49:871–878.

Rudd JHF, Myers KS, Bansilal S, et al (2007) ^{18}Fluorodeoxyglucose positron emission tomography imaging of atherosclerotic plaque inflammation is highly reproducible. Implications for atherosclerosis therapy trials. J Am Coll Cardiol 50:892–896.

Rudd JHF, Warburton EA, Fryer TD, et al (2002) Imaging atherosclerotic plaque inflammation with [^{18}F]-fluorodeoxyglucose positron emission tomography. Circulation 105:2708–2711.

Ruehm SG, Corot C, Vogt P, et al (2001) Magnetic resonance imaging of atherosclerotic plaque with ultrasmall superparamagnetic particles of iron oxide in hyperlipidemic rabbits. Circulation 103:415–422.

Sage AP, Tintut Y, Demer LL (2010) Regulatory mechanisms in vascular calcification. Nat Rev Cardiol 7:528–536.

Saraste A, Laitinen I, Weidl E, et al (2012) Diet intervention reduces uptake of αvβ3 integrin-targeted PET tracer ^{18}F-galacto-RGD in mouse atherosclerotic plaques. J Nucl Cardiol 19:775–784.

Satomi T, Ogawa M, Mori I, et al (2013) Comparison of contrast agents for atherosclerosis imaging using cultured macrophages: FDG versus ultrasmall superparamagnetic iron oxide. J Nucl Med 54:999–1004.

Scalia R, Gooszen ME, Jones SP, et al (2001) Simvastatin exerts both anti-inflammatory and cardioprotective effects in apolipoprotein E-deficient mice. Circulation 103:2598–2603.

Schatka I, Wollenweber T, Haense C, et al (2013) Peptide receptor-targeted radionuclide therapy alters inflammation in atherosclerotic plaques. J Am Coll Cardiol 62:2344–2345.

Schwartz G, Olsson A, Ezekowitz M, Ganz P (2001) Effects of atorvastatin on early recurrent ischemic events in acute coronary syndromes. JAMA 285:1711–1718.

Schwartz GG, Olsson AG, Abt M, et al (2012) Effects of dalcetrapib in patients with a recent acute coronary syndrome. N Engl J Med 367:2089–2099.

Schwarz T, Seidl C, Schiemann M, et al (2016) Increased choline uptake in macrophages and prostate cancer cells does not allow for differentiation between benign and malignant prostate pathologies. Nucl Med Biol 43:355–359.

Seo JW, Baek H, Mahakian LM, et al (2014) Cu-Labeled LyP - 1-dendrimer for PET-CT imaging of atherosclerotic plaque. Bioconjug Chem 25:231–239.

Shah PK, Chyu KY, Dimayuga PC, Nilsson J (2014) Vaccine for atherosclerosis. J Am Coll Cardiol 64:2779–2791.

Shapiro MD, Fazio S (2016) From lipids to inflammation. Circ Res 118:732–749.

Silvola JMU, Saraste A, Forsback S, et al (2011a) Detection of hypoxia by [18F]EF5 in atherosclerotic plaques in mice. Arterioscler Thromb Vasc Biol 31:1011–1015.

Silvola JMU, Saraste A, Laitinen I, et al (2011b) Effects of age, diet, and type 2 diabetes on the development and FDG uptake of atherosclerotic plaques. JACC Cardiovasc Imaging 4:1294–1301.

Skajaa T, Cormode DP, Falk E, et al (2010) High-density lipoprotein-based contrast agents for multimodal imaging of atherosclerosis. Arterioscler Thromb Vasc Biol 30:169–176.

Smith JD, Trogan E, Ginsberg M, et al (1995) Decreased atherosclerosis in mice deficient in both macrophage colony-stimulating factor (op) and apolipoprotein E. Proc Natl Acad Sci U S A 92:8264–8268.

Stamler J, Wentworth D, Neaton JD (1986) Is relationship between serum cholesterol and risk of premature death from coronary heart disease continuous and graded? Findings in 356,222 primary screenees of the Multiple Risk Factor Intervention Trial (MRFIT). JAMA 256:2823–288.

Stary H, Chandler A, Glagov S, et al (1994) A definition of initial, fatty streak, and intermediate lesions of atherosclerosis. Circulation 89:2462–2478.

Stöger JL, Gijbels MJJ, van der Velden S, et al (2012) Distribution of macrophage polarization markers in human atherosclerosis. Atherosclerosis 225:461–468.

Su H, Gorodny N, Gomez LF, et al (2014) Atherosclerotic plaque uptake of a novel integrin tracer ^{18}F-Flotegatide in a mouse model of atherosclerosis. J Nucl Cardiol 21:553–562.

Sullivan JL (2009) Iron in arterial plaque: A modifiable risk factor for atherosclerosis. Biochim Biophys Acta 1790:718–723.

Svingen GFT, Schartum-Hansen H, Pedersen ER, et al (2016) Prospective Associations of Systemic and Urinary Choline Metabolites With Incident Type 2 Diabetes. Clin Chem 765:755–765.

Tabas I, Williams KJ, Borén J (2007) Subendothelial lipoprotein retention as the initiating process in atherosclerosis: Update and therapeutic implications. Circulation 116:1832–1844.

Tahara N, Kai H, Ishibashi M, et al (2006) Simvastatin attenuates plaque inflammation. Evaluation by fluorodeoxyglucose positron emission tomography. J Am Coll Cardiol 48:1825–1831.

Tahara N, Kai H, Yamagishi S, et al (2007) Vascular inflammation evaluated by [^{18}F]-fluorodeoxyglucose positron emission tomography is associated with the metabolic syndrome. J Am Coll Cardiol 49:1533–1539.

Tahara N, Mukherjee J, de Haas HJ, et al (2014) 2-deoxy-2-[^{18}F]fluoro-D-mannose positron emission tomography imaging in atherosclerosis. Nat Med 20:215–219.

Tall AR, Yvan-Charvet L (2015) Cholesterol, inflammation and innate immunity. Nat Rev Immunol 15:104–116.

Tang TY, Howarth SPS, Miller SR, et al (2009) The ATHEROMA (Atorvastatin therapy: effects on reduction of macrophage activity) study. Evaluation using ultrasmall superparamagnetic iron oxide-enhanced magnetic resonance imaging in carotid disease. J Am Coll Cardiol 53:2039–2050.

Tarkia M, Saraste A, Stark C, et al (2015) [^{18}F]FDG accumulation in early coronary atherosclerotic lesions in pigs. PLoS One 10:e0131332.

Tarkin JM, Dweck MR, Evans NR, et al (2016) Imaging atherosclerosis. Circ Res 118:750–769.

Tawakol A, Fayad ZA, Mogg R, et al (2013) Intensification of statin therapy results in a rapid reduction in atherosclerotic inflammation: results of a multicenter fluorodeoxyglucose-positron emission tomography/computed tomography feasibility study. J Am Coll Cardiol 62:909–917.

Tawakol A, Migrino RQ, Bashian GG, et al (2006) In Vivo ^{18}F-Fluorodeoxyglucose positron emission tomography imaging provides a noninvasive measure of carotid plaque inflammation in patients. J Am Coll Cardiol 48:1818–1824.

Tawakol A, Migrino RQ, Hoffmann U, et al (2005) Noninvasive in vivo measurement of vascular inflammation with F-18 fluorodeoxyglucose positron emission tomography. J Nucl Cardiol 12:294–301.

Tawakol A, Singh P, Mojena M, et al (2015) HIF-1 and PFKFB3 mediate a tight relationship between proinflammatory activation and anerobic metabolism in atherosclerotic macrophages. Arterioscler Thromb Vasc Biol 35:1463–1471.

Tavakoli S, Zamora D, Ullevig S, Asmis R (2013) Bioenergetic profiles diverge during macrophage polarization: implications for the interpretation of ^{18}F-FDG PET imaging of atherosclerosis. J Nuc Med 54:1661–1667.

Taylor JMW, Allen A, Graham A (2014) Targeting mitochondrial 18 kDa translocator protein (TSPO) regulates macrophage cholesterol efflux and lipid phenotype. Clin Sci 127:603–613.

Thackeray JT, Bankstahl JP, Wang Y, et al (2015) Clinically relevant strategies for lowering cardiomyocyte glucose uptake for ^{18}F-FDG imaging of myocardial inflammation in mice. Eur J Nucl Med Mol Imaging 42:771–780.

Treglia G, Giovannini E, Di Franco D, et al (2012) The role of positron emission tomography using carbon-11 and fluorine-18 choline in tumors other than prostate cancer: A systematic review. Ann Nucl Med 26:451–461.

Trivedi RA, Mallawarachi C, U-King-Im JM, et al (2006) Identifying inflamed carotid plaques using in vivo USPIO-enhanced MR imaging to label plaque macrophages. Arterioscler Thromb Vasc Biol 26:1601–1606.

Tsiantoulas D, Diehl CJ, Witztum JL, Binder CJ (2014) B cells and humoral immunity in atherosclerosis. Circ Res 114:1743–1756.

Van den Maagdenberg AMJM, Hofker MH, Krimpenfort PJA, et al (1993) Transgenic mice carrying the apolipoprotein-E3-Leiden gene exhibit hyperlipoproteinemia. J Biol Chem 268:10540–10545.

Van Herck JL, De Meyer GRY, Martinet W, et al (2009) Impaired fibrillin-1 function promotes features of plaque instability in apolipoprotein E-deficient mice. Circulation 120:2478–2487.

Van Vlijmen BJM, Van Den Maagdenberg AMJM, Gijbels MJJ, et al (1994) Diet-induced hyperlipoproteinemia and atherosclerosis in

apolipoprotein E3-Leiden transgenic mice. J Clin Invest 93:1403–1410.

Varrone A, Oikonen V, Forsberg A, et al (2015) Positron emission tomography imaging of the 18-kDa translocator protein (TSPO) with [^{18}F]FEMPA in Alzheimer's disease patients and control subjects. Eur J Nucl Med Mol Imaging 42:438-446.

Véniant MM, Zlot CH, Walzem RL, et al (1998) Lipoprotein clearance mechanisms in LDL receptor-deficient "apo-B48- only" and "apo-B100-only" mice. J Clin Invest 102:1559–1568.

Vidal C, Gómez-Hernández A, Sánchez-Galán E, et al (2007) Licofelone, a balanced inhibitor of cyclooxygenase and 5-lipoxygenase, reduces inflammation in a rabbit model of atherosclerosis. J Pharmacol Exp Ther 320:108–116.

Villanueva FS, Jankowski RJ, Klibanov S, et al (1998) Microbubbles targeted to intercellular adhesion molecule-1 bind to activated coronary artery endothelial cells. Circulation 98:1–5.

Villanueva FS, Wagner WR (2008) Ultrasound molecular imaging of cardiovascular disease. Nat Clin Pract Cardiovasc Med S26–32.

Virmani R, Kolodgie FD, Burke AP, et al (2000) Lessons from sudden coronary death: a comprehensive morphological classification scheme for atherosclerotic lesions. Arterioscler Thromb Vasc Biol 20:1262–1275.

Vucic E, Calcagno C, Dickson SD, et al (2012) Regression of inflammation in atherosclerosis by the LXR agonist R211945: A noninvasive assessment and comparison with atorvastatin. JACC Cardiovasc Imaging 5:819–828.

Vucic E, Dickson SD, Calcagno C, et al (2011) Pioglitazone modulates vascular inflammation in atherosclerotic rabbits: Noninvasive assessment with FDG-PET-CT and dynamic contrast-enhanced MR imaging. JACC Cardiovasc Imaging 4:1100–1109.

Wang YX, Martin-McNulty B, Huw LY, et al (2002) Anti-atherosclerotic effect of simvastatin depends on the presence of apolipoprotein E. Atherosclerosis 162:23–31.

Watanabe T, Kawasaki M, Tanaka R, et al (2015) Anti-inflammatory and morphologic effects of pitavastatin on carotid arteries and thoracic aorta evaluated by integrated backscatter trans-esophageal ultrasound and PET/CT: a prospective randomized comparative study with pravastatin (EPICENTRE study). Cardiovasc Ultrasound 13:17.

Weber C, Noels H (2011) Atherosclerosis: current pathogenesis and therapeutic options. Nat Med 17:1410–1422.

Wenning C, Kloth C, Kuhlmann MT, et al (2014) Serial F-18-FDG PET/CT distinguishes inflamed from stable plaque phenotypes in shear-stress induced murine atherosclerosis. Atherosclerosis 234:276–282.

Westerterp M, Van Der Hoogt CC, De Haan W, et al (2006) Cholesteryl ester transfer protein decreases high-density lipoprotein and severely aggravates atherosclerosis in APOE*3-Leiden mice. Arterioscler Thromb Vasc Biol 26:2552–2559.

Westlake SL, Colebatch AN, Baird J, et al (2010) The effect of methotrexate on cardiovascular disease in patients with rheumatoid arthritis: A systematic literature review. Rheumatology 49:295–307.

White HD, Held C, Stewart R, et al (2014) Darapladib for preventing ischemic events in stable coronary heart disease. N Engl J Med 370:1702–1711.

Williams KJ, Tabas I (1995) The Response-to-retention hypothesis of early atherogenesis. Arterioscler Thromb Vasc Biol 15:551–561.

Witztum JL, Lichtman AH (2014) The influence of innate and adaptive immune responses on atherosclerosis. Annu Rev Pathol 9:73–102.

Woollard KJ, Geissmann F (2010) Monocytes in atherosclerosis: subsets and functions. Nat Rev Cardiol 7:77–86.

Wu YW, Kao HL, Huang CL, et al (2012) The effects of 3-month atorvastatin therapy on arterial inflammation, calcification, abdominal adipose tissue and circulating biomarkers. Eur J Nucl Med Mol Imaging 39:399–407.

Wyss MT, Weber B, Honer M, et al (2004) ^{18}F-choline in experimental soft tissue infection assessed with autoradiography and high-resolution PET. Eur J Nucl Med Mol Imaging 31:312–316.

Ye YX, Calcagno C, Binderup T, et al (2015) Imaging macrophage and hematopoietic progenitor proliferation in atherosclerosis. Circ Res 117:835–845.

Yun M, Jang S, Cucchiara A, et al (2002) ^{18}F-FDG uptake in the large arteries: a correlation study with the atherogenic risk factors. Semin Nucl Med 32:70–76.

Zadelaar S, Kleemann R, Verschuren L, et al (2007) Mouse models for atherosclerosis and

pharmaceutical modifiers. Arterioscler Thromb Vasc Biol 27:1706–1721.

Zernecke A (2015) Dendritic cells in atherosclerosis: evidence in mice and humans. Arterioscler Thromb Vasc Biol 35:763–770.

Zhang SH, Reddick R, Piedrahita JA, Maeda N (1992) Spontaneous hypercholesterolemia and arterial lesions in mice lacking apolipoprotein E. Science 258:468–471.

Zhang Z, Machac J, Helft G, et al (2006) Non-invasive imaging of atherosclerotic plaque macrophage in a rabbit model with F-18 FDG PET: a histopathological correlation. BMC Nucl Med 6:3.

Zimmer S, Grebe A, Latz E (2015) Danger signaling in atherosclerosis. Circ Res 116:323–340.